**Technical Report No. 32-31**



# Juno Final Report
# Volume I

# Juno I: Re-entry Test Vehicles and Explorer Satellites



**Allen E. Wolfe**
**William J. Truscott**



jpl
JET PROPULSION LABORATORY
CALIFORNIA INSTITUTE OF TECHNOLOGY
PASADENA, CALIFORNIA

September 6, 1960

[redacted]

Technical Report No. 32-31

# Juno Final Report,
# Volume I.

## Juno I: Re-entry Test Vehicles and Explorer Satellites

Allen E. Wolfe
William J. Truscott

John Small

John Small,
Juno Project Director

Copy No. HC 56
This document consists of covers and 48 leaves.



AVAILABLE TO NASA OFFICES, NASA RESEARCH CENTERS AND NASA CONTRACTORS ONLY

JET PROPULSION LABORATORY
CALIFORNIA INSTITUTE OF TECHNOLOGY
PASADENA, CALIFORNIA

September 6, 1960

[redacted]

## PREFACE

Technical Report No. 32-31, which is prepared in three volumes, is a summary of Jet Propulsion Laboratory space-flight activities utilizing the *Juno I* and *Juno II* rocket-vehicle configurations.

This volume (Volume I), describes events beginning in 1954 which led to the launching of the free-world's first earth satellite, *Explorer I*. The *Juno I* space-vehicle and flights through *Explorer V* are described.

The general program presented in this first volume was initiated and flights completed under sponsorship of the Department of the Army, Ordnance Corps, Contract No. DA-04-495-Ord-18.

Volume II of this report describes the *Juno II* rocket-vehicle and the *Pioneer III* and *Pioneer IV* lunar space-flights. Volume III, which will be released next year, will be concerned with *Juno II* earth-satellite flights. A portion of the work described in Volume II and the program presented in Volume III were conducted under sponsorship of the National Aeronautics and Space Administration, Contract No. NASw-6.

## CONTENTS

## CONTENTS (Cont'd)

## CONTENTS (Cont'd)

## CONTENTS (Cont'd)

## TABLES



## FIGURES

## FIGURES (Cont'd)

## FIGURES (Cont'd)

## ABSTRACT

The *Juno* program had for its objective the launching of satellites and space probes. The vehicle configuration consisted of scaled-down *Sergeant* solid-propellant motors and a booster of either a modified *Redstone* or a modified *Jupiter*. Volume I covers the early history of the program, a detailed description of the high-speed stages, the Microlock tracking and telemetry system, and all of the *Juno I*, or early *Explorer*, firings.

# I. INTRODUCTION

### A. General

This Report is Volume I of a three-volume series of Reports describing Jet Propulsion Laboratory participation in early space-flight activities. These activities described herein were conducted mainly under *Juno* program, although other programs—*Orbiter*, Re-entry Test Vehicle (RTV), and Microlock (tracking and telemetering)—contributed much support, research information, and experience.

*Juno* was the name given to the general program for launching satellites and space probes. This program was built around the use of a cluster of scaled-down *Sergeant* solid propellant motors for the upper stages of a vehicle in which the booster was either a modified *Redstone (Juno I)* or a modified *Jupiter (Juno II)*.

Volume I of this Report covers the early history of the program, a detailed description of the high-speed stages, the Microlock tracking and telemetry system, and all of the *Juno I* or early *Explorer* firings; Volume II (to be published shortly) covers the *Pioneer III* and *IV* lunar probes, which represented the first two flights of the *Juno II* system. The third volume will be concerned with the use of the *Juno II* for Earth satellites and will be pub lished upon completion of the program in early 1961.

The material covered in these Reports represents the work of many people at JPL and ABMA.

The bulk of the material has been taken from the documents listed in the Bibliography; no attempt has been made to make reference to specific documents.

### B. Project Orbiter

Aside from some early studies on satellite trajectories carried out for the Navy in 1945 and 1946, the first direct participation of the Jet Propulsion Laboratory in space-flight activities occurred in the joint Army-Navy *Project Orbiter* studies of 1954 and 1955.

The Jet Propulsion Laboratory was asked by the Army Ordnance Corps to assist Redstone Arsenal in the preparation of a feasibility study for a rocket vehicle capable of orbiting a small payload around the earth. Also at that time, as part of a re-entry test program, the missile laboratories at Redstone Arsenal were in the process of developing a modified high-performance version of the *Redstone* missile. This modified missile, together with a three-stage, solid-propellant rocket vehicle (as proposed by JPL), which would be launched from the *Redstone* missile, formed the Army proposal for a satellite vehicle.

The three-stage rocket proposed by the Jet Propulsion Laboratory consisted of clusters of scale *Sergeant* solid-propellant motors and had the following important characteristics. The first two stages formed the high-speed portion of the vehicle required for the re-entry test mission. For the orbiting mission a third solid-propellant stage and payload could be added to the re-entry missile without any important modifications either in the *Redstone* missile or in the first two high-speed stages.

As a part of the feasibility study for the development of an orbiting missile, this Laboratory also conducted an investigation into the problem of instrumenting such a missile. On the basis of the results obtained in these investigations, the Laboratory proposed a scheme for determining the trajectory of an orbiting missile using radio techniques.

Actual development of the orbiting vehicle, as described in the feasibility studies, was never authorized because *Project Orbiter* was cancelled in August 1955 when the *Vanguard Project* was established. However, the need for obtaining re-entry test data still remained, and Redstone Arsenal continued work toward this objective. Within the framework of the re-entry test program, the Jet Propulsion Laboratory was requested by Redstone Arsenal to undertake the development of the proposed configuration. Because this development was to be keyed to the *Redstone* re-entry test program rather than to the satellite program, the objectives and development schedules were modified accordingly.

Although the major effort of this Laboratory on the re-entry test program had been directed toward the development of the proposed design, some analysis was undertaken to explore the growth potential of the high-speed stages. On the basis of this analysis it appeared that with some minor modifications, and with some additional developments (principally on the solid-propellant motors), the high-speed stages would be capable of launching appreciably larger payloads into orbiting trajectories. Descriptions of these new developments appear in this document at points corresponding to the times when the modifications were first introduced into the flight hardware.

The RTV Program was concluded in August 1957 with the successful recovery of a scale IRBM nose cone. Three rounds had been fired. The first, round 27, was successfully fired in September 1956 to test the basic hardware. This round contained a third stage designed for the satellite rather than re-entry mission because the design was further along. Rounds 34 and 40 were true re-entry vehicles with round 40 successful, while 34 was not successful.

# PART ONE: RE-ENTRY TEST VEHICLE DESCRIPTION

## II. GENERAL DESCRIPTION OF THE RTV PROGRAM

The total effort on the re-entry test vehicle (RTV) program at this Laboratory lay in two major categories. The first category comprised the development of the high-speed stages of the rocket vehicle for use as a suitable test vehicle from which re-entry test data could be obtained, and which would still retain the capability of handling an orbiting payload. The second category comprised the development of radio instrumentation. Because the Laboratory's proposal for a trajectory measurement by radio techniques had applications in the re-entry mission as well as the orbiting mission, development continued on suitable flight and ground equipment which was adaptable to either purpose.

Because of the extremely fast time schedules required in the re-entry test program, the Jet Propulsion Laboratory was unable to follow the customary conservative procedure of thoroughly testing each component before the completion of the final design. Instead, it was necessary to base the design upon theoretical analysis and past experience. The test program, operating concurrently with the design and development of the high-speed stages, had two purposes. The first purpose was to proof-test the various components of the stages. The second purpose was to indicate what minor modifications should be incorporated into the design. Any major modification, shown by the test program to be necessary, could not be incorporated into the design without serious changes in the development schedule. No major modifications were found to be necessary. Thus, on the basis of the design, development, and testing, it appeared that the high-speed stages, together with the *Redstone* missile as a boosting rocket, was capable either of launching a 350-lb re-entry test missile along a suitable trajectory or of launching an orbiting payload of approximately 15 lb total weight into a circular orbit around the earth at an altitude of approximately 200 miles.

# III. GENERAL DESCRIPTION OF THE HIGH-SPEED STAGES

## A. Structure

The high-speed stages of the re-entry test vehicle, or *Jupiter C*, are built up as clusters of solid-propellant motors. Each motor has a diameter of 6 in., and an overall length, including the nozzle, of 47⅛ in., except for the stage 4 motor which is slightly shorter (Fig. 1). Their design is based on a scaled-down design of the *Sergeant* rocket motor, which was being developed at this Laboratory. The first high-speed stage is propelled by eleven such motors, the next by three, and the last by one. The stages are designated by the following numbering convention. The *Redstone* missile is called stage 1, or booster, the first high-speed section is stage 2, the next is stage 3, and the last, stage 4.

The eleven motors forming the propulsive unit of stage 2 are arranged in a ring with their axes parallel (Fig. 2). The radius of this ring, measured from the axis of symmetry of the stage to the axis of any one motor, is 13⅜ in. The motors are held together with three transverse bulkheads.

Inside this ring of motors is carried the group of three motors comprising the propulsive unit of stage 3 (Fig. 3).

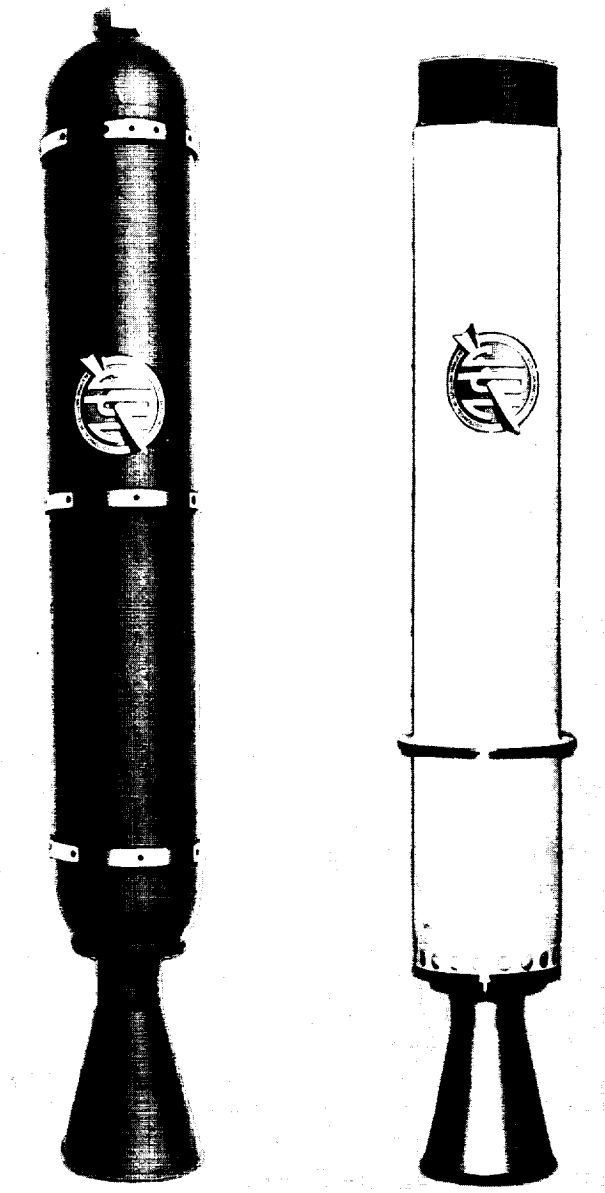

a. SECOND-AND THIRD-STAGE MOTOR

b. FOURTH-STAGE MOTOR

**Figure 1. High-speed motors**

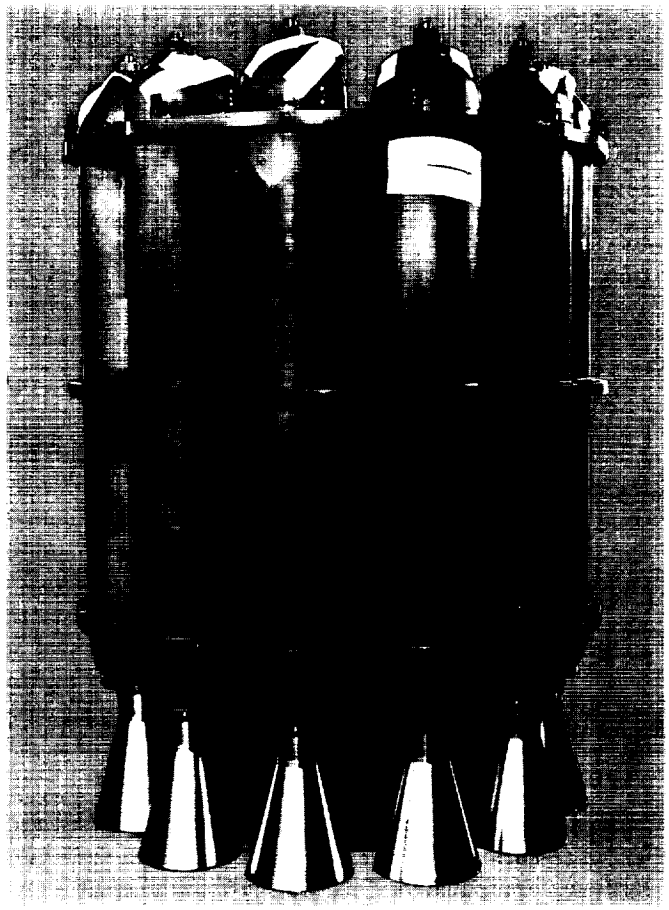

**Figure 2. Stage 2 motor assembly**

**Figure 3. Stage 3 motor assembly**

These motors, arranged with their axes parallel, are also supported by three transverse bulkheads. Extending forward from this bundle of motors is a truncated conical shell, which supports the fourth stage. A different conical shell was designed for use with the re-entry nose cone. The assembled high-speed stages and re-entry nose cone are shown in Fig. 4. The complete rocket, the *Redstone* missile with the high-speed stages mounted on the nose, is shown in Fig. 5.

The design of the high-speed stages, as described in this Report, was carried out on the basis of loads imposed and the performance required by the orbiting configuration. In this configuration the fourth stage, complete with the orbiting payload, weighed approximately 75 lb. In contrast, the re-entry vehicle which would replace stage 4 weighed 350 lb. A preliminary analysis was carried out at this Laboratory to determine what modifications were necessary in the structure of stages 2 and 3 to accommodate this heavier payload. On the basis of this analysis it appeared that no important modifications would be necessary. Thus the two-fold purpose had been successfully maintained in the design of the high-speed stages.

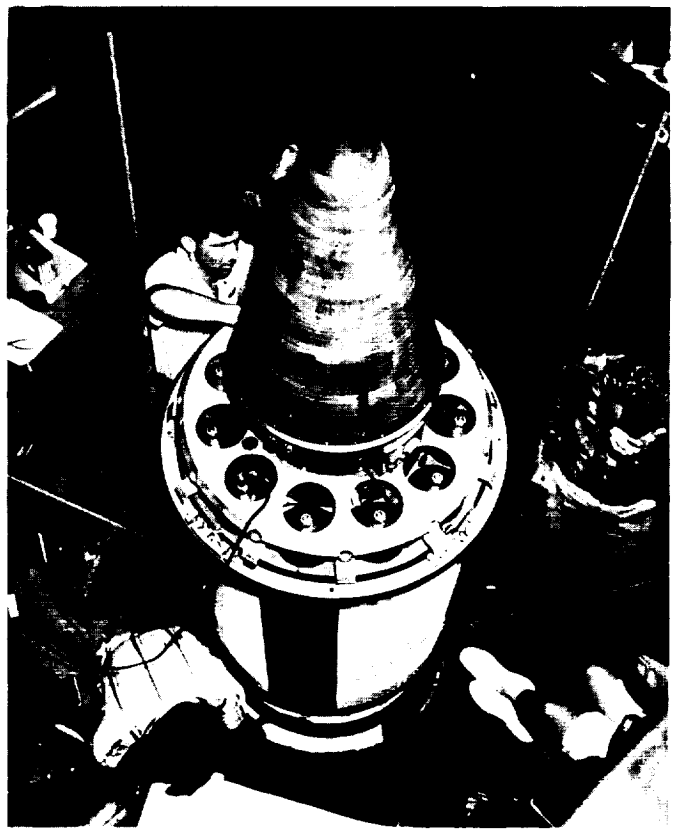

**Figure 4. Assembled high-speed stages and nose cone**

### *B. Reliability*

The choice of motors for the high-speed stages of the RTV (*Jupiter C*) was based primarily on considerations of reliability. Because the stages were to be made up of

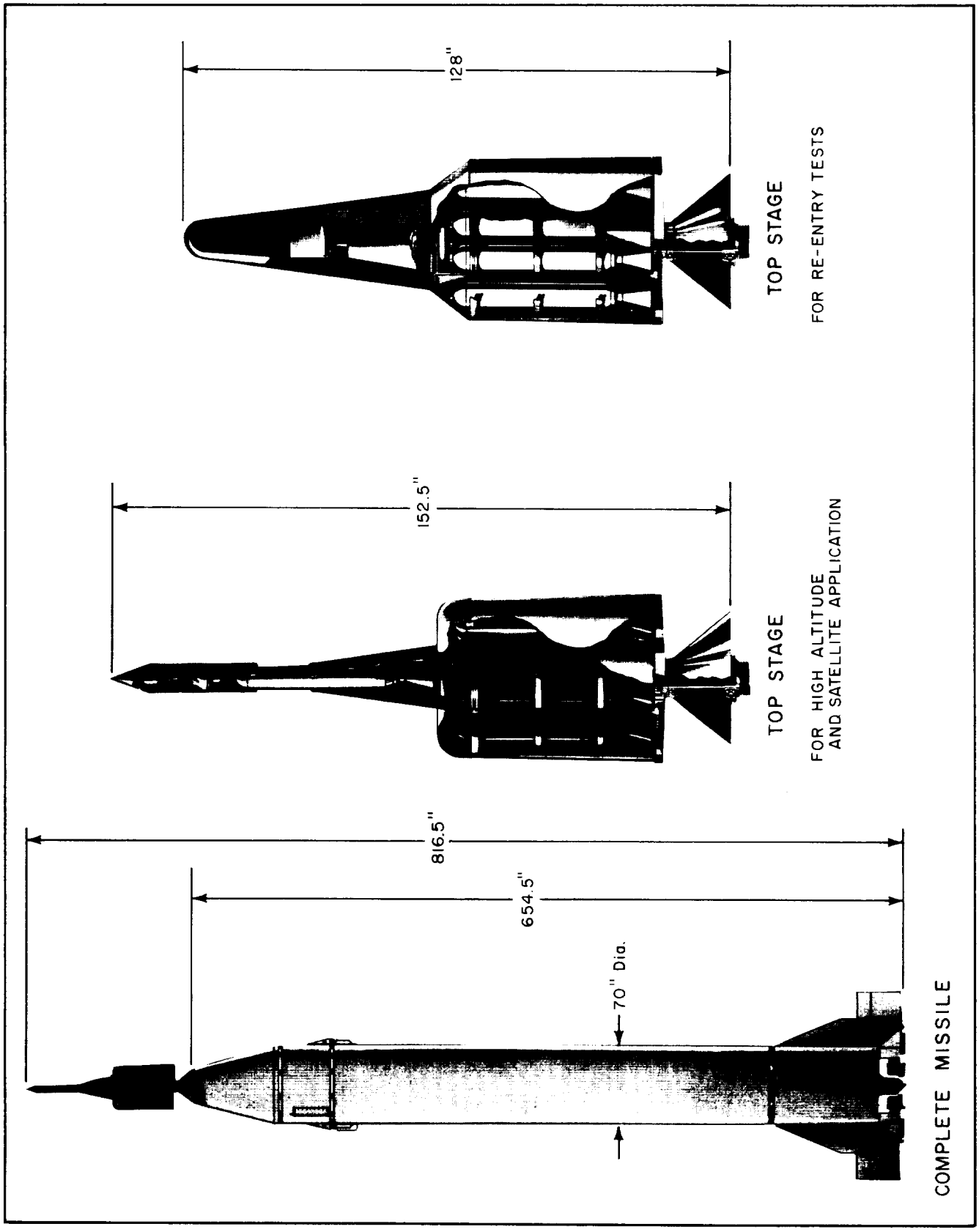


**Figure 5. Complete re-entry vehicle**

a relatively large number of readily available small rocket motors, it was considered vitally important that the reliability of the individual motors be high, so that there would be a high probability of success of the mission.

As a by-product of the development work on the *Sergeant* program at JPL, there was available a 6-in.-diameter solid-propellant motor, a scale model of the 31-in.-diameter *Sergeant* motor. Over 100 static firings in the temperature range of from −30°F to 140°F had been made on the scale motor without a single failure. The clustering of many small motors created several potentially serious problems the solution of which required a great deal of effort in several areas.

In order to ensure high accuracy, the rocket motors in stages 2 and 3 each had to fire simultaneously. The Solid Rockets Section at JPL conducted many tests to determine the potential differential, if any, in firing times of the eleven motors in stage 2 and the three in stage 3.

Using squibs to ignite the motor igniters, they found the differential was actually small, but could be reduced further by employing a manifold on stage 2 to use the hot gases to fire all eleven motors at once.

Although the manifold could have been used, it would have added weight to the stages and consequently reduced the weight available for the payload. The final solution was to use a redundant system in which two squibs were wired in parallel, for each igniter.

Another severe problem involved the guidance of the solid-propellant JPL cluster. The entire upper-stage cluster rotated on its long axis to achieve a spin stabilization effect. This rotation was achieved by means of two electric drive motors located in the instrument compartment of the booster.

The rotation of the cluster also helped equalize any variation of thrust and thrust malalignment between motors. However, there were two conflicting requirements in this condition. To increase accuracy and minimize dispersion, it was desirable to spin the cluster as fast as possible. On the other hand, certain spin rates set up a critical resonance frequency in the vehicle which could cause the vehicle to fail through vibrational loads. In any case the requirement for spin stabilization would require the careful balancing of the entire cluster.

In order to minimize the resonance problem, the rotational speed was programmed to take advantage of the fact that the critical frequency starts out at a fairly low value when the missile is fully loaded and rises steadily as the fuel is depleted during launch.

A speed regulator was developed by ABMA to program the cluster rpm from the maximum allowable at launch to the final desired rpm. The final rpm had to be reached prior to booster burnout in order that the roll control system employed after burnout would not be unduly loaded.

The cluster was driven by two General Electric direct-current aircraft motors rated 28 v, 7700 rpm, and 3.5 hp. The motors worked in parallel by means of a toothed belt. A synchro, connected by a flexible coupling to one motor shaft, provided the data for the speed regulator and an indication for a counter for accurate speed measurement. The load on the motors varied from missile take off to free flight, depending on acceleration and aerodynamic pressure. Normally, the motors operated at about 60% full load, but during the flight an overload of about 200% was to be expected.

Because an armature voltage regulation system to handle 200 amperes would be bulky and heavy, it was decided to control the speed of the motors by field regulation. The system works in a closed loop as shown in Fig. 6.

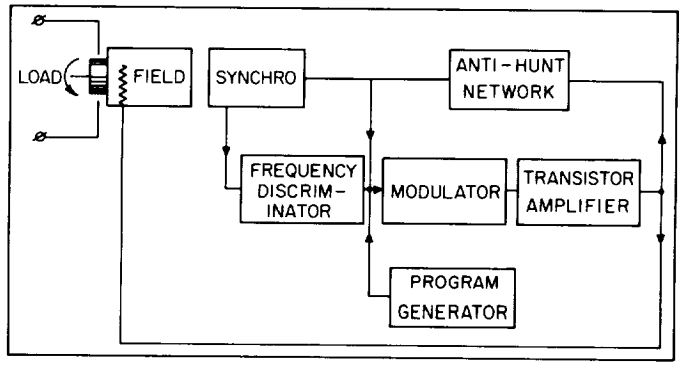


**Figure 6. Block diagram of programmed cluster speed regulator**

For the first flight, RS27, the gear ratio between the drive motor and the cluster was such that a synchro output frequency of 150 cps corresponded to 750 rpm of the cluster. This frequency was compared with a frequency reference, and the error amplified and fed back into the motor field in a direction to minimize this error. For the programmed phase of operation, a small timer motor with a gear turned a potentiometer 1 turn in about 120 sec and changed the frequency reference. The closed loop system minimized the error between the reference and the actual speed. Thus the motor changed its speed in accordance with the program, i.e., between 600 and 750 rpm in 120 sec.

The regulated motor showed a deviation of less than 3%, for a wide range of armature currents. At 750 rpm, where high accuracy is required, deviation was held to less than 1%.

Tests showed that the system could be represented essentially by a second-order system. The transient response in speed to a sudden change in load indicated an oscillation of about 0.1 cps with 40% of critical damping.

# IV. STRUCTURAL CONFIGURATION OF THE HIGH-SPEED STAGES

## A. The Complete Assembly

The complete assembly of the high-speed stages as shown in Fig. 4 has an overall length of 125⅞ in. The overall diameter, measured between the outside edges of the forward supporting lugs of stage 2, is 35¼ in. The weight of the complete assembly, less payload is 981 lb. The structure is best described in terms of the three following subassemblies which make up the complete rocket:

1. The ring of eleven motors comprising the propulsive system of stage 2.
2. The bundle of three motors and the attached forward cone which makes up the basic structure of stage 3.
3. The stage 4 assembly.

## B. The Stage-2 Ring

The ring of stage-2 motors as shown in Fig. 2 is supported in three transverse bulkheads. The method of support is as follows: three premachined steel rings, positioned to coincide with the three bulkheads, are welded to the outside of each motor case. Eleven holes are equally spaced around each bulkhead, which is machined to fit snugly over the motor rings. The bulkheads and rings are then bolted together. It is the function of the bulkheads to support the motors against radial loads imposed by the spinning motion of the rocket. The forward bulkhead serves an additional purpose. It transmits axial loads between the eleven motors and the remainder of the structure.

The three bulkheads are all similar to the design of the forward bulkhead, shown in Fig. 7. They are fabricated from flat aluminum sheet stock. The web-like structure of rings and ribs is made by removing 80% of the material from the interspaces. The forward bulkhead has four supporting lugs equally spaced around its outer circumference. These lugs fit into matching slots near the forward edge of the launching tub and serve to support the forward portion of the ring structure against transverse loads. No axial loads are taken by these lugs. On the front face of the forward bulkhead, near its inner circumference, are three equally spaced supports to hold stage 3. These supports are fitted with adjusting screws to permit alignment of stage 3 in the completed assembly. The supports transmit both axial and transverse loads from the forward bulkhead of stage 2 to stage 3.

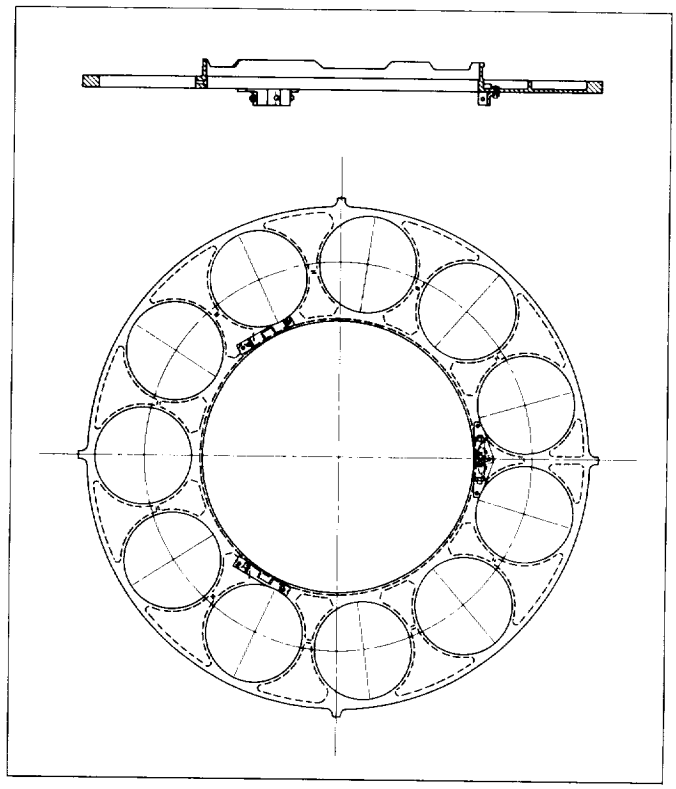

**Figure 7. Forward support assembly of stage 2**

A short cylindrical section extends aft from the inner circumference of the forward bulkhead. To this section is bolted a tube which runs from the forward bulkhead aft to a point slightly behind the nozzles of the motors in the ring. During the flight of the *Redstone* missile this tube, which rests on the base of the launching tub, transmits thrust loads from the *Redstone* to the high-speed stages.

The axial-load tube (Fig. 8), which fits the inner circumference of the ring, is bolted to each of the three bulkheads. It is made up of three pieces of aluminum sheet which are screwed together on overlap joints running lengthwise. The tube is reinforced by three doublers, also of aluminum sheet, which run between the center and forward bulkheads. At its forward end the tube is supported in a short cylindrical section running aft from the forward bulkhead, as described above. At its aft end the tube is bolted to a short ring, also made of aluminum, whose base and outer circumference are carefully machined to fit a supporting ring in the launching tub. Axial and transverse loads are taken by this ring.

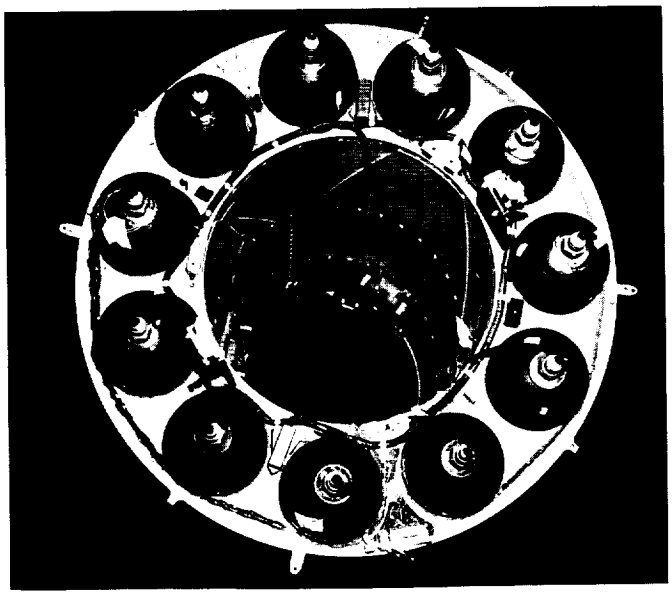

**Figure 8. Forward end of stage 2**

At the position of the aft bulkhead there are three supporting lugs equally spaced around the inside circumference of the tube. Slots are provided in these lugs which match lugs on the aft bulkhead of stage 3. In this manner the aft portion of stage 3 is supported against transverse loads; no axial loads are taken by these lugs.

### C. *The Stage-3 Assembly*

The stage-3 assembly as shown in Fig. 3 consists of two basic structures. The first structure is a bundle of three motors, held together by three transverse bulkheads. These bulkheads are fabricated in the same way as the bulkheads of the stage-2 ring. The center and aft bulkheads support the motors against the transverse loads induced by spin, while the forward bulkhead serves a dual role in supporting both transverse and axial loads. The second basic structure is the conical shell which extends forward of the front bulkhead. Two different shells were used depending upon whether the mission required the re-entry nose cone or the fourth stage and payload. Fig. 3 shows the support for stage 4 and payload.

The forward bulkhead of stage 3 has three supporting lugs equally spaced around its outer circumference. These lugs fit into the three supports which are fastened to the front face of the forward bulkhead of stage 2. During the flight of the *Redstone* missile, and stage 2, axial loads are carried into the stage-3 assembly through these supporting lugs. Extending forward of this bulkhead is a short conical section which supports the base of the conical shell.

The center bulkhead of the stage-3 assembly is lighter in construction than any of the other bulkheads since it is unnecessary to provide a rim around its outer cir-

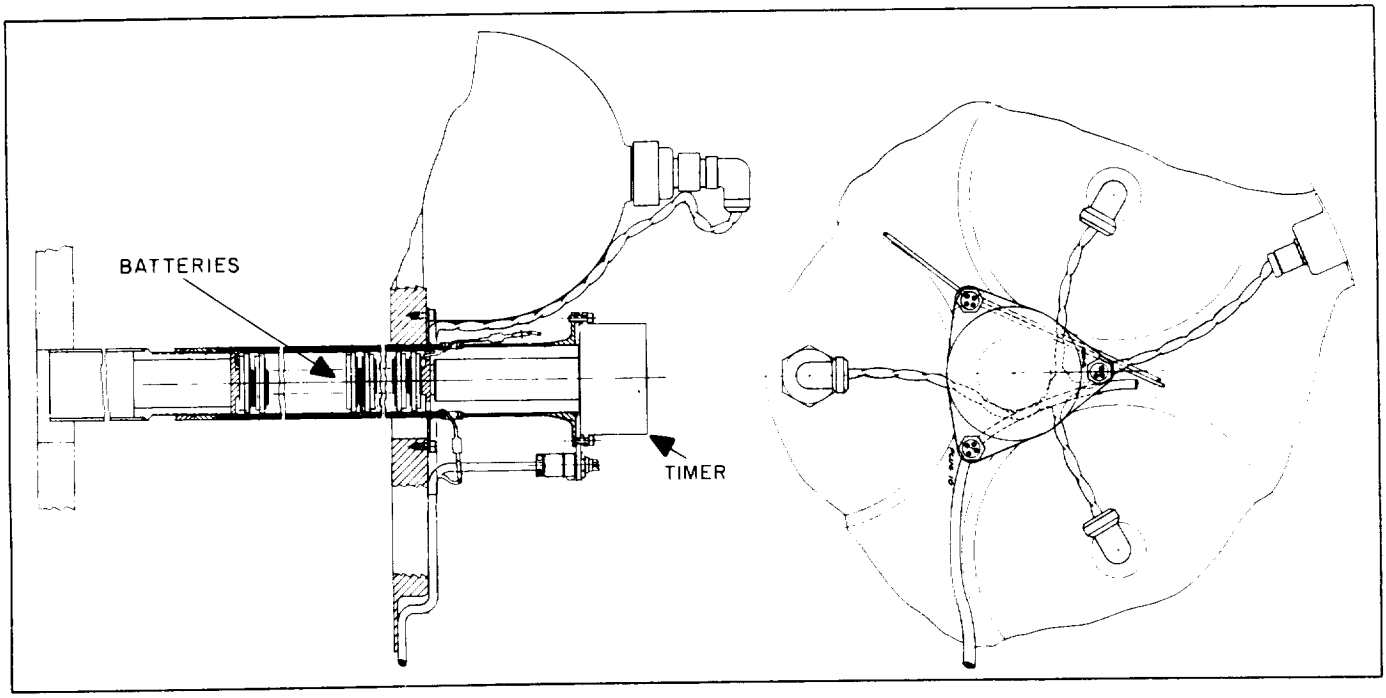


**Figure 9. Position of timer and batteries in stage 3**

cumference. The aft bulkhead has three supporting lugs equally spaced around its outer circumference. These lugs fit into the slots of the three supports attached to the inside of the tube of the stage-2 ring structure. These lugs transmit transverse loads but no axial loads into the stage-3 structure.

The conical shell, bolted onto the forward bulkhead of the stage-3 assembly, is fabricated from an aluminum spinning.

Three circular hand holes, 5¼ in. in diameter, are cut into the shell at a point just forward of the front ends of the stage-3 motors. These holes permit access to the motor heads for the purpose of installing igniters. Initial flights carried pyrotechnic flash units which were located in both stages 3 and 4. These flash units, which were fired by a timer at selected points during the burning program, were to provide trajectory information. The flash units provided for stage 3 were carried in the cone. Holes in the conical shell, through which the flashers could be fired, and fixtures to hold the flash units prior to their firing, were located just behind the aft support ring.

A triangular hole was cut in the center of each of the three bulkheads of stage 3. The dimensions of these holes are such that a 1½-in.-diameter cylinder could be carried on the centerline of stage 3, running through these holes in the bulkheads. This space was used to hold the batteries which operate the ignition and timing circuits carried in stage 3. The position of such a battery case and timer is shown in Fig. 9.

# V. THE PROPULSION SYSTEM

## A. The Propellant

The physical and ballistic characteristics of the scaled-down *Sergeant*, or RTV, motor, as adapted for the *Jupiter C* program, are given in Table 1.

**Table 1. Characteristics of RTV motors**

| | |
|---|---|
| Physical Characteristics: | |
| Diameter, in. | 6 |
| Overall length, in. (approx.) | 47 |
| Case length, in. (approx.) | 38½ |
| Throat diameter, in. | 1.732 |
| Case weight, lb | 7.0 |
| Nozzle weight, lb | 3.3 |
| Liner weight, lb | 0.5 |
| Propellant weight, lb | 48.2 |
| Total weight, lb | 59.0 |
| Performance Characteristics: | |
| Average pressure, psi | 498 |
| Effective duration, sec | 5.52 |
| Average thrust, vacuum, lb | 1830 |
| Total impulse, vacuum, lb-sec | 10,110 |

The solid propellant in this motor, designated T17-E2, is a composite formulation employing a polysulfide as fuel and ammonium perchlorate as oxidizer. The composition and characteristics of this propellant are given in Tables 2 and 3, respectively. The propellant is cast around a mandrel with a five-pointed-star configuration. A cross-section of the mandrel is shown in Fig. 10.

**Table 2. Composition of T17-E2 propellant**

| Component | Percent by weight |
|---|---|
| Ammonium perchlorate | 63.00 |
| Liquid polymer, LP-33 | 33.17 |
| Paraquinone dioxime | 2.32 |
| Diphenylguanidine | 1.16 |
| Sulfur | 0.02 |
| Nylon tow | 0.33 |

**Table 3. Performance and mechanical characteristics of T17-E2 propellant**

| | |
|---|---|
| Characteristic velocity, ft/sec | 4150 |
| Specific impulse (1000 psi, sea level), sec | 205 |
| Elongation, % | 77 |
| Breaking strength in tension, lb | 270 |
| Burning rate (70°F, 1000 psia), in./sec | 0.31 |
| Specific impulse (vacuum), sec | 218 |

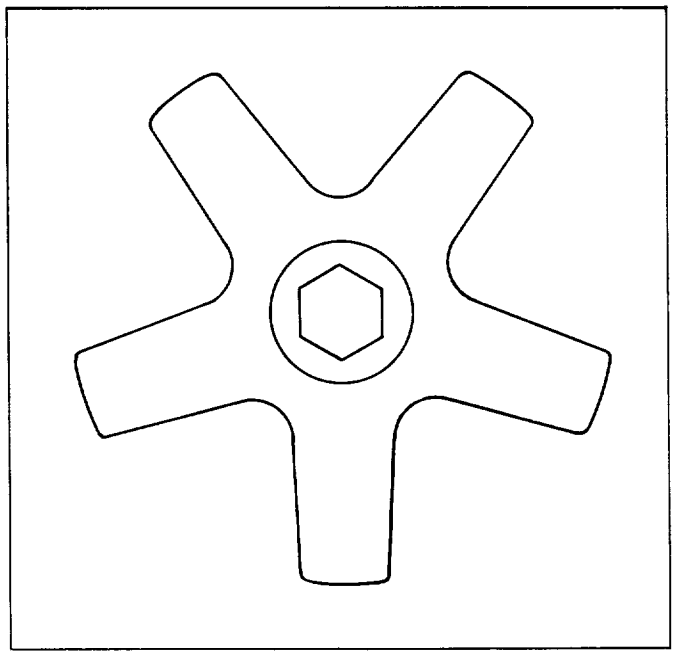

**Figure 10. Cross section of mandrel for casting RTV motor**

## B. The Motor Case

The motor cases are fabricated from No. 410 stainless steel. The cylindrical shell is rolled and welded from 0.023-in. sheet. Prefabricated rings are slipped over the case and welded in place. The forward and aft domes are fabricated as spinnings and welded to the cylindrical sections. Final machining cuts are taken to hold the nozzle axis and the center of gravity of the motor on the axis defined by the outside diameter of the rings. The nozzles are screwed into the threaded section provided on the aft end of the motor case. The motor parts are shown in Fig. 11.

## C. The Nozzle

Several nozzle designs were employed in the testing program of the RTV motor. The reason the several nozzle designs were tested is that under the combination of centrifugal loads and heating from the propellant gas, the nozzle deflects. Thus, an attempt was made to find that nozzle design for each stage which would (1) minimize the deflection and (2) cause the deflection to be reproducible from motor to motor, for minimum weight.

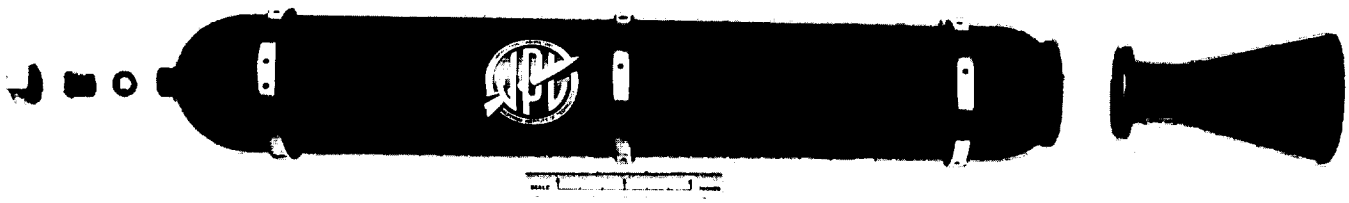

**Figure 11. RTV motor parts**

### *D. Directional Accuracy and Reproducibility of Motors*

The requirement for minimum thrust and mass unbalance could be met in either of two ways. First, all the motors of a high-speed stage could be manifolded together to ensure simultaneous ignition and operation. An analysis showed, however, that the development of a reliable manifold would be a difficult task, and that the manifold would add undesirable inert weight to the stages. Second, it might be possible, by special care in processing the propellant, to keep the motor-to-motor variation in thrust and impulse within acceptable limits.

The average between-batch variations of both thrust and burning rate were determined to be approximately 3%. The within-batch variations were approximately 0.1% for thrust, and 1.5% for burning rate.

The between-batch variation was reduced by a factor of two by loading three motors at a time from two batches of propellant, each motor receiving one-half of its load from each batch. The weights of individual motors were carefully controlled by maintaining close tolerances on metal parts and liners and by a final propellant-trimming operation. Through analysis of between-batch variations when this procedure was used, it was determined that thrust and mass unbalance could be satisfactorily limited, and only very small inaccuracies would be produced in the flight-direction angle.

# VI. IGNITION SYSTEM

## A. Description

The ignition system was designed with safety as the first consideration and reliability next in importance. For safety, the system had to be shielded from stray radio frequencies and power surges, and the final connecting of battery circuits to igniters had to be done as late as possible in the missile preflight work. To ensure reliability, duplicate circuits, batteries, switches, etc. were to be used wherever possible.

Each igniter contained two squibs wired separately. Thus, four wires were led from the igniter through the head-end fitting of the motor. This fitting also supported the igniter against axial loads. The igniter was supported against transverse loads by a set of rubber grommets (fitting inside the propellant grain) strung together with nylon line, to form an assembly which was pulled into position through the head-end of the motor. After this assembly was in place, the igniter and the head-end seal to which it was attached were installed.

Power for the ignition of the stage 2 motors was supplied by batteries located in the instrument compartment of the booster. The ignition signal was transmitted by ground command to radio-controlled equipment or by a timing device located in the booster section. Two sets of ignition leads ran through slip-rings in the base of the launcher to diametrically opposed disconnect plugs in the base of the launching tub of stage 2 and into a circular harness running around the inner circumference of the forward bulkhead of stage 2 (Fig. 12). A 2-ampere fuse was shunted across each of the two input junctions to prevent stray radiation and low-current signals from accidentally firing the motors. From the harness, pairs of wires led to each motor and connected to each igniter.

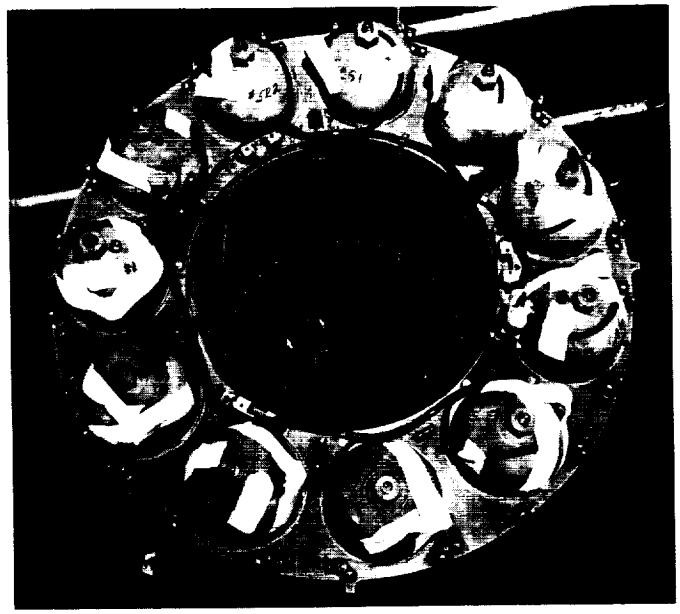

**Figure 12. Stage 2 showing ignition wiring harness**

Power for the ignition of the stage 3 motors was supplied by batteries carried in the tube running down the center of the stage 3 structure. The ignition signal was supplied by an electrically operated timer mounted on the forward end of this tube. The timer action was initiated by the closure of either one of two duplicate pressure switches mounted on two of the stage 2 motors. The switches were set to close during the ignition-pulse chamber pressure buildup of the stage 2 motors; the switch that closed first initiated the timer action. After approximately 8 sec (during which stage 2 finished burning) the timer fired the stage 3 motors.

# VII. DEVELOPMENT TESTING

## A. General

To validate assumptions on vital components of the re-entry test vehicle, it was necessary to conduct an extensive test program. This test program consisted of:

1. Pressure tests of the motor case
2. Static firing tests
3. Spin tests of motors
4. Motor firing under vacuum conditions
5. Structural tests
6. Balancing of the high-speed stages
7. RF sensitivity of ignition system.

## B. Propulsion System

### 1. Pressure Testing of Motor Case

A series of hydrostatic pressure tests was conducted on the motor case to verify its structural integrity when subjected to design loads and to determine its ultimate structural strength.

Proof pressure testing of the motor case for design structural loads was accomplished by hydrostatically applying 830 psi; this pressure was held for 5 min and then reduced to atmospheric. The cycle was repeated three times without any motor case deformation. Deflection gages mounted on the motor rings proved that these rings experienced no diameter change during the pressure rise in the chamber.

After completion of the proof pressure test, the deflection gages were removed and the pressure increased until motor case failure occurred. Bursting occurred at 1730 psi, which is more than twice the proof pressure and more than three times the actual pressure experienced by the motor under operating conditions.

### 2. Static Firing Tests

Static tests of the motors at atmospheric pressure were also carried out in test facilities at the Laboratory. From these tests, numerical data were obtained for pressure, thrust, and nozzle temperatures as functions of time. Each test provided information on the reliability of the motor.

Characteristics of the solid propellant were determined (1) by direct measurements on the propellant (to determine density) and (2) by the static-firing of batch-test motors (to determine, for example, the characteristic velocity $c^*$). Thermocouples were placed on the nozzles of motors under test to determine temperatures and gradients in nozzles of various designs and materials.

Data from 115 test motors showed that the characteristic velocity $c^*$ of T17-E2 propellant was 4152 ft/sec, with a standard deviation of 79 ft/sec. The vacuum specific impulse was computed from $c^*$ for a given nozzle as

$$I_{sp}=0.097\times C_f\times c^*/g$$

where $C_f$ was the thrust coefficient corresponding to the nozzle expansion ratio, and 0.097 was the factor usually employed to account for losses in the nozzle. The specific impulse for the motor stages 2 and 3 was 216.4 sec.

There was an alternative method for computing the vacuum specific impulse. In this second method $I_{sp}$ was given by the total thrust-time integral, obtained from the static firing tests, divided by the weight of propellant.

The values so obtained were corrected to vacuum conditions by the addition of a base drag term which was the pressure of the atmosphere times the effective area of the exit times the duration of burning divided by the weight of propellant. The correction factor due to separation effects of the flow through the nozzle was determined by a series of tests.

### 3. Spin Testing of Motors

An extensive test program was undertaken on the 6-in. *Sergeant* rocket motors to solve three important problems in the motor design:

1. Because the stage 2 motors would be located well away from the spin axis in the spinning assembly, the effects which the centrifugal forces might have on the integrity of the propellant grain or the uniformity of the combustion had to be determined.
2. The extreme directional accuracy required in the launching of the high-speed stages made it necessary that the thrust axis misalignment and mass unbalance be kept to a minimum during the launching of these stages. Tests were required to ensure that variations in ignition time, thrust, and total impulse of the different motors could be kept within the allowable limits.

3. As the high-speed stages would be required to ignite in vacuum characteristics of altitudes greater than 200 miles, the reliability of ignition under such conditions had to be demonstrated.

The spinning of the motors in the stage 2 ring subjects the solid propellant in the *Sergeant* motors to high centrifugal loads. A preliminary analysis of the effects on the propellant grain of loads such as 340 *g* at 1000 rpm indicated that the grain would not be damaged. However, configuration of the grain cross section is so complicated that a theoretical analysis can never be wholly satisfactory. Furthermore, it was almost impossible to predict what effect the spinning motion might have on the burning performance of the solid propellant. For these reasons, tests were made of both the structural integrity of the propellant grain and the burning characteristics of the propellant under spinning conditions.

The spin tests were carried out with a spin test fixture (Fig. 13) composed of two transverse arms welded to a central shaft rotated by an electric motor. A rocket motor was bolted into the hole provided in each of the transverse arms. The radius of the transverse arms from the center of the rig to the center of each motor was 15 in.

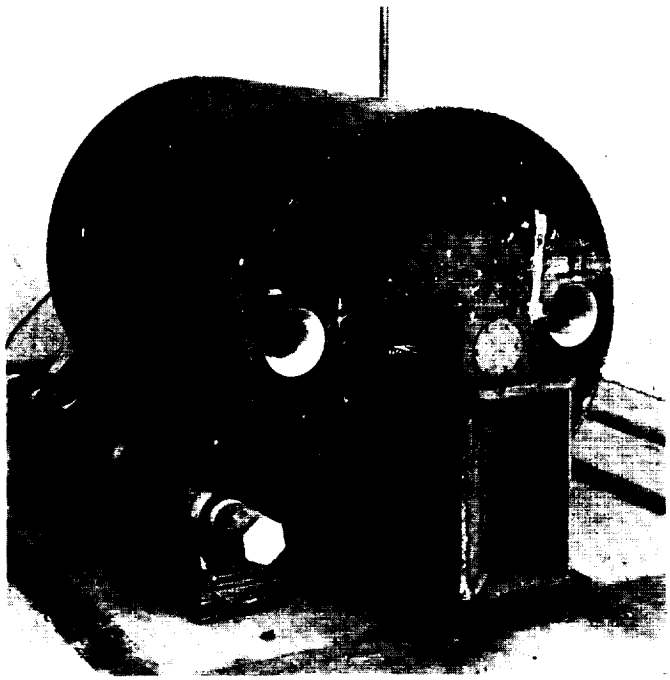

**Figure 13. Two-motor spin test fixture**

*a. Nonfiring spin tests.* The spin-test fixture was used to test the structural rigidity of the solid-propellant grain and the deflection of the motor case. Tests were conducted at several spin rates up to and including 1200 rpm, and the grains were inspected by a high-speed movie technique which employed a stroboscopic light to determine the degree of deflection of the grain (Fig. 14). The tests showed that although the grain was somewhat distorted, no cracks were formed, and the shape of the grain cross section was still acceptable for proper ballistic performance. It was evident that the grain was sufficiently rigid to withstand the spinning loads.

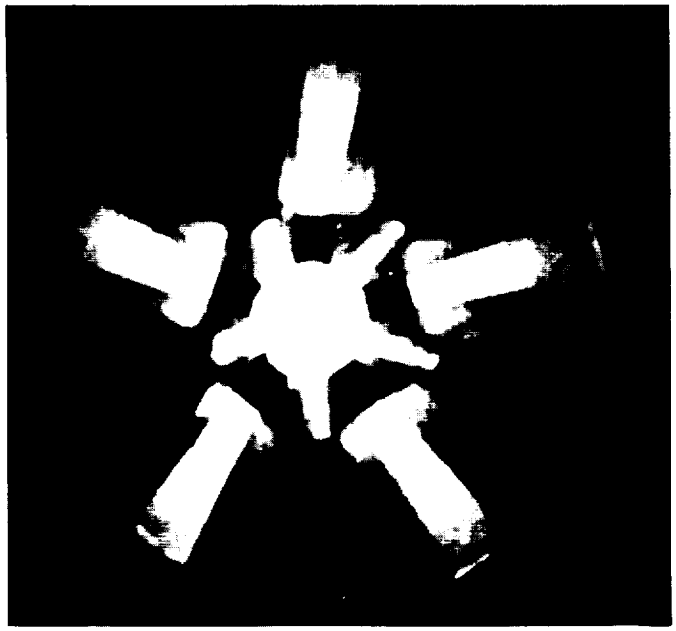

**Figure 14. Inside of propellant grain spinning at 1200 rpm**

The deflection of the loaded motor case under the spinning loads was measured by placing strain gages on the outside of the case. Although there was some deflection, it was not considered sufficient to cause any difficulty.

*b. Firing spin tests.* Firing spin tests were conducted on the spin-test fixture at various spin rates, using pressure gages to measure the chamber pressure at the head-end of the motors. The centrifugal forces on the gas stream flowing through the grain cavity caused a small change in the shape of the pressure-vs-time curve of these spin-fired motors (principally in the tail-off region) as compared with the curves for static firings. The motors, however, performed reliably and satisfactorily, producing the same total impulse as statically fired motors. Furthermore, all spin-fired motors exhibited the same type of pressure-vs-time curve.

At the conclusion of the first spin-firing tests, it was found that the motor nozzles had suffered severe outward deflections, evidently very late in the burning period. Accordingly, a nozzle-deflection gage was incorporated into the spin-test fixture, and firings were made with several different nozzle designs. Deflection was smallest in nozzles which were thicker in the region around the threads at the forward end and a heavy-base nozzle was adopted (Fig. 15).

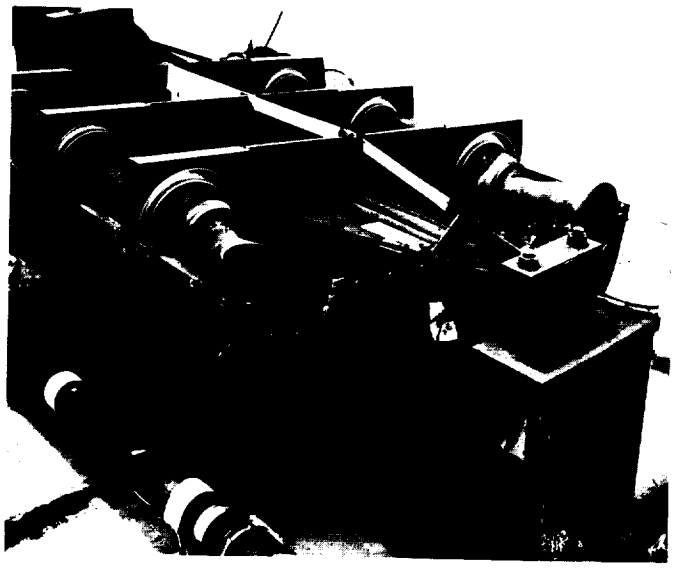

**Figure 15. RTV nozzles as deflected during spin test**

#### 4. Tests Under Vacuum Conditions

Motors were mounted in the vacuum chamber at the Army Ballistic Missile Agency. The first tests carried out with this setup were unsuccessful because of failure of the igniters, as described in the following paragraphs. In a subsequent test a nozzle seal was used and the motor operated successfully. During this test, temperature-measuring devices recorded the temperature on the nozzle of a dummy motor placed parallel to the motor being fired. This dummy motor was shielded by a metal plate, analogous to the tube running down the inside of the stage 2 ring. The purpose of the test was to determine how much heating should be expected around the aft ends of the stage 3 motors due to the flaring out of the propellant gases from the stage 2 motors operating in a vacuum. It was found that only a negligible amount of heating occurred.

When operating under normal atmospheric conditions, the igniters used in the 6-in.-scale-motor test program always operated successfully. However, the high-speed stages of the re-entry test vehicle were to be fired at extremely high altitudes. Therefore, it was necessary to test the operation of the igniters under vacuum conditions. Such tests were carried out both at this Laboratory and at the Army Ballistic Missile Agency at Redstone Arsenal.

The original igniters that were taken to Redstone Arsenal for use in these tests were found to be nonfunctional under vacuum conditions. The igniters were subjected to 2 hr of vacuum before receiving the ignition signal and failed to ignite.

Additional tests at the Jet Propulsion Laboratory showed that the composition (Thiokol X-225) was extremely difficult to ignite under a vacuum.

Several igniter designs, using a Hughes Aircraft Co. composition, were fabricated and tested and used with the Du Pont X-201E squib. These igniter designs displayed a lack of reproducibility in ignition times and in the shape of the pressure-vs-time curves.

Two alternative methods of assuring igniter reliability and reproducibility for rockets operating under vacuum conditions were used. The first method involved the use of a pressure seal for the igniter itself. Such a seal consisted of an air-tight plastic bag wrapped around the igniter. Atmospheric pressure held inside the bag until the igniter was fired. The second method consisted of sealing the whole motor under atmospheric conditions with a copper sheet soldered across the nozzle-entrance section. It was found that the seal was successful in holding atmospheric pressure of 15 psi. The average static rupture pressure for the seals tested was 25.9 psi. After rupture the seals did not interfere with the flow of gas through the nozzle.

The igniters used on Round 27 combined modified Hughes Aircraft composition of pyrotechnic and Du Pont S-89 electric squibs.

### C. *Structural Tests of the High-Speed Stages*

#### 1. Introduction

During the latter part of July 1956, a series of structural proof tests was carried out on the RTV high-speed stages. In the course of the test program, axial loads, simulating thrust, and inertial loads were applied to the high-speed stages while the complete assembly was spun in the rotational launcher. The loading program was planned in such a manner that flight conditions during stage 1 and stage 2 burning were simulated. The structure carried the applied proof loads with no yielding. On the basis of this

series of tests, it was believed that the structural strength of the RTV high-speed stages was adequate.

### 2. Structural Test Program

The following summary lists the structural test program for the RTV high-speed stages, carried out at this Laboratory:

*a. Modifications to the flight structure.* The high-speed structure used for the testing program was the second flight structure assembled by the Laboratory. Only two major modifications were necessary to allow the installation of the axial loading fixture (Fig. 16). Portions of the loading fixture attached to stage 2 had to pass through the center tube of stage 2. This necessitated cutting rectangular slots, which were then reinforced with doublers, in the center tube. Further, portions of the loading fixture extended up through stage 3 and down through the hub of the rotational launcher, in space normally occupied by slip-rings, batteries, and wiring. These portions of the wiring circuitry were not installed until the structural testing was completed.

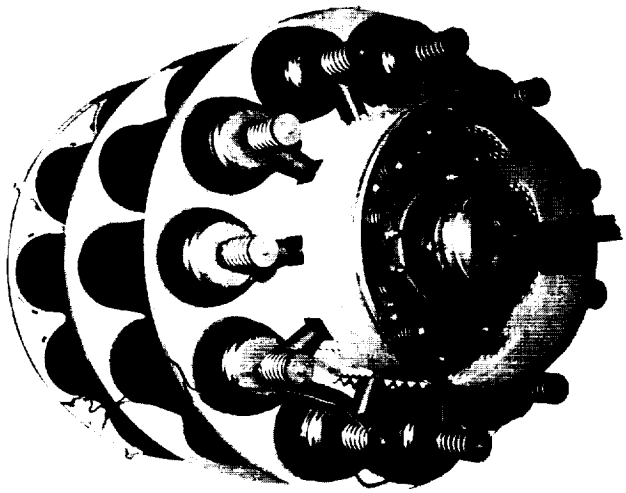

**Figure 16. Axial loading fixture installed in stages 2 and 3**

*b. The axial loading fixture.* The axial loading fixture used in the structural proof tests was a hydraulically actuated whiffletree-type fixture. One half of the whiffletree was attached to the structure of stage 2 by means of circular plates screwed into the nozzle threads at the rear of the motor cases. The other half was attached to the structure of stage 3, again by circular plates screwed into the nozzle threads. The jack mechanism applied loads through a pair of thrust bearings to the spinning structure while the jack assembly itself remained stationary. Springs were used to distribute the correct proportion of the applied gross loads to the local structure.

For the tests simulating stage 1 flight conditions, the whiffletree was actuated so that axial loads simulating the inertia loads were applied to all three stages. For the stage 2 flight conditions test, the whiffletree was actuated so that axial loads simulating thrust were applied to the stage 2 structure and axial loads simulating the inertia loads were applied to stage 3.

Although appearing quite complex, the installation and operation of the fixture during the testing was relatively trouble-free.

*c. Preliminary balancing of the structure.* Upon completion of the installation of the axial loading fixture in the high-speed stages, the entire assembly was placed in the ADC-Gisholt dynamic balancer (see Sec. VII-D). At this time, it was found that vertical clearance in the balancer was not sufficient to allow the installation of the jack mechanism during balancing operations. The jack mechanism acted as a support for the after portion of the axial loading fixture. When balancing attempts were made, the after portions of the axial loading fixture were then able to shift such that these attempts were fruitless. As a result, balancing attempts were discontinued, and the assembly was used in an unbalanced state for all the structural tests.

*d. Shake testing of the assembly.* After discontinuing balancing attempts, the assembly was installed on the structural test stand where all structural testing was carried out. Upon completing the installation and checking out the jack mechanism, a shake test was performed to determine the critical speeds of the assembly supported in this manner. With accelerometers mounted in the plane of the rotational launcher base and in the plane of the shroud-payload connector, a 25-lb electromagnetic shaker was attached to the structure. Response to the energies fed into the structure by the shaker, over the proposed operating frequency range, was measured by the accelerometer. One critical frequency was found at 11-12 cps, corresponding to approximately 700 rpm. On the basis of this test, it was decided to limit the speed during testing to 600 rpm.

*e. Stage 1 conditions tests.* Upon completion of the shake test, the fixture for holding deflection gages was mounted on the structural test stand, and stage 1 tests

were begun. Without spinning the assembly, loads simulating the inertia loads over a range of 0 to 12 *g* acceleration were applied to the entire structure. The structure was inspected both during and after loading; no yielding or deformation of any nature were observed.

Deflection gages, made using spring-loaded potentiometers with roller-tipped shafts so that the roller would follow a rotating surface, were mounted to run on the payload shell and on the upper ring of the rotational launcher and to measure the transverse deflection of these surfaces. The assembly was then spun up to 600 rpm. Axial loads simulating the inertia loads of the design range of 0 to 8.5 *g* were applied while the deflections were measured by means of the potentiometers. No difficulties were encountered during the test, and visual inspection of the structure disclosed no yielding under the combined spin and axial loads. Inspection indicated little or no transverse deflection under the loading condition.

***f. Stage 2 conditions tests.*** Upon completion of the stage 1 tests, the spring arrangement for the local load distribution and the whiffletree actuation were changed for the stage 2 tests. Without spinning the assembly, loads simulating stage 2 thrust and the inertia of stage 3, equivalent to accelerations of 9 to 57 *g*, were applied to the structure. The structure was inspected both during and after loading; no permanent deformations of any nature were observed.

Using the same deflection gages as for the stage 1 tests, the assembly was spun up to 600 rpm. The axial loads, simulating the thrust of stage 2 and the inertia of stage 3 over the design range of 0 to 48 *g* acceleration, were applied while deflections were measured. No difficulties were encountered during the test, and visual inspection of the structure disclosed no yielding under the combined spin and axial loads. Inspection of the deflection records indicated little or no transverse deflections under this loading condition.

The testing program represented a fairly complete simulation of the conditions expected during stage 1 and stage 2 flight. The one condition not tested at the Laboratory was the maximum drag and side load condition which occurred during stage 1 burning. However, a series of tests which investigated this condition was performed at Redstone Arsenal using the *Redstone* missile and the high-speed stages, and no difficulties were encountered. The flight conditions for stage 3, which were not tested, were not considered as critical as the conditions which were tested. On the basis of these tests performed it was felt that the structural strength of the high-speed stages was adequate.

### D. Dynamic Balancing and Cluster Alignment

In order to solve the dynamics problem created by spinning the cluster and minimizing the effects of vibration and precession, it was clearly necessary to have the stages precisely balanced.

The Aerophysics Development Corporation was given a contract by ABMA to develop equipment to test the balance of the cluster. The result was an ingenious rig in which the cluster was suspended on a rigid plate from cables surrounded by a rigid outer frame (Fig. 17).

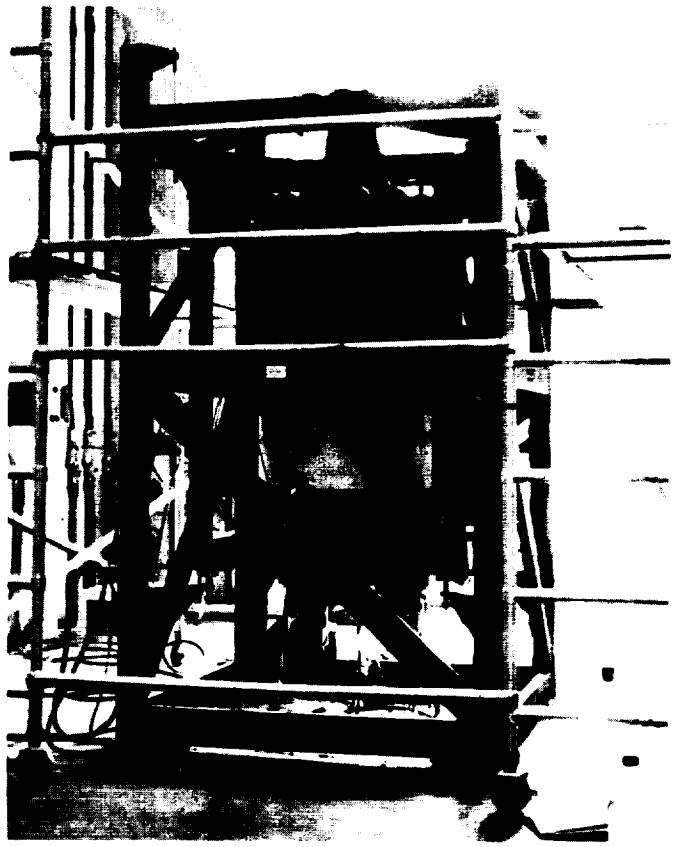

**Figure 17. Launcher, with stage 2 and stage 3 installed in dynamic balancer**

When the cluster was spun in this manner, any imperfections in the balance showed up in the form of an oscillation of the inner frame on the cables. When the cluster was perfectly balanced, it hung motionless in a vertical line even at maximum rotational speeds. Standard Gisholt velocity pickups were used to sense the motion of the inner frame and a strobe light illuminating the cluster to correlate this motion with cluster orientation.

Dynamic balancing was accomplished by the addition of small weights at appropriate locations during spin

tests. The following dynamic balancing and alignment procedure was used for each cluster:

1. Balancing of the launching tub by spinning it at speeds up to 600 rpm and adding permanent weights to the bottom and top balancing planes as required.
2. Installation of stage 2 in the launcher and alignment by controlling the runout of the forward bulkhead (measurements taken on the inner cylinder surface) by means of adjustable guides on the launcher, thereby making the forward bulkhead of stage 2 concentric with the rotational axis of the launcher.
3. Checking alignment of the aft end of inner cylinder of stage 2 for proper mating with launcher.
4. When alignment requirements are satisfied, the composite mass of stage 2 plus launcher was dynamically balanced for the 600-rpm condition. Stage 2 was then pulled out and permanent balancing weights attached to the top and bottom bulkheads. Stage 2 was reinstalled and check-balanced prior to stage 3 tests.
5. The stage 3 assembly was installed in the stage 2 cylinder and aligned. Alignment was accomplished by bringing the vertical axis of stage 3 parallel to the rotational axis of the launcher.
6. After stage 3 alignment, the composite mass of launcher, stage 2 and stage 3, was dynamically balanced for the 600-rpm condition (Fig. 17). The temporary balance weights for the launcher, stage 2 condition, were removed and another set of temporary weights installed to effect a balance for the buildup to this point.
7. Payload balancing was accomplished separately and the necessary permanent balancing weights installed. Then the payload was mounted on the complete buildup in the dynamic balancer. The orientation of the payload with respect to stage 4 was selected for minimum runout. The bolts attaching the payload to stage 4 were tightened and the entire unit was check-balanced. For reproducibility of alignment, the payload was dowel pinned to stage 4.
8. All temporary weights were removed, and permanent weights representing composite corrections for the entire unit were installed.

### E. Accidental Ignition of Igniters

There is always a danger of accidental ignition of sensitive electrical igniters when they or their connecting circuits are exposed to high-energy electromagnetic fields. Since the high-speed stages of the RTV used electrical squibs to initiate the firing sequence, a study was undertaken to determine the susceptibility of the RTV ignition system to accidental firing. The squibs used in the igniters were Du Pont type S-89. In the design of the squib-firing circuits, every reasonable effort was made to minimize the pickup of stray energy.

In one series, two tests were made: the first was to excite the wiring harness with an approximately known field strength and note the power absorbed in a 50-ohm thermistor element connected in place of a squib inside one of the motor cases; the second test consisted of illuminating the harness as strongly as possible with the antenna radiation in an attempt to ignite one of the squibs. All measurements possible in the time allotted were made under conditions that would provide the greatest chance of igniting a squib. Although, in some of the tests, the thermistor indicated that sufficient power for ignition was available in the circuit, no squib ignited during any of the experiments with the harness. This was interpreted as an indication of the lack of sufficient impedance transformation between the source (excited harness) and the low-impedance igniter to effect ignition of the squib.

Approximate calculations and experimental measurements indicated that the shielding and twisting of the harness provided protection of the order of 20 db. Disregarding this 20-db margin, a power density of 0.3 watt per square meter is a potential hazard at any frequency. The safest way devised to prevent accidental ignition was to store the igniters in their sealed metal shipping containers; the second safest way was to keep them in the motor case with the harness disconnected and the pins shorted.

As an example of the calculations made to determine the danger from radio-frequency sources, two known hazards at the Patrick Air Force Base firing range were considered: the 2-kw, 37-mc base DOVAP (Doppler Velocity and Position) transmitter located approximately 1,000 ft behind the launcher, and the tracking radars at the Central Control. In the case of the DOVAP transmitter, there is a shielding effectiveness of 23 db; with the 25 dbm required for ignition, this gives an expected safety margin of 31 db over the 17 dbm received by the igniter harness. In the case of the tracking radars there is a shielding effectiveness of 22 db which, with the 25 dbm required for ignition, gives an expected safety margin of 34 db over the 13 dbm received by the igniter harness.

Other potential sources of accidental ignition were considered, such as the static electrical charge on a human body, lightning storms, and high-power electrical machinery and lines.

As a safety precaution, no operations were performed on the igniters when an electrical storm was within 12 miles. When a storm was likely to occur within 2 miles, the igniters were disconnected from the harness and shorted before the storm came within the 12-mile range. If a storm came within 2 miles and the harness was still connected to the igniters, the area was cleared of personnel.

# VIII. MICROLOCK: MISSILE TRACKING AND TELEMETERING SYSTEM

## A. General

The launching of a small vehicle into an orbit around the Earth would be pointless unless some means were available to demonstrate the existence of the orbited object and to receive intelligence from the object. Conventional optical tracking of small orbiting objects or of high-altitude long-range missiles such as the RTV would be difficult, thus a minimum-weight tracking mechanism that was independent of light and weather conditions was required.

The Jet Propulsion Laboratory had been conducting experiments that led to the development of a low-signal-level missile tracking and telemetering system called Microlock. Microlock is a phase-locked loop system in which the receiver in the ground station is locked to a signal from the transmitter located in the missile. The system is built upon basic electronic circuits and techniques but uses new combinations of these to accomplish the desired performance. The main feature of this system was its ability to lock to an extremely low-level signal; for instance, the system could maintain lock on a milliwatt signal at a distance of nearly 6000 miles under ideal conditions. The missile payload transmitter consisted of a crystal-controlled oscillator which was phase-modulated by telemetering signals. The re-entry vehicle also included five channels of minimum-weight telemetering for the high-speed stages plus telemetry located in the *Redstone* or first stage.

In addition to the capability of tracking signals at a very low level and extracting telemetered information from the phase-modulated carrier, Microlock has the ability of locating an orbiting object. The simplest method of satellite radio tracking is by the doppler frequency method. In this method, the received satellite frequency is plotted as a function of time during a satellite transit. Despite the simplicity of this method, it yields such data as height at perigee and apogee, period, and inclination, and hence the complete orbit, with surprising accuracy if enough satellite transits are tracked. To reduce the number of transits required to determine the orbit, a system of three or more doppler stations may be used to triangulate the position of the satellite constantly during a transit.

A second method of tracking, to which Microlock lends itself readily, is interferometry. In this method, the times at which the satellite passes through the nulls of a special antenna system are recorded. The angular position of the satellite as a function of time is then determined from this data.

## B. Microlock Operation Description

### 1. Overall Microlock System

A block diagram of the overall Microlock system is shown in Figure 18. The missile transmitter as originally conceived consisted of two crystal-controlled oscillators which were phase-modulated by telemetering signals. The use of two transmitters was to add a degree of redundancy as well as increase the telemetry capabilities. Telemetering was accomplished with frequency-modulated subcarriers of which as many as five could be accommodated.

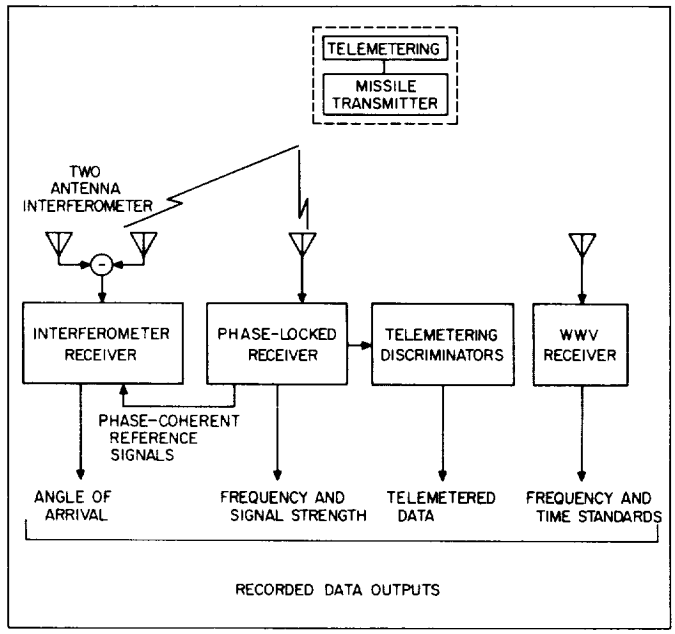


**Figure 18. Block diagram of Microlock system**

The transmitter design began as the result of investigations into the high-frequency properties of transistors; a 30-mc crystal-controlled oscillator was constructed using a Philco surface-barrier transistor. The unit operated well but was capable of only 50 microwatts output. Such a low power was felt to be useless for any practical applications until calculations were made which indicated that a 50-microwatt signal might be observed at several hundred miles line-of-sight distance if an appropriate phase-locked

receiver were used. A receiver was assembled and bench tests were performed as shown in Fig. 19. The signal from the transistor oscillator was sent through a resistive attenuator which simulated the attenuation in free space for line-of-sight transmission. The receiver consisted of a high-gain 30-mc amplifier and a mixer which produced an audio beat frequency which was then detected in an audio phase-locked system. The system was demonstrated to operate satisfactorily with attenuation equivalent to as much as 1000 miles of free space transmission. The same transmitter was subsequently flown suspended from a weather balloon and the signal was tracked with the receiver as used in bench tests. The balloon went to a maximum distance of 40 miles at an altitude of 100,000 feet. The signal received from the balloon-borne transmitter was 10 db above the ambient noise level in the vicinity of this Laboratory. This ambient noise level has been estimated to be more than 20 db above thermal noise. This was the first demonstration of communication with a micropower beacon.

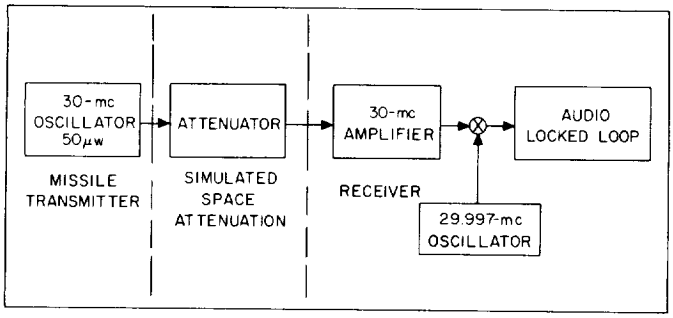


**Figure 19. Bench test setup (Microlock)**

The primary unit of the ground station is a phase-locked receiver which had been designed to detect the beacon signal and to track doppler shift automatically. The phase-locked receiver provides phase-coherent reference signals to an interferometer receiver, to allow correlation detection of the signal received on a two-aerial interferometer such as is commonly used in radio astronomy. Correlation detection, rather than linear or square-law detection, in the interferometer receiver results in much less noise in the angle-of-arrival data. An accuracy of 1 mil was expected for the angle data.

The telemetering subcarriers are received in the phase-locked receiver and sent through discriminators to recover the original data. Phase-locked discriminators were used, in order to provide the best possible data outputs.

Frequency and time standards were obtained from WWV transmissions. In this way, data taken from several tracking stations can be correlated. Two complete ground stations were proposed for tracking. The theory of phase-locked systems has been reported by Rechtin and Jaffe (see Bibliography). Phase-locked systems at frequencies ranging from low audio to X-band had been constructed and tested, providing a wealth of information on the practical performance of such systems. In general, performance was exactly as predicted by theory. Phase-locked loops were also used successfully in guidance techniques developed by this Laboratory. Details of such systems may be found in the *Corporal Bimonthly Summaries 39a through 44a* and the *Guided Missile Summaries* beginning with No. 45 (see Bibliography).

### 2. Phase-Locked Loop Receiver

The simple phase-locked loop shown in Fig. 20 is a servo system which locks a voltage-controlled oscillator (VCO) in phase synchronism with a sine-wave signal input despite a large amount of noise that may also be present at the input. If the system is assumed to be initially in lock (i.e., the VCO has exactly the same frequency as the input signal) the output of the phase detector will be directly proportional to the cosine of the phase difference between the signal and the VCO output. This phase detector output, when filtered by the low-pass filter, is a control voltage which will maintain phase synchronism with the VCO output 90 deg from the input signal. The low-pass filter effectively removes the noise from the control voltage so that the VCO output is very clean and is a good measure of signal frequency and phase. In a second channel, the signal is shifted in phase by 90 deg so that it is in phase with the VCO output. The phase detector in this channel then produces a dc voltage which is proportional to the signal amplitude. In this manner the signal is completely detected by the phase-locked loop, i.e., the frequency, phase, and amplitude are determined.

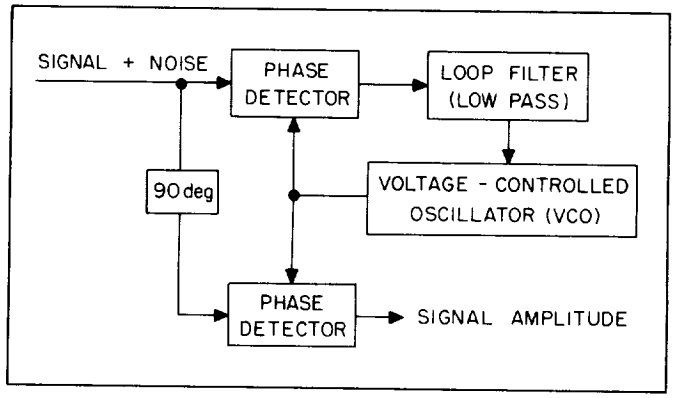


**Figure 20. Basic phase-lock loop**

In this description of the phase-locked loop, it was assumed that the loop was initially locked. Initial acquisition of the signal may be accomplished by slowly sweeping the VCO frequency across the signal frequency. As the beat between the signal and the VCO output goes to zero, the system acquires phase lock and thereafter retains synchronism unless signal level becomes so small that the available control voltage can no longer overcome the effects of the small amount of noise which appears at the output of the low-pass filter.

### 3. System Testing

The first field test of the system occurred 22 March 1956 when the ground station was set up under simulated field conditions near this Laboratory. A beacon, towed by a helicopter, was used to check out the operation of the ground station and to get a first measurement of the performance of the system when receiving very small signals. A more complete ground station was assembled at Earthquake Valley (EQV) in San Diego County, and helicopter tests were performed for the purpose of checking the angle measurement portions of the system. These tests were performed during the period of 14 to 25 May 1956. The primary purposes of the Earthquake Valley tests were to gain experience with the interferometer antenna system which had been proposed for angle measurement and to evaluate the accuracy of such an antenna in conjunction with the Microlock receiver. The ambient (external) noise level at EQV was found to be about 6 db above thermal noise; consequently, it was possible to measure the performance of the system when tracking very small signals under essentially the conditions assumed for the theoretical analysis of the system. In addition, much valuable experience was gained in the operation of the Microlock ground station equipment and a set of procedures for the checkout and calibration of the equipment was generated.

The general layout of the interferometer system is shown in Fig. 21 and 22. The three antenna units comprising the single-axis interferometer are constructed of

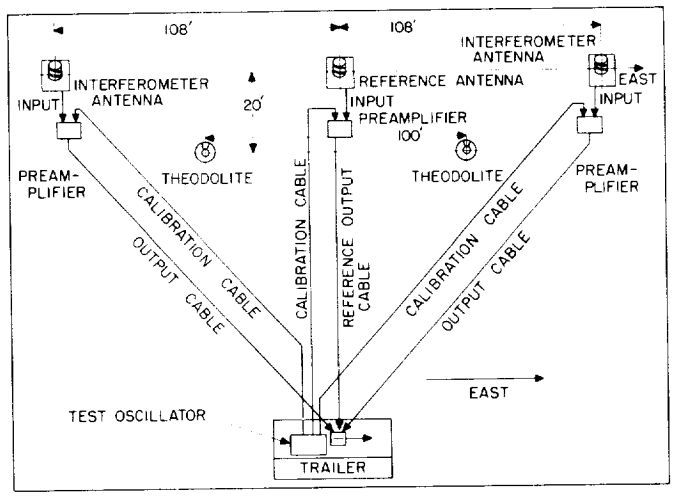


**Figure 21. Earthquake Valley interferometer antenna system**

**Figure 22. Interferometer setup at Earthquake Valley**

a rugged welded aluminum frame with a perforated sheet aluminum covering, and a fiberglass drum with a tape helix wound upon it. The structure is supported by two adjustable feet and two sets of telescoping tubes at the rear; these latter permit the units to be tilted to any prescribed angle between 45 and 90 deg, in addition to the flat position. The three antenna units were set on a baseline of twenty wavelengths, which at the operating frequency chosen required a little over 200-ft separation between the end antennas. This separation causes nulls in the multilobed interferometer pattern at intervals of about 50 angular mils. A null separation of 50 mils was thought to be a good compromise between the opposed problems of null ambiguity and system mismatch errors. Phototheodolites (Fig. 23) were used for checking the system angular accuracy. As shown in Fig. 21, these were placed between and somewhat to the rear of the antennas. Before emplacement at the site the theodolites were adjusted and tested for accuracy at JPL. The tests indicated that these instruments had no inherent source of errors greater than 0.5 mil. One limitation of the theodolites as used was in the lenses, which were found to possess serious aberrations off axis. As the object being tracked does not necessarily lie in the center of the frame, a data error could occur from this defect, depending on the centering of the object in the frame.

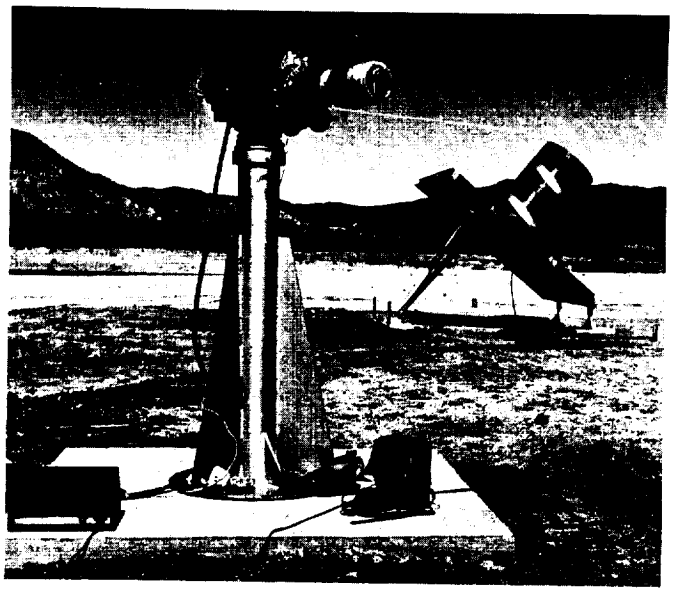

**Figure 23. Mitchell theodolite at Earthquake Valley**

In order to have a correlation between the expected interferometer pattern and the tracking theodolite data, the positions of the antennas, the theodolites, and the target cards were accurately surveyed and recorded. Upon conclusion of each tracking run, the theodolites were sighted on the target cards. At this time, both static pictures of the card and sweeping pictures of the card were taken, in order to have a measure of backlash in the theodolite gear train as well as card angular position. The interferometer output was continuously recorded during each test run, which together with a timing reference appearing on both the interferometer output recorder and the theodolite film allowed a direct comparison of expected null position and observed null position.

Electrical calibrations of the station were performed by inserting equal phase signals at the preamps or antennas by means of calibrated equal-length cables. The electrical portions of the system were then adjusted to provide a null indication. Such a procedure would result in a null in the plane perpendicular to the antenna axis.

The airborne radio source used in the Earthquake Valley field test was a low power crystal-controlled beacon transmitter mounted in a helicopter. The antenna was a quarter-wave stub mounted vertically in the rear section of the helicopter. The helicopter was flown at an altitude of 5,000 ft. above the test site. In general the runs were in a west-east direction, i.e., parallel to the line through the three interferometer antennas, and at a ground range of roughly a mile. A few runs were made in a northeast direction with the idea that a cyclical ground reflection error might easily be identified in this type of run.

Reduction of the data was done in the standard manner, with each camera corrected for its position parallax individually. The small discrepancies between the two sets of theodolite data were then averaged, as there did not appear to be any a priori reason for biasing the final data toward either one. Figure 24 is a plot of the azimuth error versus elevation angle for four typical northeast

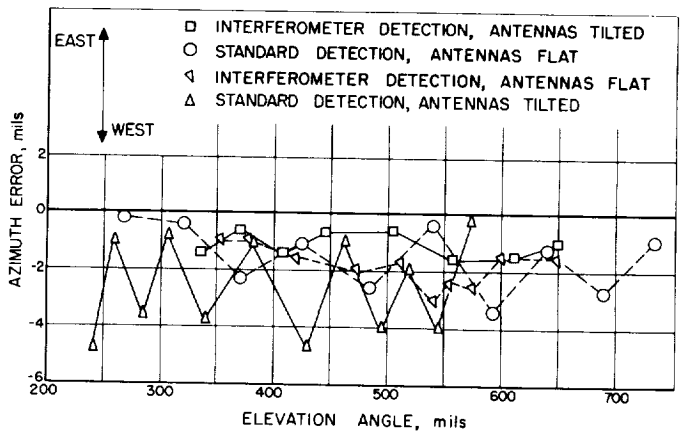


**Figure 24. Azimuth error vs elevation angle**

runs. Since there was evidence of a deleterious amount of leakage from the reference channel to the interferometer channel, two runs labeled "interferometer detection" were taken with the reference antenna disconnected and the receiver locked to the differencing junction output. Figure 24 indicates less error with only a single channel in use. The antennas were used in two different positions, flat and tilted to 45 deg. Less ground reflection error was expected in the flat position. This was apparently not the case, probably due to the fact that the terrain had a slight slope in the easterly direction whereas the antennas were laid in level. Figure 24 indicates that even when the reference leakage is eliminated a bias on the order of one mil in the westerly direction was present. In addition, a cyclical ground reflection error of about one mil peak-to-peak was present.

In conclusion, the interferometer system with 20-wavelength spacing, as tested at Earthquake Valley, exhibited errors of 2 or 3 mils. Probable sources of the observed errors are (1) antenna emplacement, (2) calibration procedures, and (3) cross-coupling between adjacent channels in the receiver. Work in these problem areas succeeded in reducing angle measurement errors to less than 1 mil in subsequent operations.

The sensitivity of the Microlock receiver was measured at Earthquake Valley on 22 May 1956. A Microlock beacon was placed in a bomb and towed approximately 500 ft behind the helicopter. The power output of the beacon was attenuated to −50 dbm (0.01 microwatt) by placing small resistors across the antenna gap. The power output was measured using a dipole signal generator and a receiver. The position of the helicopter was determined by an optical tracker while recordings were made of appropriate voltages in the Microlock receiver. While the beacon was being towed at a distance of 5 miles, the signal was observed to be 12 db above the threshold of the receiver (i.e., 12 db above the point at which the receiver could no longer retain phase lock). Extrapolating from this observation, the same received signal level would be obtained from a beacon radiating one milliwatt (0 dbm) at a distance of 1500 miles. Such a beacon would have to proceed to a distance of 6,000 miles before the received signal would approach the threshold of the Microlock receiver.

It should be noted that the performance of the receiver would be severely degraded if the ground station were to be located in a region of much higher ambient noise level. As an example, if the receiver were located at JPL or Cape Canaveral where the noise level has been measured at 20 db above thermal noise, the threshold distance would be reduced to 1,200 miles with a 1-mw beacon.

In addition to the equipment described in the referenced publications, interferometer lobe switching and a total noise detector were incorporated in the receiving station at Grand Turk Island during the firing of round 27. The addition of this equipment provided for the use of noise signals, received from known radio stars, in the calibration of the interferometer antenna system. With this arrangement, the output of the receiver is a square wave when a radio star appears in the region of a null in the interferometer antenna pattern, and is some dc voltage at other times. The receiver output and an indication of the switch position are recorded simultaneously.

In order to reduce the recorded data, the amplitude and phase of the square wave component of receiver output are taken as an indication of the apparent position of the radio star. By comparing the apparent position with the known position as a function of time, it is possible to arrive at a calibration correction for the interferometer antenna system. Such a calibration is extremely useful in determining the accuracy of angle measurement in such a system, under field conditions, where comparisons by optical tracking of an airborne beacon may be particularly difficult and time consuming.

Very good correlation existed between the expected null times as predicted from the known positions of the radio stars in Cassiopeia and Cygnus and the observed times as indicated by the recordings. However, the resolution available from the recorded data is equivalent to an rms error of 2 angular mils. Therefore, least-squares averaging techniques are required in order to obtain satisfactory estimates of interferometer accuracy.

The radio-star calibration equipment used at Grand Turk Island in September 1956 was primitive and suffered unnecessarily from the effects of noise, which made data reduction very difficult.

#### 4. Beacon Transmitter

The Microlock system, as previously described, was a dual system involving two missile transmitters and two receivers for the purpose of increasing system reliability. Because of the pressure of time schedule and difficulty in obtaining a suitable duplexing network to match the two transmitters to a common antenna, and at the same time isolate them from each other, it was decided to use but one single frequency transmitter for round 27. Telemetering of two temperature measurements was eliminated as a result of the reduction of one of the transmitters. The beacon transmitter as flown in early rounds is shown schematically in Fig. 25.



[redacted]

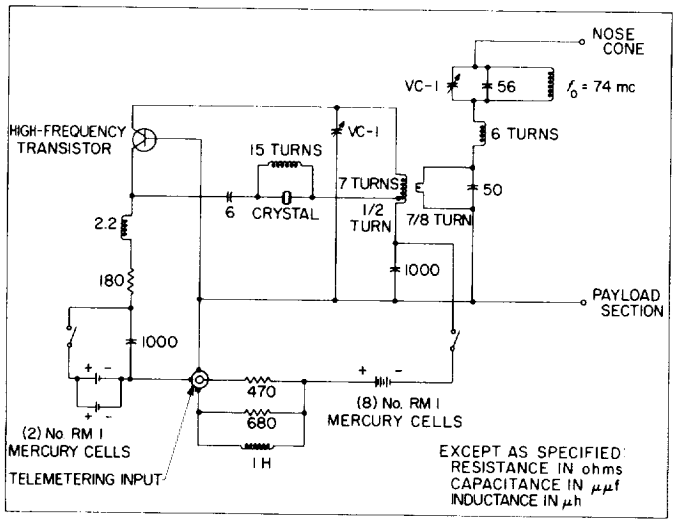


**Figure 25. Single beacon and antenna system circuit**

The final weight of the beacon, including batteries, was 380 grams. Power measurements from the actual flight configuration show that all the beacons radiate approximately 10 mw. The internal battery supply was sufficient for operation at this power level for approximately 1 week. One of the flight transmitters, prepared for shipment, is shown in Fig. 26.

The supporting structure for the beacon was designed so that all thrust and spin loading was taken up by mechanically interlocked parts instead of by glued joints. In this way the structure could be partly disassembled (after wiring was completed) if necessary, for replacing or checking of components. The battery ring was also removable to simplify changing batteries for test purposes. Subcarrier oscillators, for the purpose of telemetering temperature data, were designed for channels 2 through 5.

### 5. RTV Telemetering

*a. Introduction.* A small, lightweight, 5-channel telemeter was fabricated for flight instrumentation of RTV flight 27. It was an FM-PM system in which the output of five subcarrier oscillators frequency-modulated the transmitter of the Microlock tracking system by means of an interconnecting cable, which carried the mixed tones from the telemetering package, located in the nozzle end of stage 4, into the payload.

*b. Measurements.* The five measurements made were as follows:

Channel 1, igniter current to 2nd stage motors blip

Channel 2, operation of pressure switches of 2nd stage motors blip

Channel 3, timer operation of 3rd stage

Channel 4, lateral acceleration of 3rd stage ±50 *g* blip

Channel 5, lateral acceleration of 3rd stage ±50 *g* blip

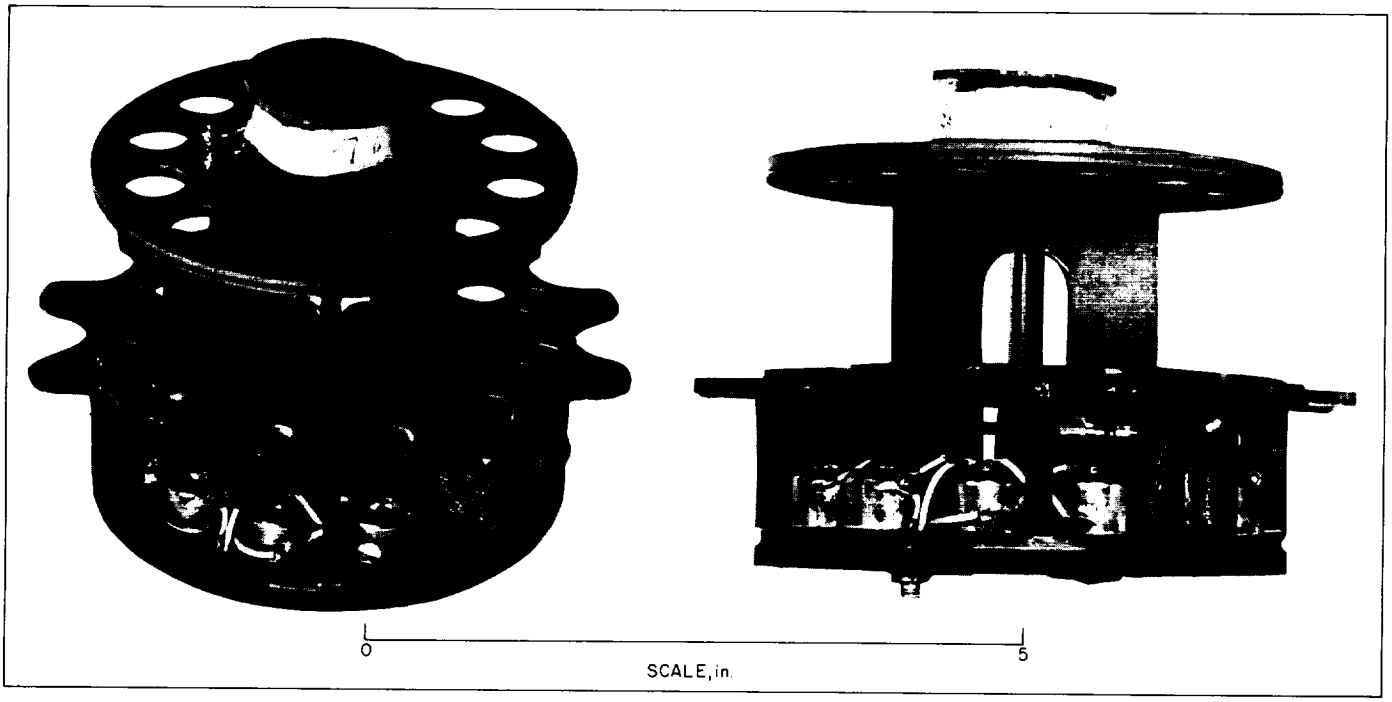


**Figure 26. Flight transmitter**

### 6. Telemetering System

The telemetering system and battery pack was contained in a cylindrical package 4 in. in diameter and approximately 18 in. in length. The entire telemetering system is composed of two vibration amplifiers, five bistable multivibrators, five current-controlled oscillators, and one output amplifier as shown in the block diagram of Figure 27. Each of the five telemetering subcarrier frequencies is generated by a current-controlled oscillator (ICO) (Fig. 28). The input function to these ICO's must be expressed as a variable current between 0 and 1 milliampere in order to deviate the oscillator frequency a full rdb bandwidth. Each ICO is preceded by a modified bistable multivibrator or flip-flop whose primary function is to provide a memory circuit for each telemetered signal. A memory device was necessary because the Microlock tracking equipment is a phase-locked loop system and in the event that the system was not in lock during the separation of the various stages of the missile, or at the time that any of the measured functions occurred, the memory circuit would retain and continue to transmit the desired information throughout the missile flight.

The battery pack for the telemetering system is composed of two batteries in parallel, each consisting of 18 Mallory RM-1R mercury cells in series. The life test on one battery was observed to be about 27 hr for a 30 milliampere load. The telemetering system requires approximately 0.88 watts of power, excluding, of course, the Microlock transmitter power requirements. The estimated life of the battery pack, supplying 0.88 watts, was about 40 hr of operation.

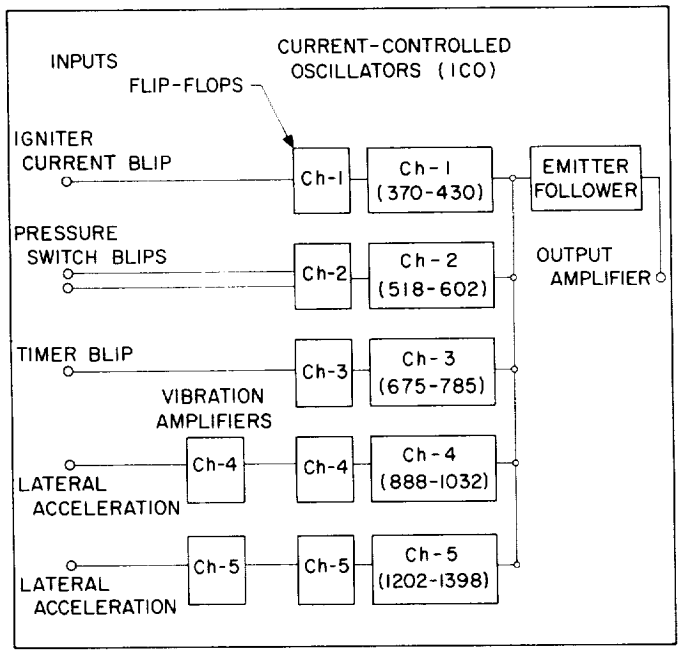


**Figure 27. Block diagram of RTV telemetering system**

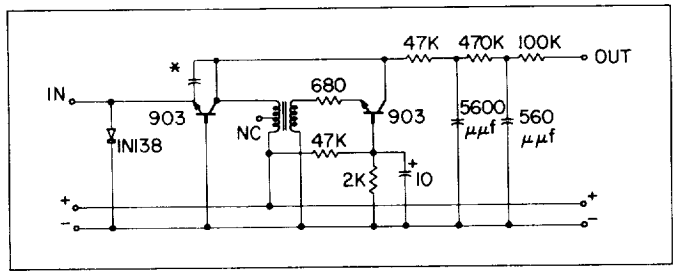


**Figure 28. Current-controlled oscillator (ICO)**

# IX. MISSILE 27

## A. Description

The *Jupiter C* missile 27 (Fig. 29) was the first vehicle to be fired in the re-entry test program. It was a modified missile with the fourth stage replaced by an inert mass. The principal objectives of this firing were:

1. To test staging techniques for a three-stage missile for future testing of model nose cones for the *Jupiter* missile.
2. To test missile structures in the three-stage configuration.
3. To test the booster thrust unit power plant performance during increased time of motor operation.
4. To investigate the operation and use of pyrotechnic flares during ascent and at the apex.
5. To investigate operation of a miniature version of the DOVAP transponder and Microlock instrumentation.
6. To attain ranges of at least 465 miles for the first stage, at least 1170 miles for the second stage, and a total of 2500 miles.

The payload consisted of a hollow truncated cone which was attached to the forward end of a single inert scaled-down *Sergeant* rocket. This cone was supported by a transverse bulkhead connected to the forward ring of a stage 3 cone (Fig. 30) and by radial support at four points on the rim of the rotational launcher.

Contained in the payload were a miniaturized DOVAP transponder to be used after burnout of the booster, and a 10-mw Microlock beacon with a frequency of 108 mc.

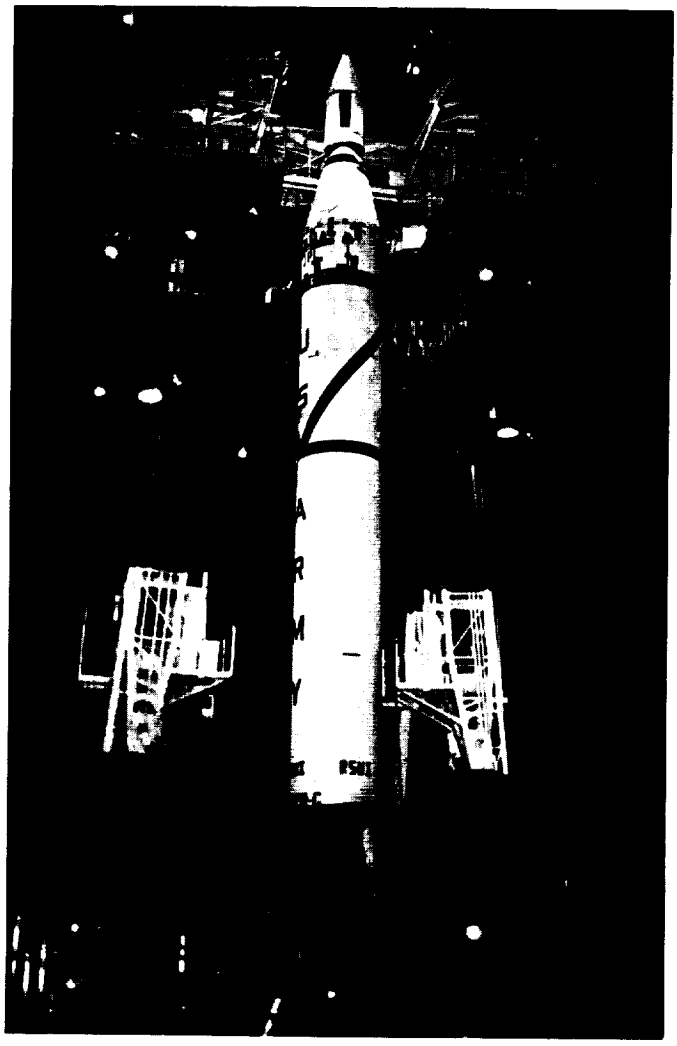

**Figure 29. *Jupiter*-C, round 27**

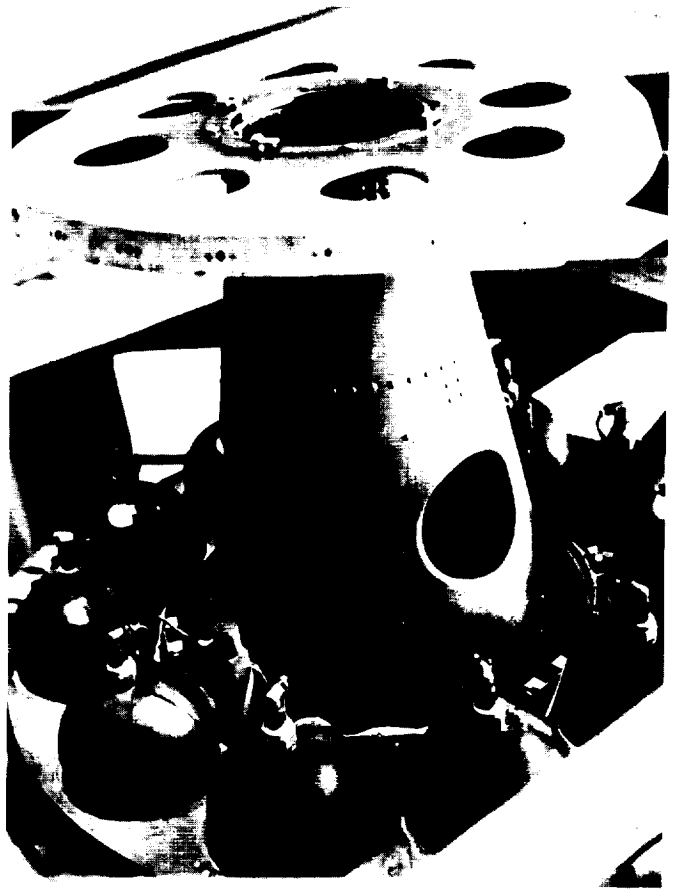

**Figure 30. Launcher with assembled stages 2 and 3**

Five channels of telemetry were superimposed on the Microlock carrier. (Refer to Sec. VIII-A-5.)

Microlock ground stations were set up at the launching site at Cape Canaveral and downrange at Grand Turk Island. The antenna at the Cape station consisted of a four-helix array directed down the firing azimuth (Fig. 31). Grand Turk had a reference helix and two interferometer helices each 100 ft. from the reference (Fig. 32). The interferometer array was installed with the zero or center null directed true north.

**Figure 31. Microlock station**

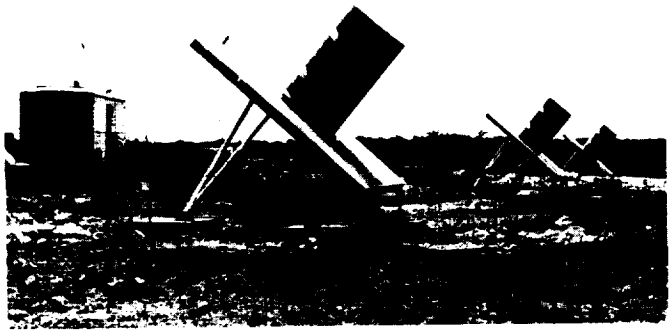

**Figure 32. Antenna installation at Grand Turk Island**

The complete assembly of the high-speed cluster, launching tub, and payload had an overall length of 125⅝ in. The overall diameter was 35¼ in. measured between the outside edges of the second stage forward support lugs. The overall weight was 1214 lb; the payload weighed 86.5 lb.

The upper stage assembly enclosed in the tub was run up to a spin rate of 549 rpm, just before take-off, by two electric motors mounted in the forward end of the booster unit. The motors continued to rotate the assembly until separation of the booster from the high-speed stages, at which time the speed reached 810 rpm. The rate of rotation was automatically increased at chosen points of the first-stage trajectory to avoid resonance with the natural frequency of the missile structure.

At 0147 EST, 20 September 1956, missile 27 was launched at AFMTC, Cape Canaveral, Florida, with an aiming azimuth 100 deg east of true north. The pyrotechnic flashes in the payload were completely lost because of heavy cloud cover and an excess of light from the full moon, but all other missions of the flight were exceptionally successful. The missile attained an altitude of 682 miles and a distance of 3350 miles. The firing proved the propulsive power of the A-5 engine, and verified the aerodynamic design of the *Jupiter-C* configuration. Data on the entire flight were received by tracking stations from the transponder and transmitter and indicated fulfillment of the desired objectives.

### B. Flight Test Results, Microlock Operation

Figure 33 indicates the signal level as recorded at Cape Canaveral. The signal was tracked for 1007 sec. The dip in the signal levels which occurs at approximately 60 and 225 sec was caused by the tail null of the missile antenna pattern sweeping across the receiving antenna. Receiver

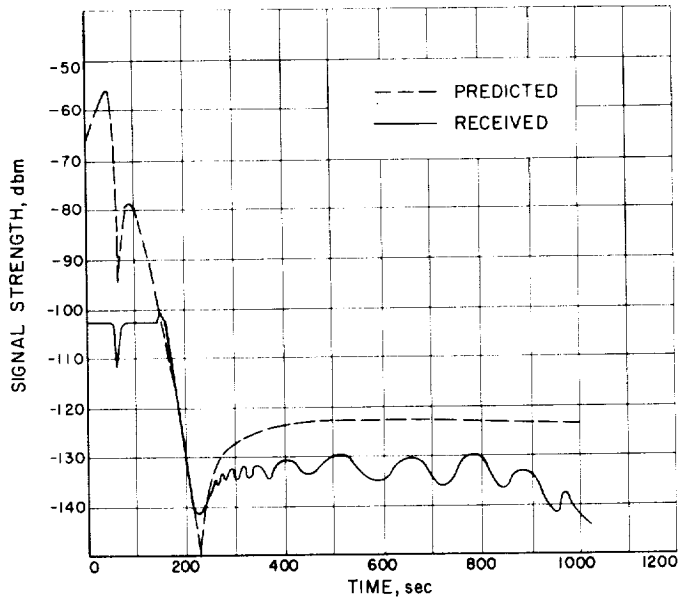


**Figure 33. Signal strength, round 27, Cape Canaveral**

saturation caused the large discrepancy between the predicted and received signal levels from 0 to 150 sec.

The model that was used to predict the flight antenna pattern did not contain the shroud that was used on the final flight unit. The effect of this shroud was to broaden the tail null and to increase the bandwidth of the sidelobes. Since the antenna was looking down the tail null at the Cape Canaveral station, the received signal was about 10 db lower than was predicted from the pattern measured on a model.

Figure 34 indicates the frequency shift as received at the Cape Canaveral station. The predicted curve indicates doppler shift and the received curve indicates doppler shift plus beacon-oscillator drift. The beacon drift after cutoff is approximately 1 cps in the negative direction. The initial frequency was measured to be 107.99879 mc.

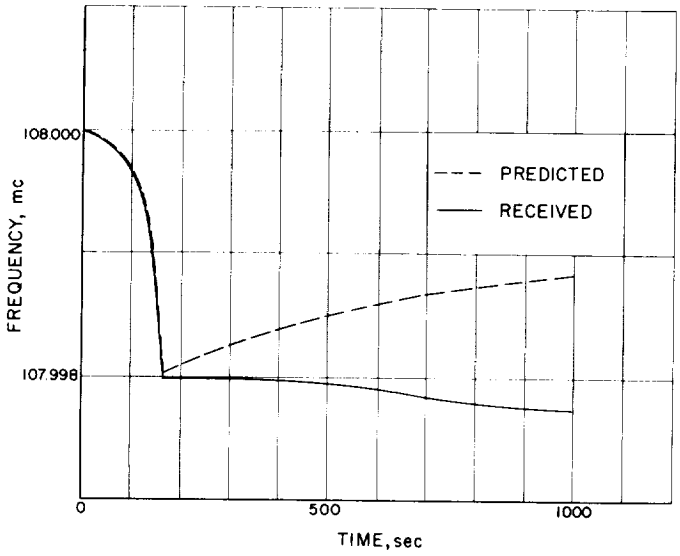


**Figure 34. Frequency shift, round 27, Cape Canaveral**

Figure 35 indicates the signal level received at the station on Grand Turk Island. The predicted and received levels correspond fairly well except for the predicted null at 345 sec and the periodic variations (as in Fig. 33). The null was predicted on the basis of the model antenna pattern; the flight antenna did not have this null. This again is due to the addition of the shroud. The signal was acquired at 196 sec at Grand Turk Island and was tracked until approximately 1170 sec. The signal level was extremely low and the station dropped lock at 650 sec, regaining lock at 690 sec.

Figure 36 indicates the frequency shift as received from the Grand Turk Island station. Again the predicted curve indicates the doppler shift, and the received curve indicates the doppler shift plus beacon-oscillator drift.

The indicated beacon-oscillator drift correlates nicely between the two ground stations. The Grand Turk Island station measured the initial frequency at 2.3 kc lower than the Cape Canaveral station measurement. The measurement made from Cape Canaveral is believed to be the more accurate of the two.

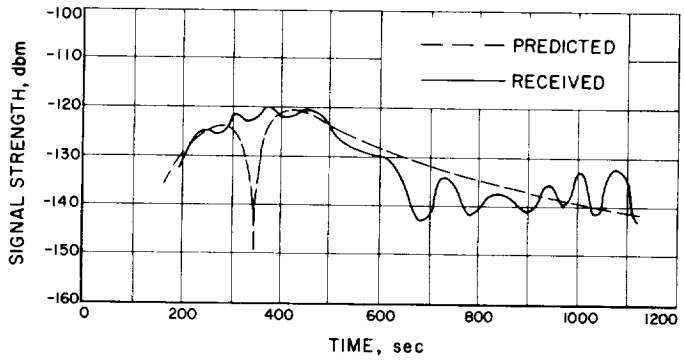


**Figure 35. Signal strength, round 27, Grand Turk Island**

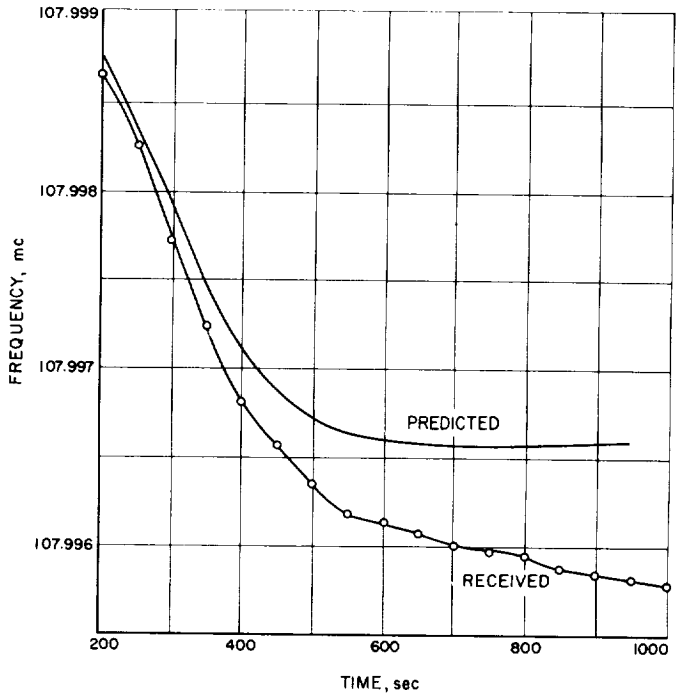


**Figure 36. Frequency shift, round 27, Grand Turk Island**

### C. *Telemetering*

Telemetering for this flight consisted of the first five RDB channels, as shown in Fig. 27, received through the

Microlock system. Channel information was of the event type and since the noise level was expected to be high, a memory was included in the flight unit in the form of flip-flop circuits, which could be triggered only once.

As was expected, the data was extremely noisy. This presented an excellent opportunity to try out data reduction by use of the phase-locked loop discriminators or tracking filter recently designed specifically for telemetry. Anticipation of this flight allowed enough lead time to procure filters for the occasion. Because of the limited available equipment, each channel had to be reduced singly. Data reduction consisted of two parts: these were reduction with and without the tracking filter as shown in Fig. 37.

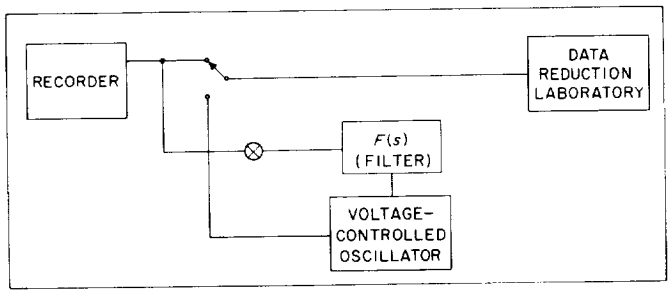


**Figure 37. Recovery of telemetered data**

A summary of the reduced telemetering data is presented in Fig. 38. Channels 1, 2, 4, and 5 show the data obtained through use of the phase-locked tracking filters, whereas channel 3 allows a comparison with representative results obtained with a standard pulse-counting discriminator. A considerable difference in noise level may be noted. Channels 4 and 5, lateral accelerometers, were not expected to trigger under normal conditions in the operation of the high-speed stages. The trigger level was set by mounting the accelerometer on a shake table and adjusting the trigger level with a 50 g peak sine wave. Triggering of channel 5 occurred at stage 3 ignition, whereas the channel-4 accelerometer (mounted at right angles to that for channel 5) did not trigger. The exact source of the observed shock cannot be determined. The trigger might have been caused by either the ignition of a stage 3 motor located adjacent to the accelerometer or by some mechanical interference during the separation of stages 2 and 3.

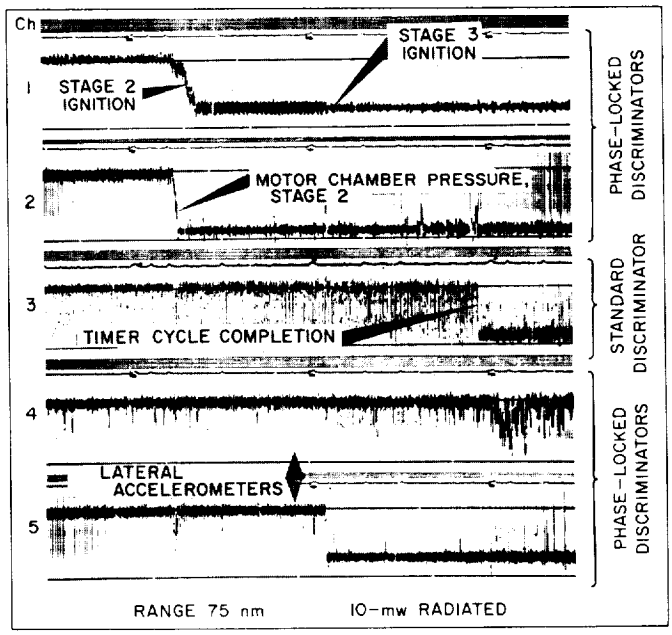


**Figure 38. Summary of telemetered data**

# X. RTV FLIGHTS, NOSE CONE RECOVERY

## A. Description of Mission

The missile system for the re-entry tests consisted of three propulsive stages, the *Jupiter*-scale nose cone or payload, and the Cook Recovery Package contained within the payload.

The three propulsive stages – the *Redstone* booster and two RTV high-speed stages – were identical to the system described previously. The third stage, however, had the conical section designed to support the 300-lb re-entry cone.

The scale re-entry nose cone was a one-tenth scale model of the *Jupiter* nose cone. The basic structure was welded steel cone covered with fiberglass varying in thickness from 1 to 3 in. A magnesium severance ring was bolted to the aft end of the fiberglass shell. This ring formed the mechanical attachment between the payload and support structure on stage 3. Separation from stage 3 was to be effected when a primacord located in the mechanical joint was detonated, severing the magnesium ring at a special "necked" down area. Figures 39 and 40 show the top of the cluster and the nose cone with and without the protective shroud.

The Cook Recovery Package, contained within the payload, was a system devised by Cook Research Laboratory to allow physical recovery of the payload after re-entry. The recovery system can best be explained by a discussion of the expected overall flight sequence.

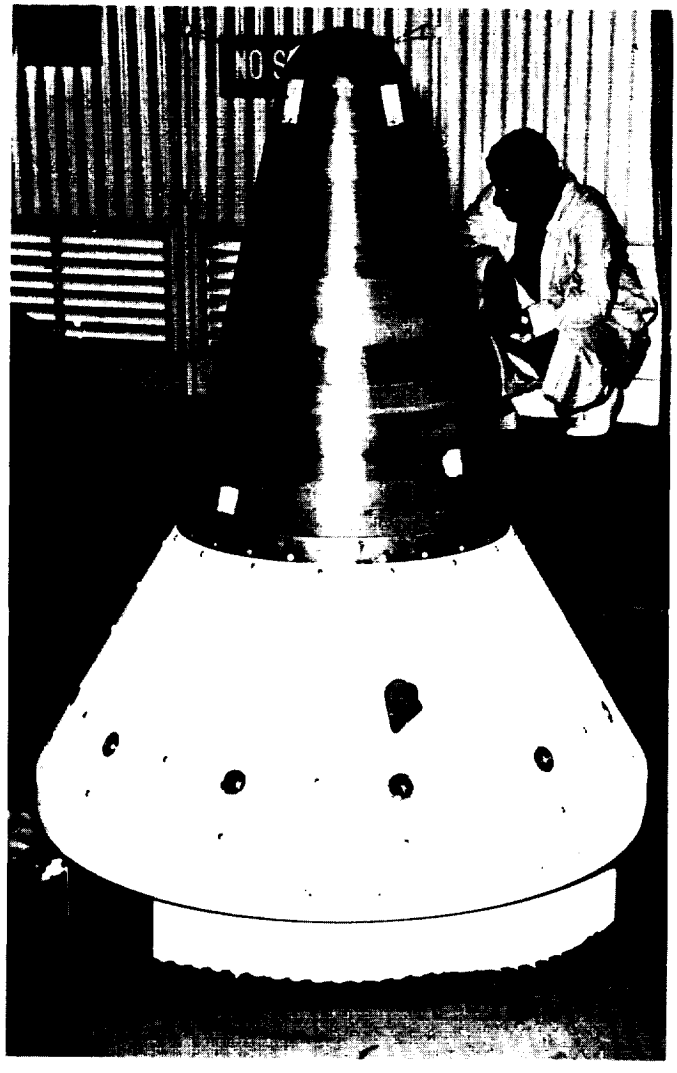

Figure 39. Cluster and nose cone with protective shroud

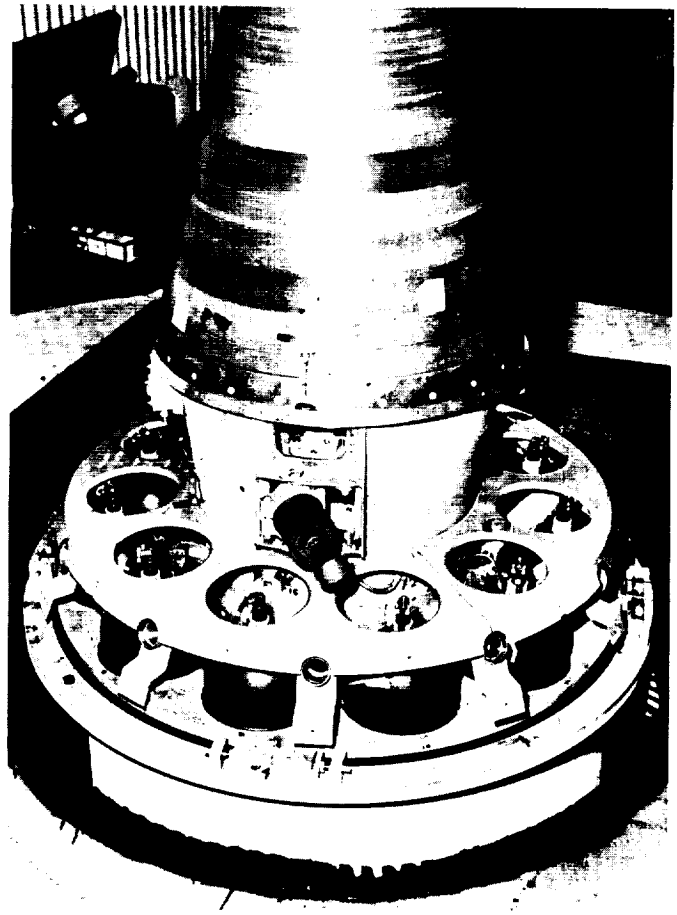

Figure 40. Cluster and nose cone without protective shroud

Ignition of the second stage is initiated from the booster when cutoff of the booster occurs. Cutoff is effected using an integrator cutoff control, which actuates cutoff after the proper velocity has been attained by the booster. Upon ignition of stage 2, there is an acceleration phase of approximately 5½ to 6 sec until burnout occurs. Simultaneously with the ignition and attainment of pressure in the motors of stage 2, a timer in stage 3 is activated by a pressure switch in stage 2. Exactly 8 sec after the ignition of stage 2, stage 3 is ignited by a pulse from the timer. With the ignition of stage 3, separation of stage 3 from stage 2 occurs. Upon this separation, a lanyard from a detonator block on stage 3 to an attachment on stage 2 is pulled, arming the detonator block–primacord system for separating the payload. Nominal burning time for stage 3 is also 5½ to 6 sec. At 64 sec after the ignition of stage 2, the antispin motors are fired (see Sec. X-C). These are two small rocket motors mounted in the stage 3 structure to produce a torque impulse to despin stage 3 and the payload. This despinning is necessary for the successful operation of the recovery system. Four seconds after the antispin motors are fired, the primacord is detonated separating the payload from stage 3. Upon separation, two lanyards between the payload and stage 3 are pulled, arming the recovery system.

Upon completion of the re-entry portion of the trajectory, but before impact, the nose cone will go from supersonic to subsonic velocities (at approximately 15,000 ft). An accelerometer sensing the corresponding changes in drag forces activates a number of powder delay trains within the recovery package. The first of these delay trains sets off a number of explosive bolts, blowing off the rear cover of the payload. A few seconds later, the second delay train causes a parachute to be blown out the rear of the payload. The air forces on the parachute cause a deflated balloon to be pulled out of the package as the parachute inflates. A third delay train ruptures the seals on two air bottles, inflating the balloon. Upon inflation of the balloon, the connecting air line is severed and the balloon then trails above the inflated parachute on a lone line attached to the payload. Simultaneously with the inflation of the balloon, a SOFAR bomb is released from the package, falling into the sea. The SOFAR bomb is a powder charge set off by a pressure-sensitive fuse preset to go off when the bomb sinks to a prescribed depth. The resultant shock wave can be picked up and a position bearing taken using SONAR techniques with equipment aboard naval vessels stationed in the impact area. Upon entry into the water, the payload sinks until the balloon strikes the water and slack in the connecting line is taken up; the balloon then acts as a buoy, supporting the payload and acting as a marker. Three additional location-determination systems are carried in packets in the balloon cover and are activated by squibs sensitive to salt water immersion. The first of these is a small radio beacon (SARAH) which automatically broadcasts a homing signal when the batteries are activated by salt water. This signal can be received by planes in the impact area. In addition, there is a small flashing light beacon activated by sea water, and there are several packets of dye marker.

### B. Estimated Dispersion for the High-Speed Stages of the RTV, Round 34

To facilitate the recovery of the nose cone, an analysis of the dispersion to be expected from the flight of the high-speed stages of the RTV, round 34, was made. This analysis made use of currently available information on the structural rigidity of the assembly of high-speed stages and of the launching tub. Statistics describing the uneven burning among the motors in the clusters of stages 2 and 3 were used in the calculations.

Two types of effects make important contributions to the dispersion. The first of these is a thrust-upsetting moment which occurs when the line of thrust action, as extended forward, passes a nonzero distance $\Delta$ from the center of gravity of the missile. It is convenient to break down the possible causes for such a malalignment into three groups, as follows:

1. Malalignment of structural parts resulting in an offset between the center of gravity of the missile and the nominal axis.

2. Malalignment of the rocket nozzle (or nozzles) leading to both an angularity between the thrust axis and the axis of the missile, and a displacement (parallel to itself) of the thrust axis away from the axis of the missile.

3. For missiles using more than one rocket motor, uneven burning among the various motors, which leads to a displacement of the total thrust vector, as well as (eventually) to a malalignment of weight.

The second important effect contributing to the dispersion of spinning missiles is a nonzero rate of yaw at launch (denoted by $\zeta i$). Such a yaw rate will occur, for missiles launched while spinning, whenever there is an angle between the axis about which the missile is constrained to spin in the launcher and the principal axis of inertia of the missile itself. It is convenient to consider such an angularity between the two axes as arising from two types of malalignment, which are:

1. Malalignment of the structural parts of the missile, which gives rise to an angularity between the principal axis of inertia and the nominal axis of symmetry.
2. Tipping of the initial spin axis due to bending of the launching structure or malalignment of the launching supports.

When the dispersive effects are small, the equations describing the motion of the missile are linear. In this case each type of effect can be analyzed separately, and the overall dispersion computed. The magnitudes of these effects are given in Table 4.

Using a burning time of 5.5 sec and the average ratio of roll-moment of inertia to pitch-moment of inertia, the results shown in Fig. 41 are obtained for expected dispersion (angular radius of the CPE) in a coordinate system in which the high-speed stages are initially at rest. Figure 42 gives the expected dispersion in a coordinate system incorporating the initial velocity of the high-speed stages. The nominal spin rate of the high-speed stages of round 34 is 380 rpm.

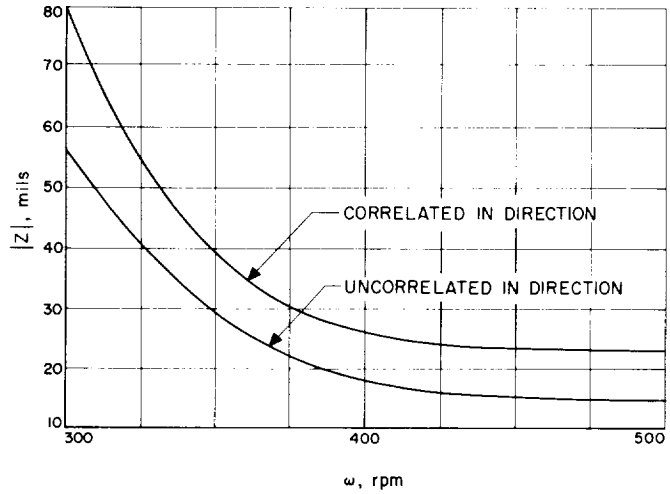


**Figure 41. Expected dispersion, initial = 0**

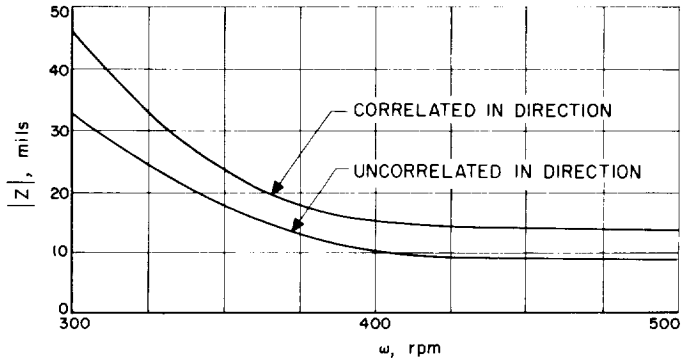


**Figure 42. Expected dispersion, initial velocity = 2313 meters/sec**

## C. *Anti-Spin Rocket Motors*

Round 34 in the re-entry test vehicle program required that the spinning payload have a portion of its spin removed upon re-entry. The requirements were to lower the spin rate from 380 to approximately 90 rpm. It was decided that this could be done most easily and reliably by using a pair of rocket motors placed 180 deg apart in the hardware immediately below the Cook re-entry package.

The two motors (Fig. 43 and 44) are held in brackets which were positioned to produce sufficient torque, counter to the spin direction, in order to lower the spin rate as indicated above. The rocket motor jets exhausted to the exterior through ceramic-coated steel ducts.

**Table 4. Effects contributing to the dispersion of the flight 27 configuration (stages 2 and 3)**

| Stage | Type of effect | Size of effect | Dispersive effect, mils | | | | | |
|---|---|---|---|---|---|---|---|---|
| | | | Spin rate, rad/sec | | | | | |
| | | | 20 | 30 | 40 | 60 | 80 | 100 |
| 2 | Δ, due to malalignment of parts | $1.1 \times 10^{-3}$ ft | 68 | 28 | 12 | 1.5 | 4 | 1.5 |
| | Δ, due to uneven burning | $3.0 \times 10^{-3}$ ft | 288 | 115 | 34 | 5 | 11 | 4 |
| | $\lvert\xi i\rvert$, due to malalignment of parts | $0.15\omega$ mil/sec | 7.5 | 8.5 | 9.5 | 9.5 | 8 | 6.5 |
| | $\lvert\xi i\rvert$, due to bending of tub base | $\omega \cdot b(\omega)$ mil/sec* | 0 | 0 | 1 | 27 | 3.5 | 2 |
| 3 | Δ, due to malalignment of parts | $1.3 \times 10^{-3}$ ft | 30 | 16 | 9.5 | 3.5 | 2 | 1 |
| | Δ, due to uneven burning | $1.0 \times 10^{-3}$ ft | 24 | 12 | 7 | 3 | 1.5 | 1 |
| | $\lvert\xi i\rvert$, due to malalignment of parts | $0.08\omega$ mil/sec | 4.5 | 5.5 | 5.5 | 5 | 4.5 | 4 |
| | $\lvert\xi i\rvert$, due to launcher-support tolerances | $0.35\omega$ mil/sec | 20 | 22 | 24 | 21 | 20 | 18 |

$$*b(\omega) = \frac{(\omega/61.8)^2 \times 1/40}{1 - (\omega/61.8)^2}$$

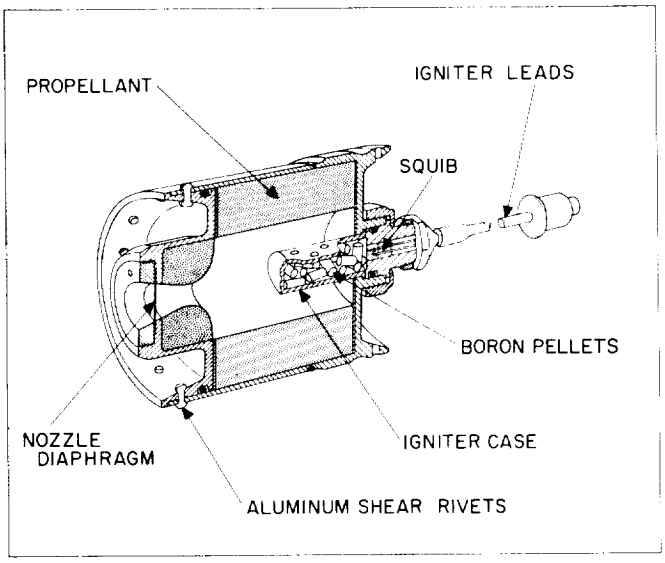


**Figure 43. Cutaway view of assembled anti-spin motor**

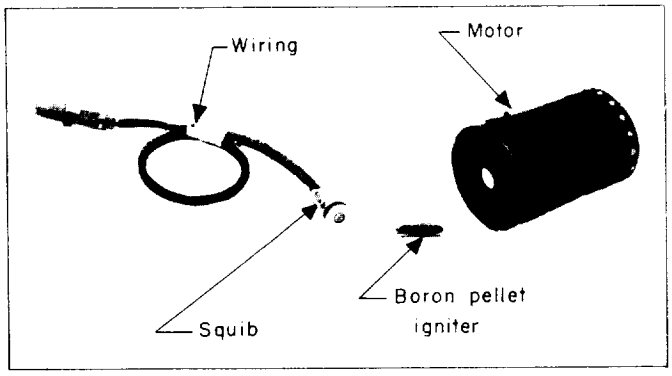


**Figure 44. Anti-spin motor components**

The principal data of the anti-spin rocket motor are listed in Table 5. The design principle used was to maintain a very high reliability factor for all the components involved. A conventional motor chamber was used and the nozzle end of the motor was attached with aluminum shear rivets designed to shear at 1100 psi pressure. The direction of the nozzle would be away from the payload. Thus, a failure would not destroy the re-entry package. The propellant was JPL 136, a polysulfide–ammonium perchlorate type which was case bonded in the motor chamber. Typical thrust-time curves are shown in Fig. 45. The initial and final pressures corresponding to initial and final thrust are 300 and 780 psi.

The conventional ignition systems used previously (metal-oxidant jellyroll igniters) were unsuccessful in this application and it was necessary to design a new unit.

**Table 5. Principal data of anti-spin rocket motor**

| | |
|---|---|
| Length (overall), in. | 4.20 |
| Outside diameter, in. | 2.77 |
| Weight, lb | |
| Loaded | 1.90 |
| Expended | 1.34 |
| Total impulse, vacuum, lb-sec | 116.7 |
| Propellant type | Polysulfide-perchlorate |
| Charge design | Internal burning, tubular |
| Total propellant weight, lb | 0.56 |
| Design parameters | |
| Nozzle diameter, in. | 0.280 |
| Expansion ratio, in. | 4.0 |
| Burning-surface-to-throat-area ratio, $K_n$ | 160 |
| Port-to-throat-area, ratio $H$ | 20 |

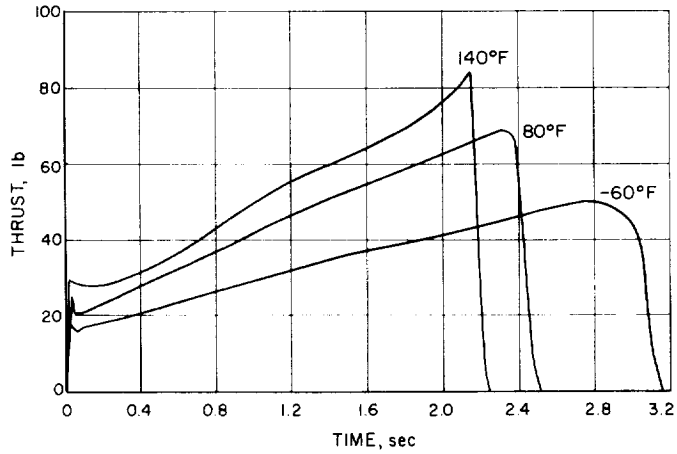


**Figure 45. Thrust-time curves for anti-spin motor**

The unit used consisted of a perforated tube holding a thin (0.005 in. wall thickness) polyethylene sack which contained 1.5 grams of boron pellets. Holding the perforated tube in place and providing a pressure tight seal was a specially designed squib.[1] The squib pyrotechnic material was a mix developed for use at extremely high altitudes (125,000 ft).

The rocket motor was sealed at the nozzle end by an aluminum diaphragm. Ignition reliability was maintained at a high level by (1) making the rocket motor a sealed unit, (2) making the igniter a sealed unit, and (3) making all static test firings at low pressure (1 to 2 mm of mercury). There were no igniter malfunctions in the tests conducted.

Table 6 presents data obtained on batch check rocket motors. A total of 14 motors were made, of which 10 were static tested and 4 were sent to Patrick Air Force Base

[1]McCormick Selph Associates, Hollister, California

**Table 6. Static test data for anti-spin motors being used for round 34***

| | |
|---|---|
| 1. Total impulse, vacuum, avg, lb-sec | 116.7 |
| Estimate of standard deviation σ, lb-sec | 1.09 |
| Standard deviation σ, % | 0.94 |
| Range, lb-sec | 3.31 |
| 2. Burning time, avg, sec | 2.62 |
| Estimate of standard deviation σ, sec | 0.033 |
| Standard deviation σ, % | 1.26 |
| 3. Ignition-delay for all tests, millisec | less than 5 |

*Conditions of tests were as follows:
All motors tested were cast from same batch of propellant.
All squibs and igniters were from same lot.
Diaphragms, 100-psi burst pressure, installed in all motors.
Items 1, 2, and 3 hold for the four units used for round 34.
Test temperature, 80°F.

for round 34. Four additional motors were delivered to ABMA for calibrating the position of the anti-spin rocket motor brackets. The tests were completely successful.

### D. Telemetry System

Because of severe space problems on the re-entry rounds it was not possible to incorporate a separate telemetry system in the cluster. However the Microlock techniques previously developed made possible the recovery of very low-level telemetry modulation from the miniature DOVAP transponder. (Fig. 46)

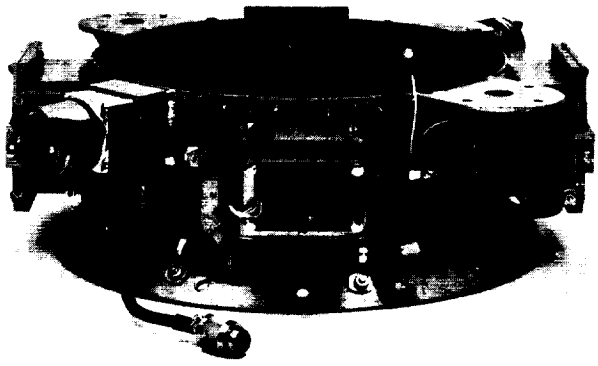

**Figure 46. Round 34 cluster telemetry package**

The operation of the DOVAP-Microlock telemetering system is much the same as a normal Microlock operation in which the telemetering subcarrier oscillators phase-modulate the transmitter. The peak phase-modulation is 0.1 radian or less, and this amount is too small to interfere with the DOVAP system. The Microlock system is easily capable of detecting this modulation since it was designed to track a transmitter with much lower output than the DOVAP transponder. Figure 47 illustrates the operational theory of the DOVAP-Microlock system. The DOVAP station operates in the normal manner. The Microlock station receives both the signal from the missile and from the DOVAP ground station and is capable of producing the doppler tone; its main purpose, however, is to recover the telemetering information. The Microlock telemetering system was modified to operate at the DOVAP frequency of 73.88 mc instead of the normal operating frequency of 108 mc.

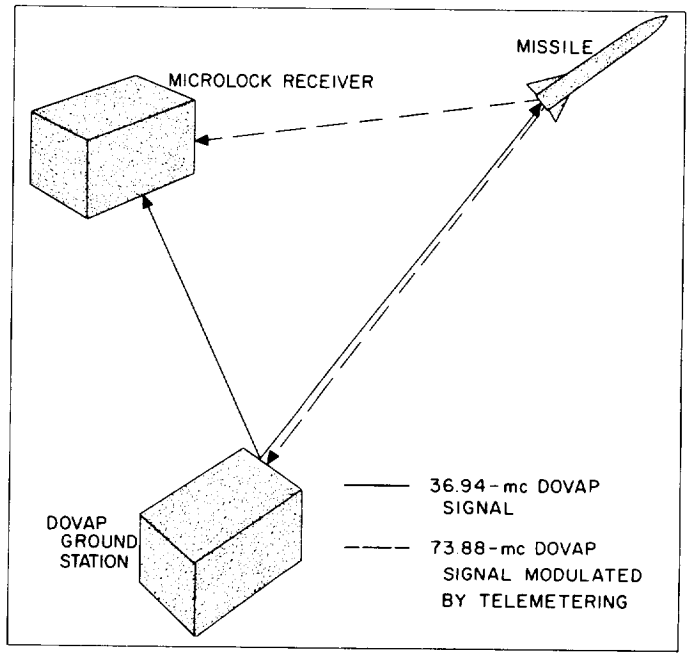


**Figure 47. Functional operation of DOVAP-Microlock telemetering**

The modulation system for use with a round 34 cluster-type DOVAP was developed concurrently at JPL and ABMA, with ABMA having the prime responsibility for the final system and modification of the flight units. At JPL, the variable capacity characteristics of a silicon diode with variations in back voltage were used to vary the tuning of one of the plate tank circuits just before the doubler (Fig. 48). This circuit yielded the desired phase modulation, although there was a small variation of modulation index with RF amplitude. Later tests with this system also showed interference with DOVAP data reduction because of an AM component when a modulation index of 0.1 radian was used.

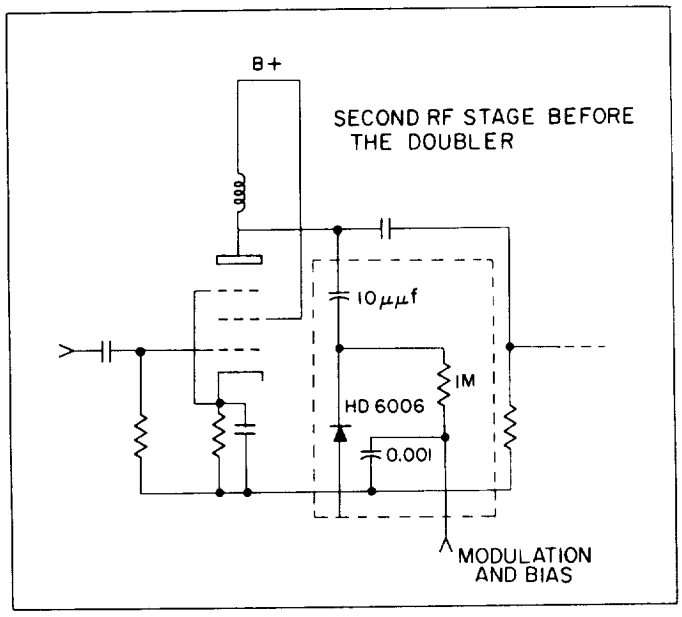


**Figure 48. DOVAP-Microlock**

A second modulation system was then proposed by ABMA that employed a feedback circuit from plate to grid in an early stage of the transponder. This circuit, although more complex, produced PM without the serious AM component.

### E. Missile 34

*Jupiter-C* missile 34 was the second test missile fired in the re-entry test program. It was the first to be fired with a scaled-down version of the *Jupiter* nose cone for study of the thermal behavior during re-entry.

The principal objectives of this launching were:

1. To flight test the second A-5 type production engine using the two high-speed cluster stages in the rotational launcher.
2. To test the material used for protection of the payload (which included the recovery package) against overheating.
3. To test the rocket motors used for decreasing the rotation of the third stage prior to separation.
4. To test the operation of the Cook recovery package and to recover the nose cone.

At 0255 EST, 15 May 1957, missile 34 was launched at AFMTC, Cape Canaveral, Florida, with an aiming azimuth of 105 deg east of north. The first stage was under full control and operated according to plan until 6 sec prior to cutoff. At that time the missile began to respond to an erroneous pitch gyro position. Just prior to cutoff, control of vane 2 was completely lost. At cutoff, an angle of attack of about 60 deg had been built up and, as a result, the spinning high-speed cluster stages were fired almost vertically and slightly backwards. The thrust vector moved along a precession cone with a half angle of 44 deg so as to give a lateral velocity component to the left.

The apex of this flight was 102 miles higher and the distance traveled by the missile was 365 miles less than predicted (see Fig. 49). Radio contact was maintained with this missile for 795 sec.

The launching tub rotation, which was 246 rpm at launching time, increased to 380 rpm at cluster ignition. The anti-spin rocket motors fired at 203.5 seconds, almost exactly as scheduled. This reduced the rotational speed of the re-entry body from 380 to 185 rpm, about 80 rpm more than the precalculated final spin of 106 rpm.

The primacord did not ignite, and 55 sec after burnout of the last stage the nose cone had failed to detach itself from the empty third stage. Retention of the third stage, which acted as an antenna for the nose cone, provided an extra 180 sec of telemeter signals and 413 extra sec of DOVAP beat.

A single SOFAR bomb explosion was recorded. The signal was well received by all stations and confirmed the ballistic information of the flight. It is not known whether the bomb was ejected at, or prior to, water impact or whether the nose cone with both SOFAR bombs sank on impact. The elapsed time between ballistic impact and the bomb explosion was close to the precalculated sinking time of an ejected bomb.

The main mission of this second firing, recovery of the nose cone, was not accomplished.

The DOVAP-Microlock telemetering system was used on the flight of *Jupiter-C* round 34 to provide telemetering of the high-speed stages. The Microlock receiver operated normally and satisfactorily throughout the flight. Because the DOVAP transponders radiated such high power compared to the Microlock beacon, attenuators were placed between the antenna and the preamplifier and between the preamplifier and the mixer, in the receiver.

### F. Missile 40

*Jupiter-C* missile 40 was the third missile fired in the re-entry test vehicle program, and the second test in

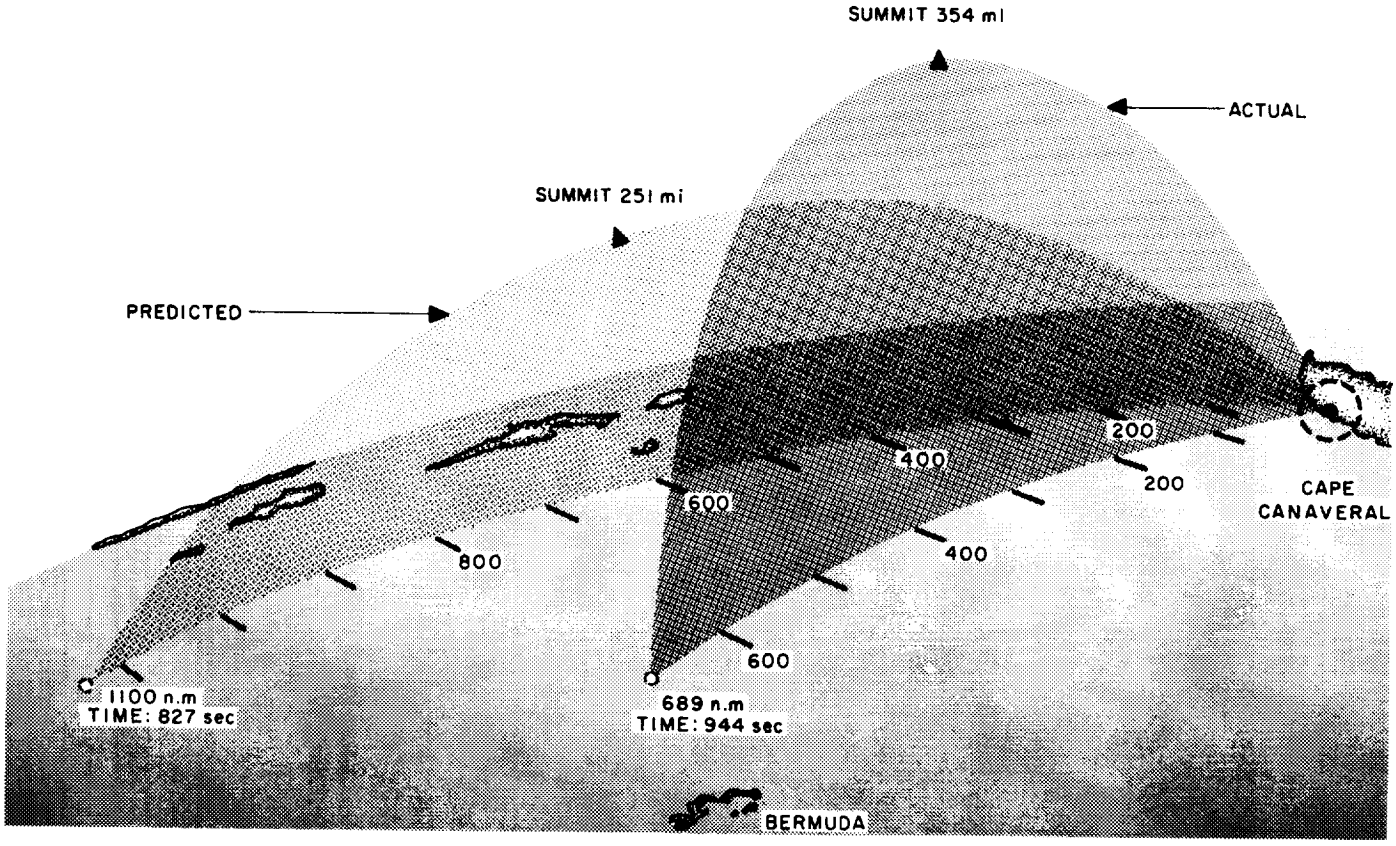


**Figure 49. Predicted and actual trajectories of missile 34**

which a scaled-down version of the *Jupiter* nose cone was used.

The objectives of this flight were the same as for round 34.

At 0159 EST, 8 August 1957, missile 40 was fired from a launching site at AFMTC. The booster and the high-speed stages operated very well. The LEV-3 autopilot control system which controlled the jet vanes and air rudders worked properly through the booster flight. The launching tub was rotated at 240 rpm prior to take-off, but after 124 sec of flight time the speed increased to 463 rpm instead of the planned 380 rpm and remained at this speed until cluster separation.

A short in the circuit of the flash battery prevented the ignition of the anti-spin motors. This failure left a highly stabilizing spin, which led to a high ballistic factor. Failure of the nose cone to separate changed the re-entry trajectory, reducing the large angle of attack upon re-entry to approximately 10 deg at the maximum heating period. Nonseparation of the nose cone from the last stage contributed to stability and corresponding high restoring moments, tending also to reduce the angle of attack.

Failure of separation and nonfiring of the antispin rockets however did not affect the recovery of the nose cone. The recovery system depended on the separation of the nose cone from the last stage for arming. This separation was apparently achieved during the early part of re-entry by the melting of the magnesium separation point. The recovery sequence was designed to separate the nose cone and simultaneously arm the system not later than 17 sec before the re-entry deceleration switch operated. The rear cover of the nose cone was blown off 3 sec after activation of the deceleration switch. The parachute was ejected 4 sec later at an altitude of 11,080 ft when the deceleration was about 3 $g$.

At 6 sec after parachute ejection, a Marman clamp was fired, which released the recovery package basket. The basket ejected the two SOFAR bombs and at the same time released the balloon at 9820 ft. At this time the velocity of descent was 118 ft/sec.

In 10 sec the balloon was fully inflated and released from the compressed air bottles and the ties which held it adjacent to the recovery basket. The balloon descended the remaining 8500 ft in about 81 sec.

Upon water impact, the battery activated by salt water, actuated release and erection of the antenna, closure of a number of other circuits, illumination of the beacon, and radio transmission. In addition, dye markers were released, and shark repellant was expelled.

The nose cone was recovered by the U. S. S. Escape at a range of 1160 miles (57 miles greater than predicted) with an almost negligible lateral deviation of 1.36 miles to the right.

Although ablation type re-entry heat protection protected the nose cone from overheating, the reduced angle of attack diminished nose cone heating conditions.

Examinations and tests made on the recovered nose cone showed that ablation of the glass fiber laminate was essentially uniform and was approximately 1½% of the radius. No detrimental effects on joints or adhesive lines were noted except for a slight pitting tendency in the cross-laminate flow areas near the stagnation point.

# PART TWO: JUNO I (EXPLORERS I-V)

## XI. GENERAL DESCRIPTION OF PROGRAM

Following the successful completion of the re-entry test program, the Department of Defense authorized the Army and JPL to modify the *Jupiter-C* into a satellite-launching vehicle. Such satellites were to carry scientific payloads as part of the IGY program.

The name *Juno* was given to the satellite program. This program was divided into two series of space flights. The first series, *Juno I*, used *Redstone* missiles as the first stage to place Earth satellites in orbit which were designated *Explorer I—V*. See Table 7 for a summary of RTV and *Juno I* launchings. The second series, *Juno II*, used the *Jupiter* IRBM instead of the *Redstone* as the first stage.

The DOD authorization called for the preparation of two satellite vehicles and payloads. JPL was to supply the cluster of high-speed stages and the payloads. Plans for the two payloads were approved by the Technical Panel on the Earth Satellite Program on 6 November 1957.

The first experiment was to be performed at the earliest possible date; its objective was to: (1) gather environmental data, (2) flight-test major items of hardware, and (3) make certain measurements of scientific value. The total electronic payload weight was to be 11.8 lb. The total payload weight including structure and antennas was 18.2 lb. The total weight of the orbiting satellite, including the empty stage 4 motor, was 31 lb.

The second experiment, originally planned for the *Vanguard* as part of the IGY program, was the State University of Iowa (SUI) cosmic-ray experiment modified for the *Jupiter-C* configuration. The major objective of the SUI cosmic-ray experiment was to make an extensive survey of primary cosmic-ray intensity. The payload and its total weight was approximately the same as for the first experiment.

A micrometeorite experiment was included in each payload. This experiment, originally planned as part of

**Table 7. RTV and *Juno* launchings**

| Program | Flight or round and date | Duplicate designations | Stages | Mission | Results |
|---|---|---|---|---|---|
| *RTV* | Round 27, *Jupiter-C* 9/20/56 | | 3 | Proof test of re-entry test vehicle and Microlock | Successful<br>Range: 3300 mi.<br>Height: 650 mi. |
| *RTV* | Round 34, *Jupiter-C* 5/15/57 | | 3 | Nose cone test and recovery | No recovery of nose cone |
| *RTV* | Round 40, *Jupiter-C* 8/8/57 | | 3 | Nose cone test | Successful recovery of nose cone |
| *Juno 1* | Round 29, *Jupiter-C* 1/31/58 | *Explorer I*<br>*1958 Alpha* | 4 | Earth satellite | In orbit |
| *Juno 1* | Round 26, *Jupiter-C* 3/5/58 | *Explorer II* | 4 | Earth satellite | 4th stage did not function |
| *Juno 1* | Round 24, *Jupiter-C* 3/26/58 | *Explorer III*<br>*1958 Gamma* | 4 | Earth satellite | In orbit |
| *Juno 1* | Round 44, *Jupiter-C* 7/26/58 | *Explorer IV*<br>*1958 Epsilon* | 4 | Earth satellite | In orbit |
| *Juno 1* | Round 47, *Jupiter-C* 8/24/58 | *Explorer V* | 4 | Earth satellite | Failed to orbit |
| *Juno 1* | Round 49, *Jupiter-C* 10/22/58 | *Deal III*<br>Beacon | 4 | Earth satellite | Failed to orbit |

the SUI experiment, was performed in cooperation with the Air Force Cambridge Research Center (AFCRC).

The *Jupiter-C* launcher rotated the payload at a higher speed (750 rpm) than the *Vanguard* launcher. Except for this one more stringent requirement, the *Jupiter-C* environment approximated that of *Vanguard*. Environmental testing of the payload for the first experiment was completed at this Laboratory by 31 December 1957.

# XII. DESCRIPTION OF THE LAUNCHING VEHICLES

## A. General Description of Explorer I

The *Juno I* configuration (Fig. 50) is similar to that of the *Jupiter-C*, but with the addition of a fourth stage and a payload. Other changes included a different shroud, over the stage 2 motor domeheads, and a new high-performance fuel—unsymmetrical dimethylhydrazine (UDMH) and dietylene triamine (DETA) in the booster.

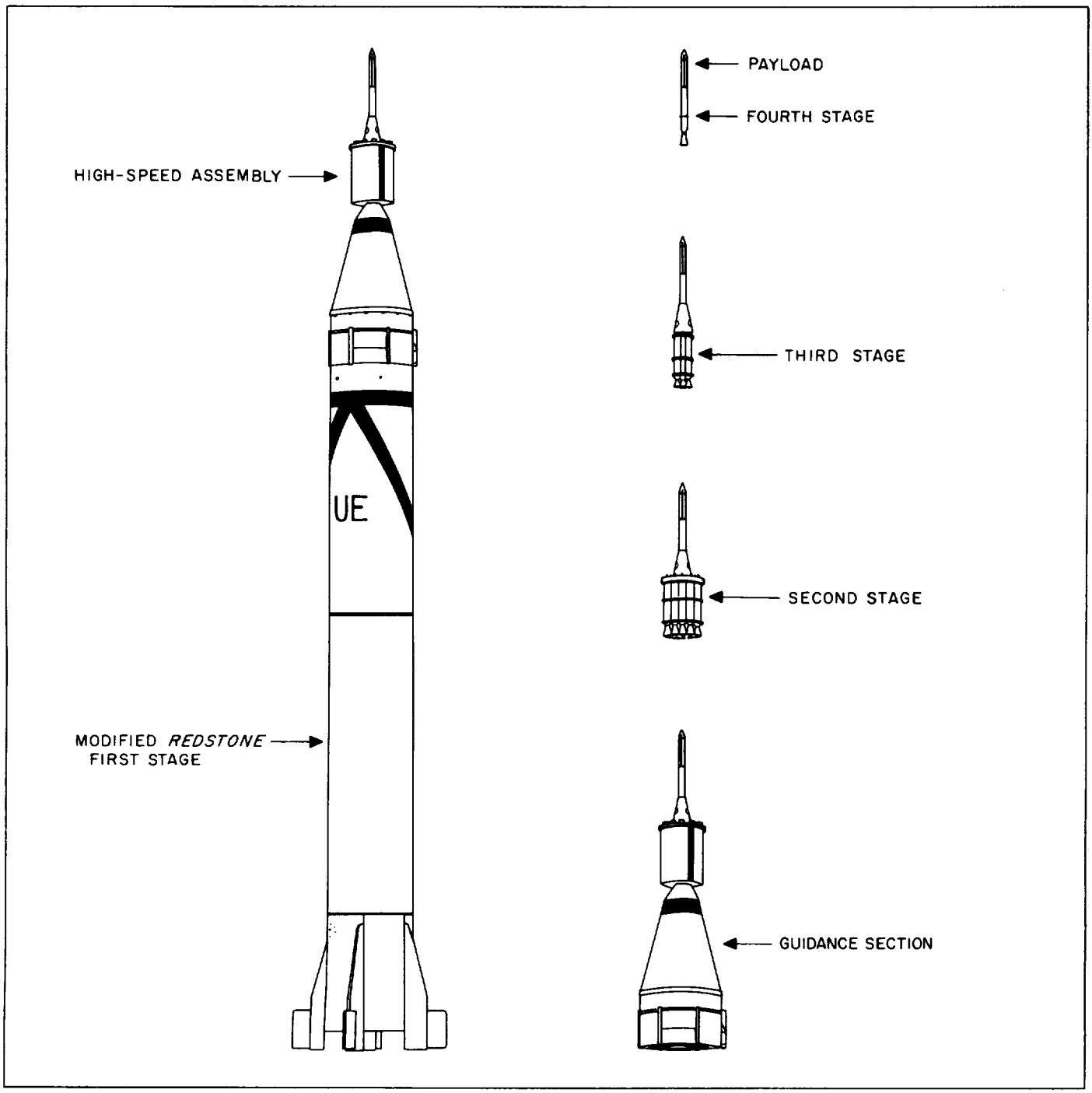


**Figure 50. The *Jupiter-C***

The first stage consisted of two major parts: (1) the main body with its propulsion system, which also was the chief source of power during the initial phase of flight, and (2) the guidance section which houses the guidance, spatial-attitude control, and cluster drive systems.

The second and third stages were similar to the *Jupiter-C* and consisted of clusters of RTV motors as described in Part One of this volume. Stage 3 did have a support cone designed to support the fourth stage. This cone, described in Sec. XII-B, was similar to that flown on round 27.

The fourth stage used a regular RTV motor case, but differed from the stage 2 and 3 motors in the propellant, igniter, size of nozzle, and support attachment.

### B. *Stage 4 Support Cone*

The support cone for stage 4 is shown in Fig. 51. The forward ring, made of steel, projects outside the forward diameter of the conical shell. This increased diameter was necessary from strength considerations. The conical shell, an aluminum alloy, was tapered down to and riveted to the inner diameter of this ring, thus providing a smooth continuous inner surface for the cone-ring combination. This decreased the possibility that stage 4 will hang up in the cone during launch.

Axial thrust applied to stage 4 during the burning of earlier stages was carried on the front surface of the forward support ring. The aft support ring carried only transverse loads and was fabricated from aluminum as a webbed structure. It was riveted to the conical shell, and

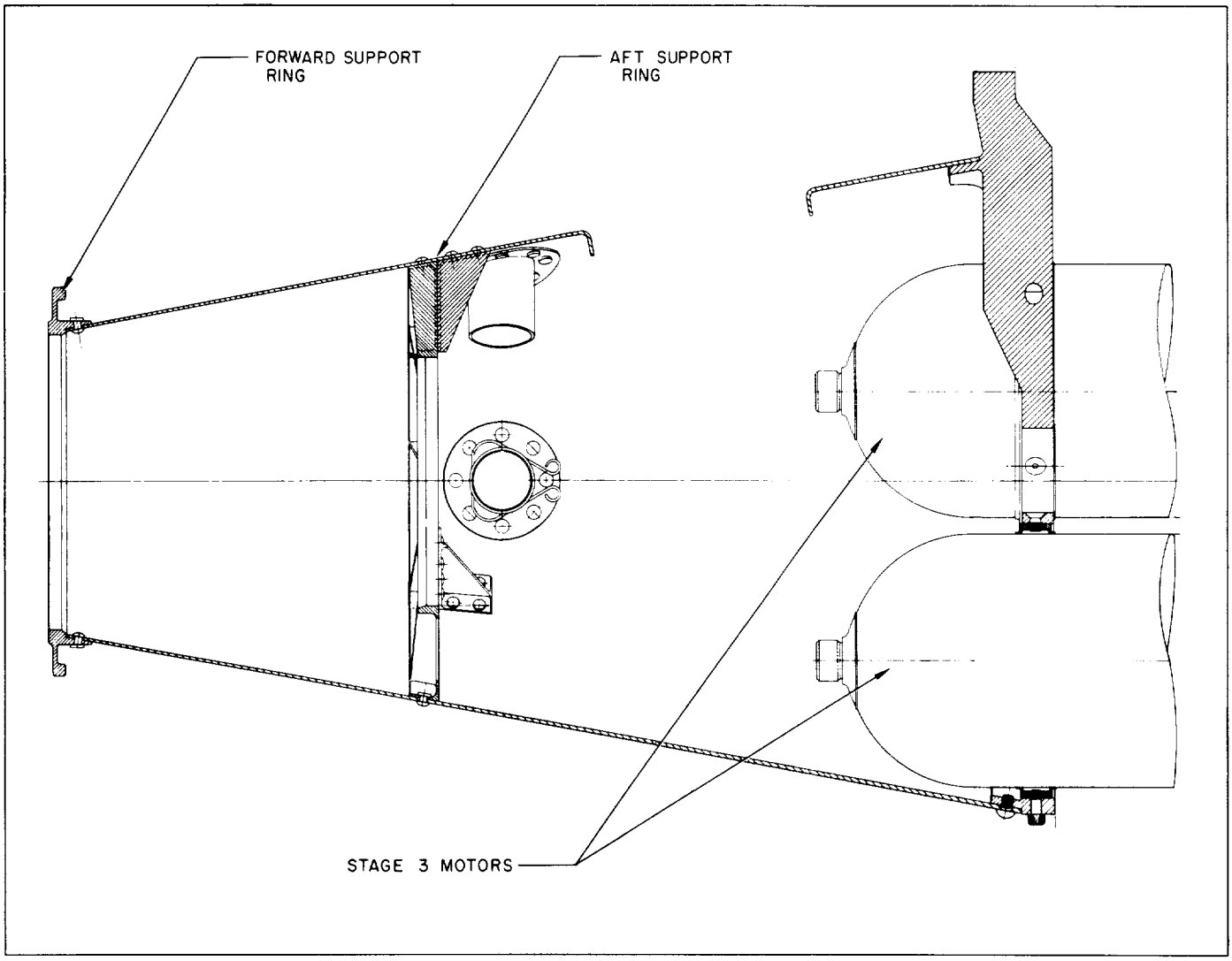


**Figure 51. Assembly of stage 3 propulsion unit**

the joint between the ring and shell was reinforced by buttresses between the aft face of the ring and the inner surface of the shell. The skin thickness of the shell tapered from 0.09 in. at the base to 0.06 in. at the forward end.

### C. The Stage 4 Assembly

Figure 1 shows a comparison between the stage 4 and stages 2 and 3 motors. The two rings near the aft end of the stage 4 motor support this stage in the matching rings of the stage 4 support cone. The forward ring, which was welded to the outside of the motor case, had a cylindrical surface to transmit transverse loads and a lip on the forward edge of the cylinder to transmit axial loads. Both the cylindrical surface and the bearing surface of the lip were carefully machined to permit accurate alignment of stage 4 in stage 3. Three shear pins prevented stage 4 from working its way out of the support cone due to vibration. The aft ring was welded to the aft domehead. Only a cylindrical bearing surface was machined on this ring since it is to carry only transverse loads.

The nozzle of the stage 4 motor is slightly shorter and slightly smaller in its maximum (aft) diameter than the motors of the other stages. This is to permit adequate clearance, during the launching of stage 4, between the stage 4 nozzle and the stage 3 cone.

The propellant in stage 4 was a higher performance JPL 136 propellant. Table 8 shows the 136 formulation.

**Figure 52. Second and third stages of high-speed assembly**

**Table 8. Composition of JPL 136**

| Component | Percent by weight |
|---|---|
| Ammonium perchlorate | 72.0 |
| Liquid polymer, LP-33 | 25.7 |
| Paraquinone dioxime | 1.7 |
| Sulfur | 0.10 |
| Monoastrol blue | 0.50 |

The use of a different propellant in stage 4 is more readily accommodated because the motor is on the spin axis where the flight environment isn't as severe. The design of the payload attachment on the forward end of the stage 4 motor depends, of course, upon the design of the payload itself. For the early *Explorers*, there was a short cylindrical section attached to the forward domehead of the motor and fabricated as an integral part of the domehead. The aft end of the payload shell was bolted and pinned to this section.

### D. The Shroud

A spun aluminum shroud (Fig. 52) covered the stage 2 motor domeheads and ignition wiring in order to protect them from the aerodynamic heating. This shroud was attached to the forward bulkhead in stage 2. The covers over each motor were removable to provide access for igniter insertion and connection. The access ports in the stage 4 support cone were also shrouded after completion of work.

### E. Ignition System

The igniters for the stage 2 and 3 motors were identical to the earlier RTV igniters and were installed through

the motor domehead fittings. Because the payload section was mounted forward of the stage 4 domehead and because it was undesirable to have the stage 4 ignition wires cemented to the outside of the motor case, it was necessary to install the igniter (Fig. 53) through the aft end of the motor prior to mating with the third stage.

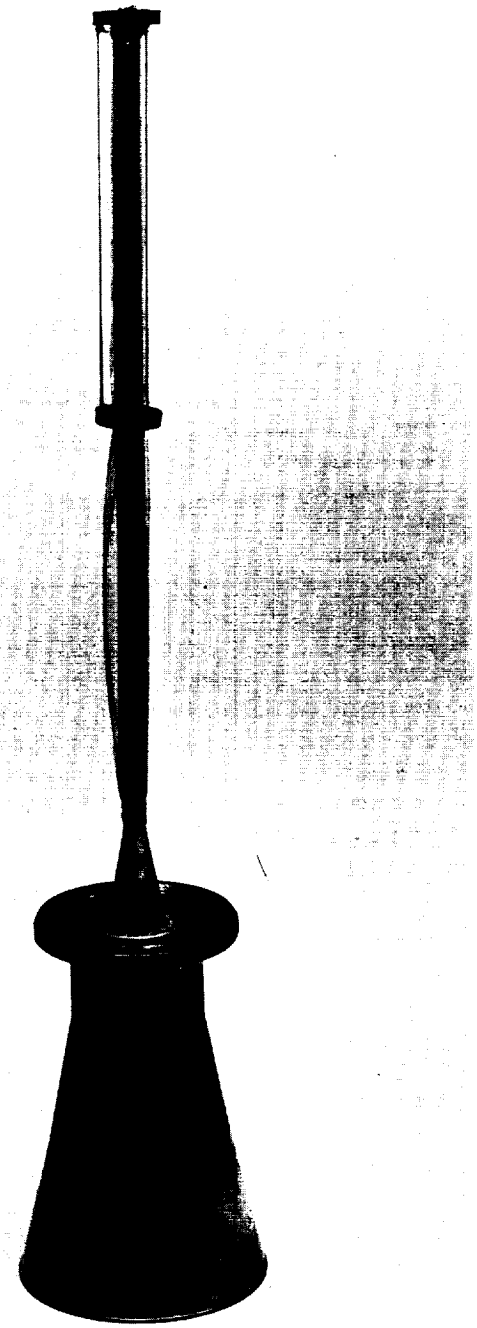

Figure 53. Fourth stage igniter

The ignition signal for stage 2 was supplied by a ground command to radio-controlled equipment, installed in the guidance section. To safeguard ignition in the event that the command signal was not received on board, a flight timer would cause second-stage ignition. The timer was set to operate 10 sec after the time of standard ignition, at 404 sec after liftoff.

Ignition of stage 3 and 4 was controlled by a motor-driven timer (Fig. 54) located in the top center of stage 3. The timer was started by the closure of either one of two pressure switches mounted on two of the stage 2 motors. These switches were actuated by chamber-pressure buildup after stage 2 ignition. Once the timer started, it continued to run through one full cycle (20 sec) even though the start circuit was broken when stage 3 separated from stage 2. The battery tube was lengthened so that separate batteries could be included for the ignition of stages 3 and 4. Approximately 9 sec after ignition of stage 2, the timer fired stage 3, and 9 sec later stage 4. These timers were set so that the preceding stage had finished burning before the next stage was fired. Access to the timer assembly was through three exhaust holes in the support cone for stage 4.

Figure 54. Igniter timer

# XIII. OPERATIONS DESCRIPTION

After burnout of the booster at about 100 km the motor and tank section separated from the rest of the vehicle. The guidance section with the high-speed stages and payload then coasted to the apex of the preprogrammed trajectory (approximately 360 km). During the time between the first separation and the time that the vehicle reached the apex of its trajectory (free-coast period), the spatial-attitude control located in the guidance unit positioned the high-speed cluster so that the spin axis was approximately parallel to the Earth's suface at the trajectory apex (Fig. 55).

The spatial-attitude control system used compressed air nozzled through the eight air jets, tangentially located on four fin-like protuberances at the aft end of the guidance compartment.

As with the *Jupiter-C*, two electric motors housed within the guidance section were used to spin the high-speed stages at about 750 rpm in order to provide directional stability. The guidance section was prevented from rotating by the action of the spatial-attitude control positioning air jets. If the guidance section were to rotate, the guidance gyros would tumble and the guidance reference would be lost.

The operation and orientation of the instrument compartment and the spatial-attitude system were continuously telemetered until the launching of the second stage. Using prepared nomographs, the exact point of apex was computed, based on information received from radar, DOVAP, etc. When the apex had been achieved, a radio signal from the launching site was used to relay the fire order to the launching vehicle to fire the second-stage rockets.

A typical gain in velocity from the three solid-propellant high-speed stages amounted successively to: II = 1571 m/sec; III = 1534 m/sec; and IV = 2189 m/sec, which resulted in a total velocity at final burnout of 7684 m/sec.

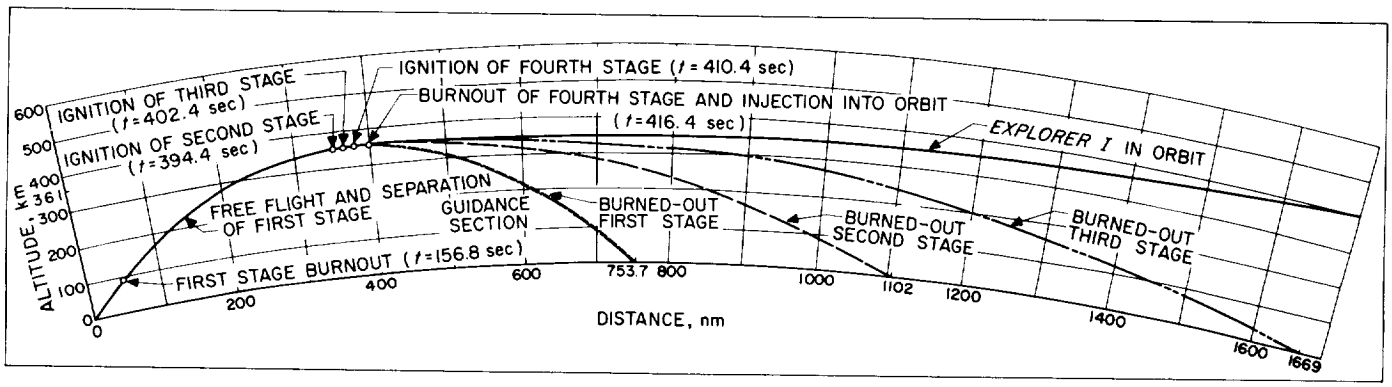


**Figure 55. Launching geometry**

# XIV. SATELLITE DESCRIPTION

## A. General Description

Each satellite consisted of two main elements: the instrumented payload and the shell of the last-stage rocket motor. These two items form the 80-in.-long, 6-in.-diameter structure shown in Fig. 56. The cylindrical rather than spherical shape of the instrumentation sec-

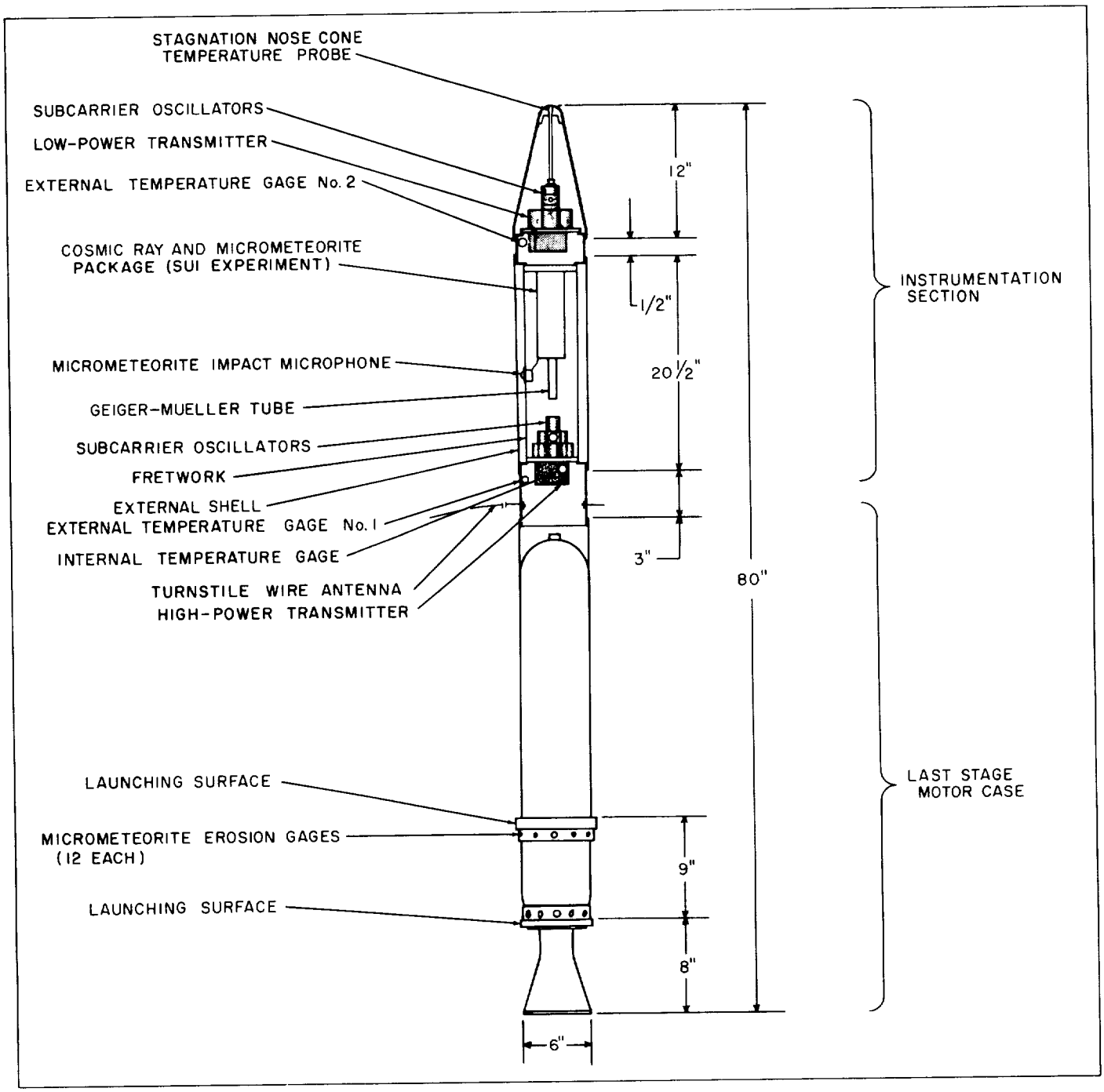


**Figure 56. Internal view of *Explorer I***

tion permits the rocket motor case and the nose cone to become an integral part of the orbiting vehicle. The attached motor case increases the overall size of the satellite, which aids in visual sightings. It also serves as part of the antenna system for the low-power transmitter.

The instrumentation section and integral nose cone of the first satellite were coated with Rokide-A (aluminum oxide) stripes, for purposes of temperature control with a ratio of 25/75 and 30/70 of Rokide/steel on the body and nose cone, respectively. The pattern of this coating is shown in Fig. 57.

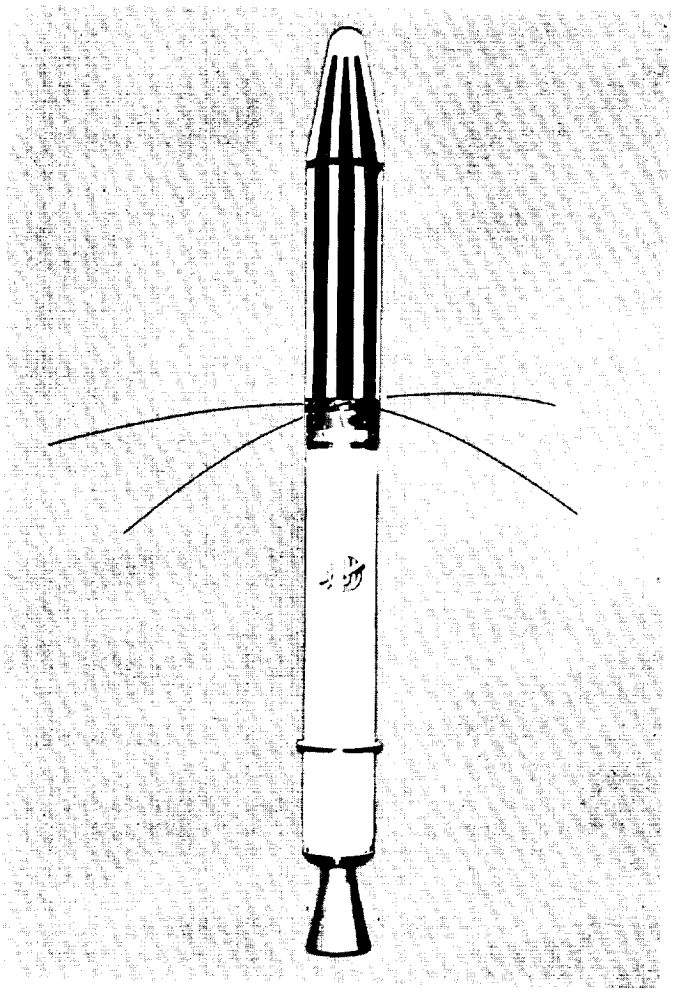

**Figure 57. External view of *Explorer I***

### B. Scientific Information

Three basic types of information were telemetered to ground stations: temperature measurements, micrometeorite impact and erosion data, and incident cosmic-ray count. Ground observations of the satellite were expected to provide additional data about the Earth's ionosphere, geomagnetic field intensity, and atmospheric density. These observations were to be made by both radio and optical means.

### C. Satellite Communications

Because of the restrictions imposed by weight, size, and power consumption, it is necessary for the communication system that is used with a small satellite to be as efficient as possible. It should be noted that in terms of satellite application, efficient circuit design means highest radiated power and longer instrumentation life per battery weight. In the case of the *Explorer* satellite, the Microlock system developed by the Jet Propulsion Laboratory, and described in Part One, was used. The essential feature of the Microlock system is the phase-locked receiver which allows a very narrow bandwidth to be used and therefore made it possible for a very sensitive system to be built.

The transfer of intelligence from the satellite to the earth was to be accomplished by two completely redundant telemetering systems. This dual approach to the transmission of satellite data was taken for two reasons: (1) it enabled greater overall data handling capability, and (2) it permitted a partial backup system.

Each of the transmitters had its own set of subcarrier oscillators. Standard FM/FM Channels 2, 3, 4, and 5 were selected for convenience in data reduction. Channels 2 and 3 are used for temperature measurements in both transmitters, channel 4 for erosion, and channel 5 for cosmic-ray data.

Both telemetering systems (Fig. 58) with their associated instrumentation were completely transistorized for two reasons: (1) transistors permitted the design and building of systems which were capable of withstanding both the severe shocks imposed during the launch phase and the extreme thermal variations to be expected during the orbital portion of the satellite life, (2) transistors exhibit inherent low-power consumption characteristics which permitted the design and development of extremely efficient circuitry.

One transmitter, which was referred to as the high-power transmitter, radiated approximately 50 mw of RF power via a circularly polarized turnstile antenna, at a frequency of 108.03 mc. The four subcarrier oscillators amplitude-modulated this transmitter with a level of 50%.

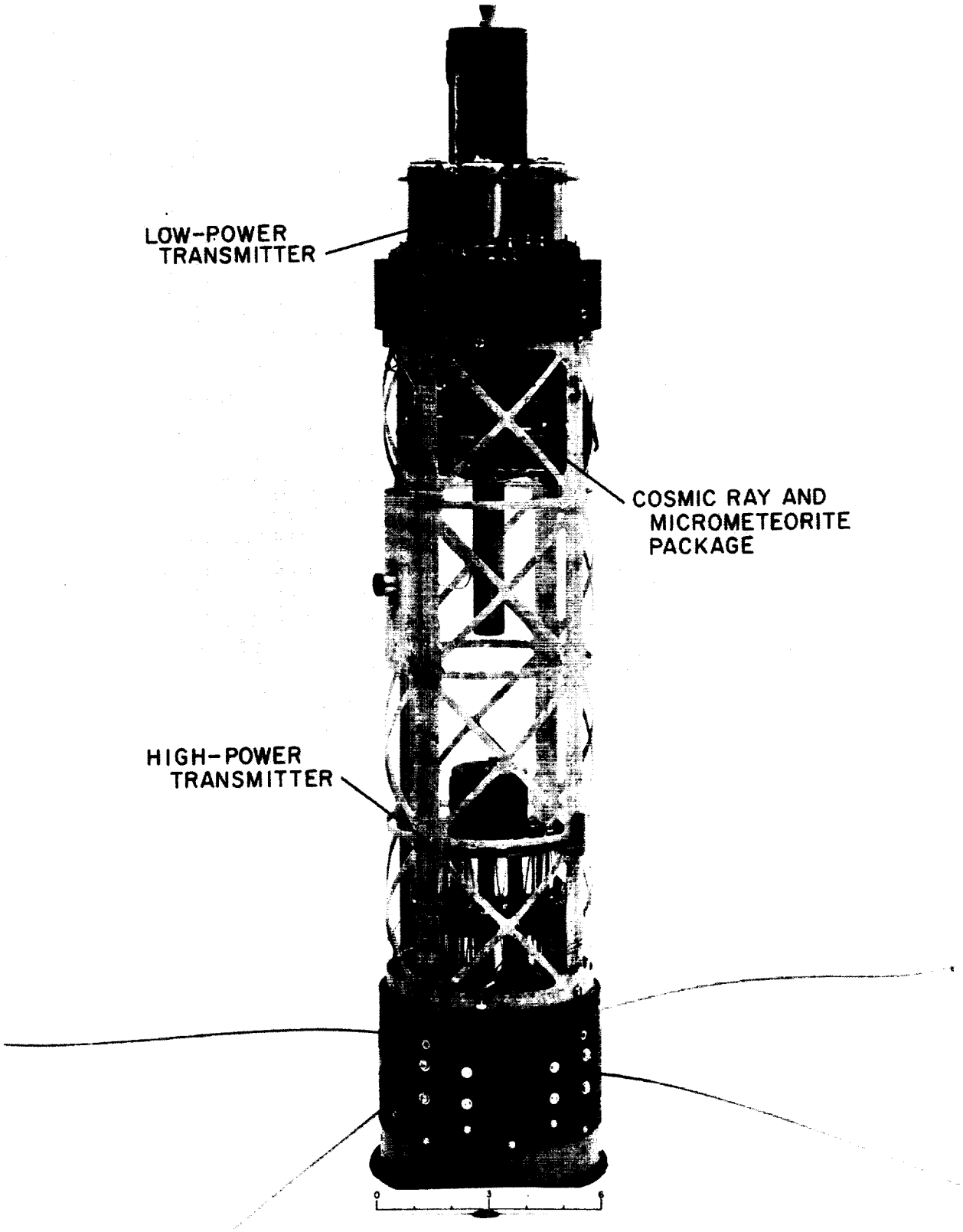


**Figure 58. *Explorer I* payload instrumentation**

This signal was to be received by the Minitrack net and used for precise orbit determination. The life expectancy of the high-power transmitter was approximately 2 weeks.

The second, or low-power transmitter, which was phase-modulated to a level of 45 deg rms delivered 10 mw of power to its linearly polarized dipole antenna at a frequency of 108.00 mc. One of the unique features of the low-power transmitter was its long (approximately 1500 hr) operating-life-to-battery-weight ratio. Signals from the high-power transmitter could be satisfactorily received by the Minitrack system or by any comparable sensitive receiver. However, to obtain the telemetering information from the low-power phase-modulated transmitter it was necessary to use a Microlock type of system.

In order to improve the sensitivity of the Microlock system, phase-locked discriminators were used to recover the telemetry data, and bandwidths as low as about 1 cps were used. It was possible to effect this improvement because, except for the cosmic-ray count, the information rate of the telemetering channels was quite low.

# XV. TEST AND CALIBRATION OF *EXPLORER* SATELLITES

Environmental test specifications for the *Explorer* satellite prescribed two complete testing procedures: flight-acceptance and type-approval tests. The use of dual test specifications is characteristic of the philosophy of the Jet Propulsion Laboratory on environmental testing in research and development programs. Flight-acceptance tests, applied to all units prepared for flight, were designed to subject the units to an environment simulating that encountered in flight. Type-approval tests, applied to a sample payload, were designed to verify that the payload design was capable of surviving the flight-acceptance test and the flight.

In the *Explorer* program, the use of the 100% flight-acceptance testing in reference to any sampling or test-to-failure plan was dictated by the complete lack of statistical information concerning the test units and by the high reliability required. Furthermore, flight-acceptance testing was the only technique which could provide assurance that the custom-made RF transmitters, such as the Microlock beacons, would provide satisfactory signals for low-power reception while subjected to the severe environmental conditions expected in the launch and orbiting phases.

Both the flight-acceptance and type-approval test specifications for the *Explorer* satellite were divided into two categories: mechanical and thermal. Various tests, both flight-acceptance and type-approval, are listed below. Brief discussions of the reasons for their selection are included.

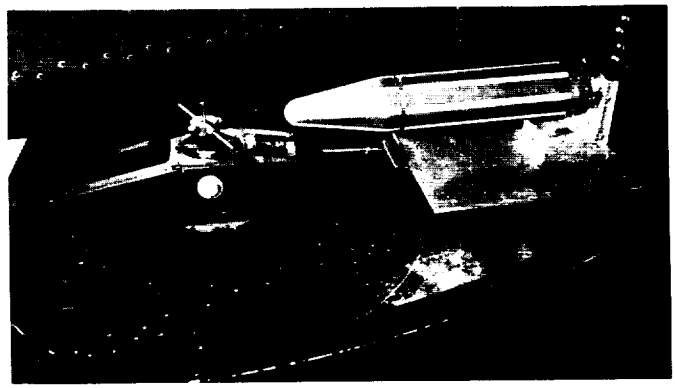

**Figure 59. Centrifuge test**

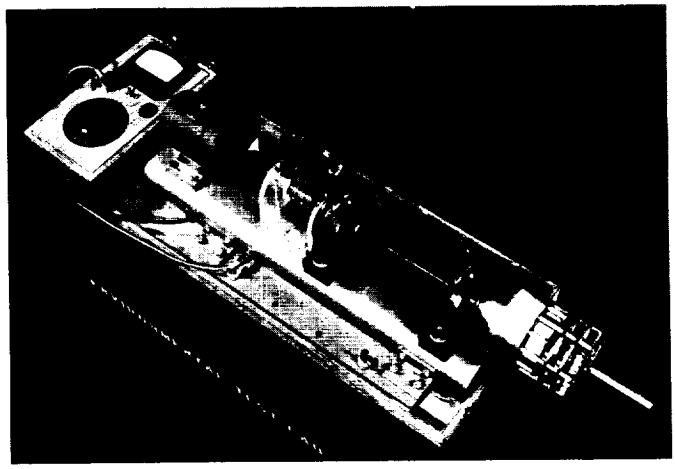

**Figure 60. Spin test**

## A. Mechanical Environmental Tests

Mechanical tests prescribed by this specification were performed on complete *Explorer* payloads.

### 1. Static Accelerations

The payload was expected to experience static accelerations as great as 60 *g* during the launching phase. Type-approval tests were therefore made on a centrifuge (Fig. 59) in order to produce stresses greater than 60 *g* for periods of up to 5 min.

### 2. Rotation

The high-speed stages of the *Jupiter-C* were spin-stabilized. Since the effect of this rotation on the payload components should be independent of total time, units were tested at the expected spin rates (Fig. 60) for short times. Flight-acceptance test units were spun at 750 rpm for 1 min around the thrust axis, whereas type-approval units were required to withstand a spin rate of 1500 rpm for 10 min in order to pass their tests.

### 3. Vibration

Tests of the satellites were based on estimates of the vibration which the fourth-stage rocket motor would produce at the joint between the motor case and the payload. Estimates of this vibrational data were determined by several restrained motor test firings. Calculations to determine the effects of the test stand measured data and the loading effects on the payload structure by the rocket motor vibration were also made.

Some of the most severe vibration experienced by the *Explorer* payloads was expected to be produced by the stage 4 motor. Since little was known about the coupling

and attenuation characteristics of the clustered motors of the *Jupiter-C* configuration, the payload vibration tests (Fig. 61) included three types, expected to be produced by the fourth-stage rocket motor. It should be noted that the vibration produced by the booster motor and by aerodynamic effects was considered negligible compared to that produced by the solid-propellant motors.

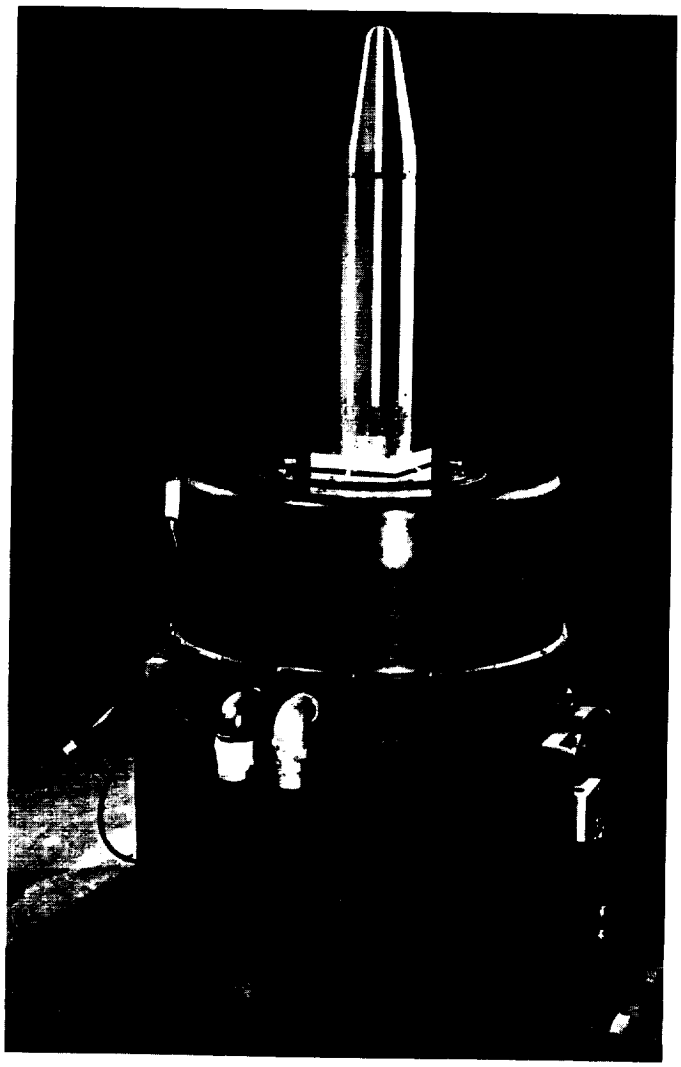

**Figure 61. Vibration test**

4. Shock

Vibration measurements on restrained firings of solid-propellant motors of the type used in the *Jupiter-C* configuration indicated that the *Explorer* payload would experience shocks of between 50- and 75-*g* peak value as a result of motor ignition. Flight-acceptance tests for the *Explorer* satellite incorporated shock tests with the vibration tests by the use of 0.1-sec bursts of high-level noise. Type-approval specification prescribed shocks of 100 *g* excited at the payload base by means of a ballistic shock machine.

### B. Thermal Environmental Tests

The philosophy employed in the thermal environmental testing was somewhat different from that of the mechanical testing. The justification for this difference was the absence of fatigue effects associated with temperature changes in the vehicle.

Thermal flight-acceptance tests were performed (Fig. 62) to determine that the payload subassemblies were capable of operating at temperatures between 0 and 50°C, the expected range of the internal temperature of the satellite. These tests were often performed simultaneously with the calibration of instrumentation for measuring the temperature at various places in the payload.

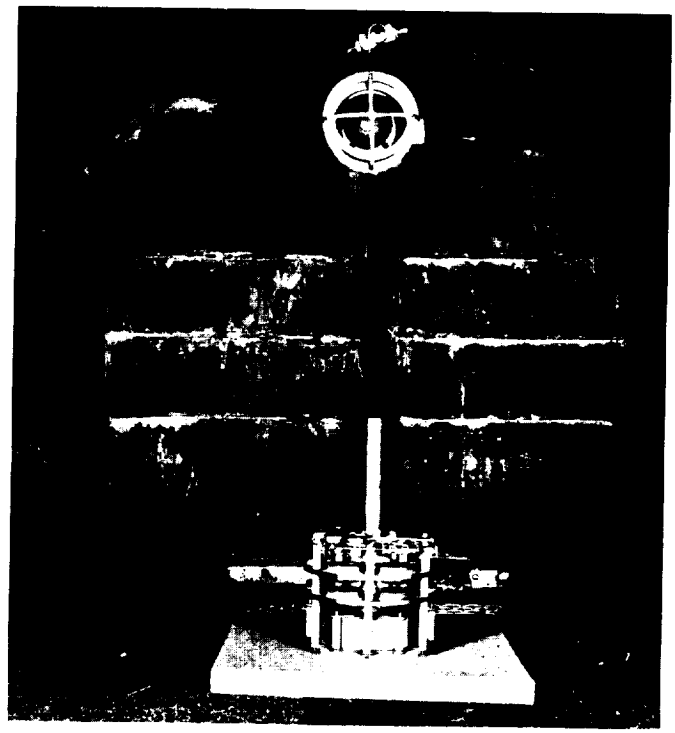

**Figure 62. Thermal test**

### C. Electronic Checkout Equipment at Launch Site

No special equipment was required. The limited amount of testing necessary was done by monitoring transmitted signals with the Microlock station.

# XVI. JUNO I TRACKING SYSTEM

## A. Satellite Tracking Stations

The ground links with the *Explorer I* satellite experiment were the ground instrumentation stations. Their purposes were twofold: (1) to determine orbital data and (2) to receive telemetered satellite environmental data. From these two sources of information, many important scientific investigations as to the properties and characteristics of both outer space and the Earth were conducted.

Orbital determination for the IGY program was made primarily by the Minitrack network, a tracking system developed by the Naval Research Laboratory. The Minitrack system consisted of a 10-station network lying on a line running north and south along the 75th meridian.

By a system of phase-comparison techniques, these stations measured the angular-position of the satellite as it passed through a fan-shaped (10-deg-wide) antenna pattern. During the time the satellite was passing through the antenna pattern, the Minitrack station also received and recorded the data being telemetered from the amplitude-modulated high-power transmitter in the satellite. All telemetered environmental data which was part of this experiment was channeled through this Laboratory for reduction and dissemination to cognizant organizations for interpretation.

The JPL-developed Microlock tracking and telemetering system was primarily interested in the output of the satellite low-power transmitter which operated for a longer period of time than the high-power transmitter. The Microlock Gold Station, however, telemetered, recorded, and tracked both the high- and low-power transmitters.

The Microlock system (see Sec. XVII) consisted of four Microlock stations spread in a band around the Earth; each station had the ability to track and receive data from horizon to horizon (180 deg of arc). Some tracking passes have lasted as long as 30 min.

## B. Doppler Station

This station, located on Antigua, B. W. I., to obtain doppler data only during launch, was operated in conjunction with the Antigua Minitrack network. Data were used for initial orbit determination.

The equipment was installed and operated by three JPL men. It was operated only during the launching and was not used to obtain telemetered data. The doppler data were printed digitally on a paper tape and sent by teletype to the JPL Message Center at Cape Canaveral and retransmitted to Pasadena.

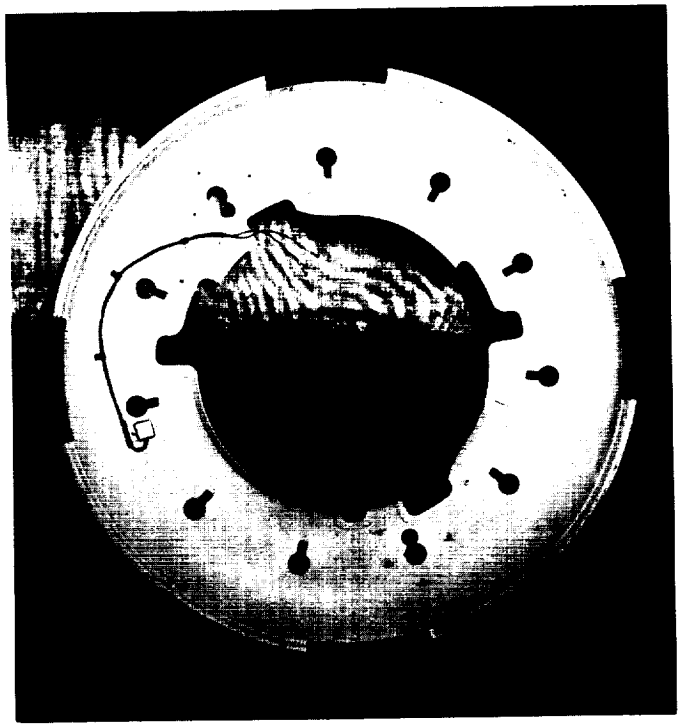

**Figure 63. Second-stage shroud and temperature sensor**

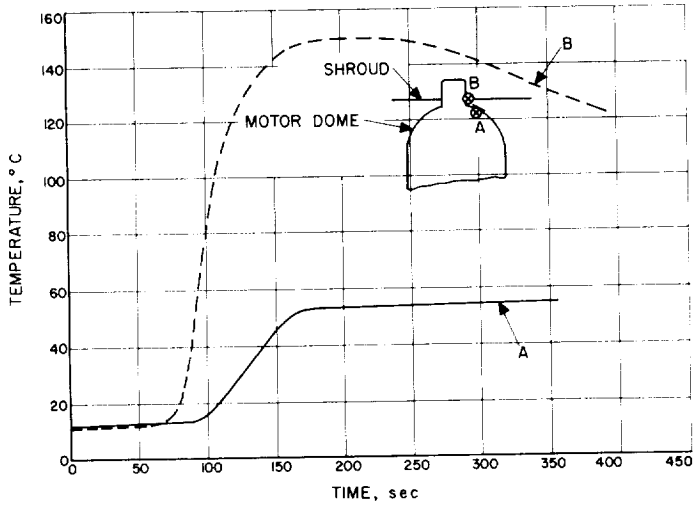


**Figure 64. Shroud and motor dome temperatures**

## C. Telemetered Data

### 1. *Redstone* Booster

*a. Shroud skin temperature.* A temperature sensor (Fig. 63) was mounted on the shroud of the high-speed stages midway between two motor domeheads. The sensor (calibrated and supplied by ABMA and installed by JPL) was connected to the ABMA telemetering equipment in the guidance section of the *Redstone* through three pairs of slip-rings. The information (Fig. 64) telemetered from this source was used to evaluate the shroud design.

### 2. Payload Telemetering

This was used for payload information only, as described in Sec. XIV-C.

# XVII. OPERATION OF MICROLOCK NETWORK

## A. Ground Stations

### 1. General

The network of Microlock stations used in the re-entry test vehicle (RTV) program has been described previously. The Microlock network as used in the *Explorer* launchings by the Jet Propulsion Laboratory consisted of two Microlock stations, the Red Station at Earthquake Valley, California, (later shifted to Goldstone Lake, California) and the Gold Station at the Air Force Missile Test Center (AFMTC) in Florida. The Gold Station was used in the testing and launching phases of the satellite experiment in addition to its function of tracking the satellite passes. Two stations, designated Black and Silver, were prepared at the Laboratory and were sent to University College, Ibadan, Nigeria and to Malaya University, Singapore, respectively. Personnel at these institutions operated this equipment under cooperation with the British IGY committee.

The prime purpose of these stations was to collect telemetering information from the low-power (10 mw) transmitter of the satellite. This information was transmitted in the form of phase modulation which the Microlock receiver was designed to recover. The Gold and Red Stations also furnished doppler information to the JPL computing center for orbital calculations. In addition, Gold Station provided interferometer data at launch which provided azimuth angle data to extreme ranges.

The Red and two other stations formed a Spheredop network, which by a method of triangulation was able to provide orbital information from doppler data. Two Microlock stations were designed at JPL to be built using commercial radio receivers and components for most of the station (see Bibliography). Such stations were constructed and operated by the San Gabriel Valley Radio Amateur Club, Temple City, California, and the Naval Ordnance Test Station, Inyokern, California. These three stations were tied together through the JPL Message Center to the Laboratory computing center.

### 2. Description of Stations

*a. Black and Silver Stations.* The Black and Silver Stations were designed with the minimum equipment necessary to collect the telemetering data on the cosmic-ray and micrometeorite experiments. These stations consisted of a single rack containing the following equipment: a Microlock receiver, a test oscillator, an auto-transformer (to adapt to either 110 vac or 220 vac), a WWV receiver, and a portable Ampex (two-track) magnetic tape recorder, converted to operate at 50 cps (Fig. 65).

Radio station WWV in Washington, D. C., was received and used as a reference in Africa, and in Singapore station JJY in Japan was used to provide a reference signal.

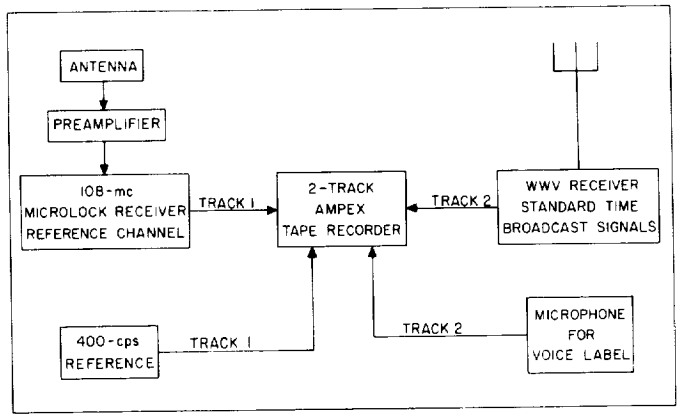


**Figure 65. Black and silver telemetering stations**

*b. Red Station.* Earthquake Valley had been chosen in 1956 as a site for testing the Microlock system because of its low radio noise environment. The Red Station was used to observe *Sputnik* (1957 Alpha); the Microlock receiver was converted to operate 40 mc for that operation.

For the *Explorer* operations, the Red Station did not provide interferometer data but in all other respects it was a standard Microlock station. It was installed in a 26-ft van and included an air conditioner, two 30-kw generators, a helix antenna, and a house trailer for personnel.

For the *Explorer* launchings, an improved doppler readout system was added to both Red and Gold Stations. Figure 66 shows the Red Station block diagram. The heart of the data recording system was a Hewlett-Packard frequency counter (Model HP-524A). The reference oscillator in this unit was checked for stability against an oscillator stable to several parts in $10^9$, and its stability was found to be several parts in $10^7$ when kept in a stable environment (stable voltage, temperature, etc.). This frequency was used to indicate the frequency shift of the voltage-controlled oscillator (VCO) of the Microlock receiver. During a pass this VCO was locked to the frequency of the satellite transmitter. As the apparent transmitter frequency varied during a pass due to the doppler

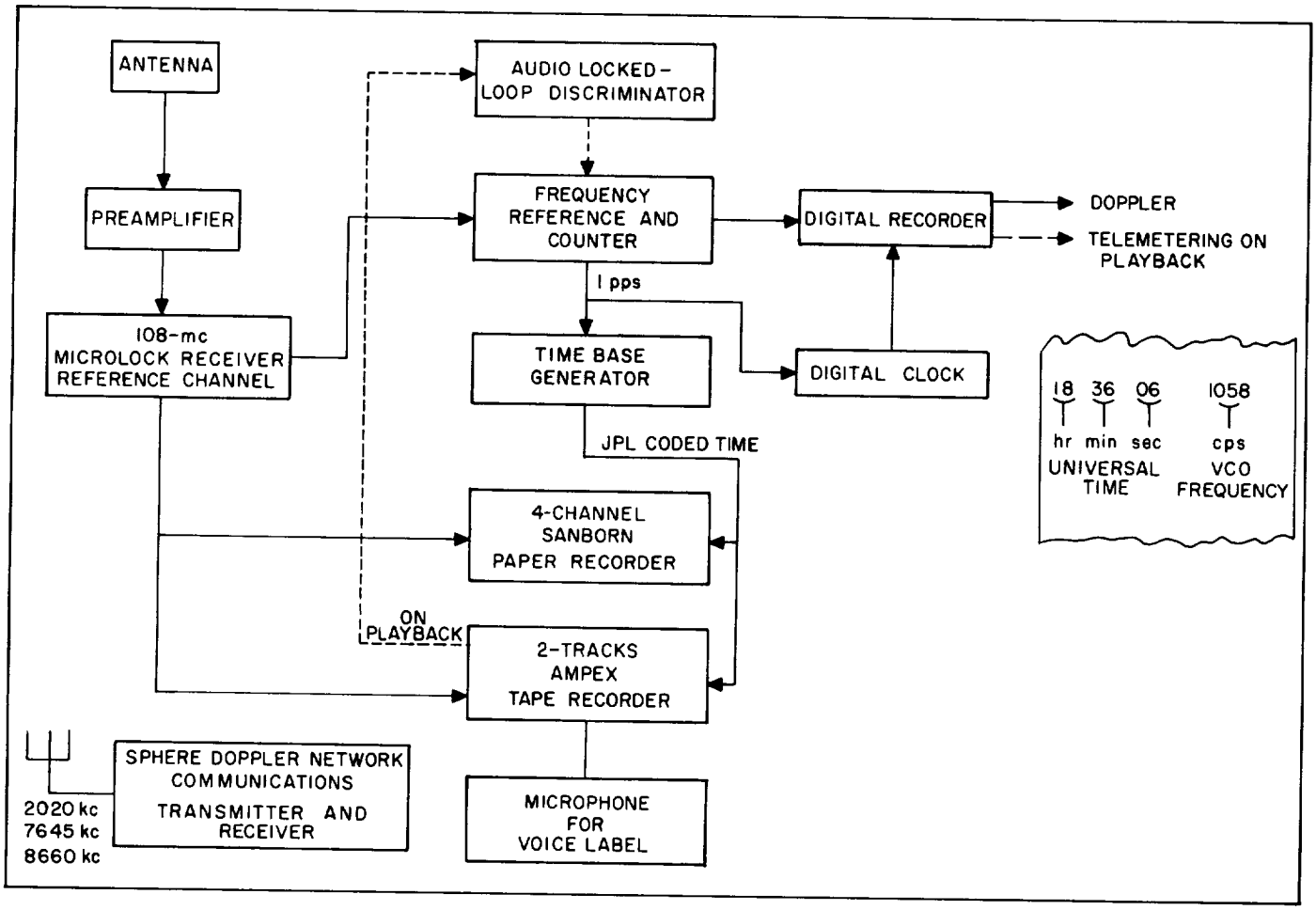


**Figure 66. Microlock Red Station**

effect, the VCO frequency followed it. The VCO frequency was then recorded by a counter and a digital recorder. The recorder then printed out the last four digits of the VCO frequency on a paper tape. A plot of the frequency shift vs time provided the data required for orbital calculations.

The frequency counter also provided a 1-pps signal which drove a time-base generator and a digital clock. The time-base generator provided timing for the other recorders. A digital clock controlled six printing wheels in the digital recorder which in turn printed out in Universal-time units of hours, minutes, and seconds. The printed time represented the end of a 1-sec counting interval and agreed with the time signals from the station WWV to within a few millisec.

A further addition to Red Station for the *Explorer* operations was the incorporation of a radio set (transmitter and receiver) to enable communication with and through the JPL message center.

*c. Gold Station.* This Microlock station at AFMTC had the following five basic requirements: (1) to perform the preflight checkouts of the payloads, (2) to provide the azimuth angle of the payload near the point of injection and near the horizon, (3) to provide doppler information during and after high-speed stage burning, (4) to monitor performance of the telemetering channels during launch, and (5) to obtain doppler and telemetering information on subsequent passes.

This station was installed in two Helicop-Huts (Fig. 67). The doppler printout equipment such as installed in the Red Station was added and the Ampex (two-track) magnetic tape recorder was replaced by a seven-track machine. A block diagram of the system is shown in Fig. 68. The system included a single-axis interferometer receiver (108.00 mc) for the angle determination.

The Gold Station received and recorded (on magnetic tape) telemetering information from both 108.00- and 108.03-mc transmitters of *Explorer I*. For *Explorers II* and

**Figure 67. Microlock Gold Station**

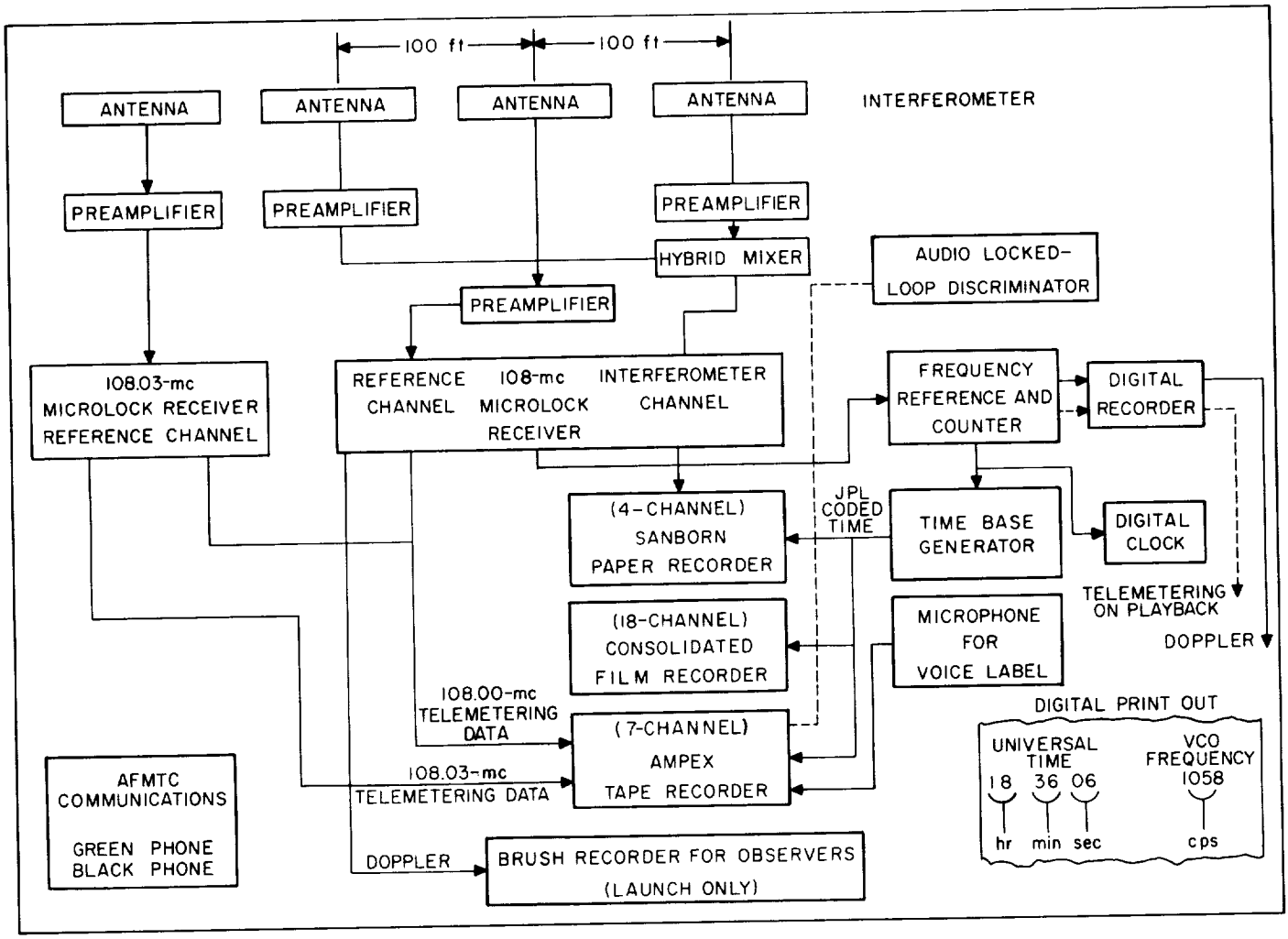


**Figure 68. Block diagram of Microlock Gold Station**

*III* only the data from the low-power (108.00-mc) transmitter was recorded. Doppler information of launch was also provided by the Gold Station to the JPL computing center at AFMTC.

## B. Spheredop Net

### 1. Description

The JPL Spheredop network was a group of tracking stations possessing equipment capable of rapidly determining the exact nature of the doppler shift of signals transmitted from satellite vehicles.

At the time of the first *Explorer*, the Spheredop network consisted of the following stations: Naval Ordnance Test Station (NOTS), China Lake, California; San Gabriel Valley Radio Club, Temple City, California; Ballistic Research Laboratory, (BRL), White Sands Missile Range, New Mexico; Collins Radio Company, Cedar Rapids, Iowa; ABMA, Huntsville, Alabama. In addition, data were available from the prime Microlock station located at Earthquake Valley, California. The NOTS, San Gabriel, and Collins installations consisted of amateur Microlock systems. The BRL, White Sands, installation consisted of the normal BRL doppler tracking setup. The ABMA operation employed the JPL audio lock-loop system that was used on Antigua Island. All the stations used modifications of the JPL Microlock system. All stations used some form of phase coherent detection in conjunction with a device for automatically printing out in digital form numbers related to the satellite carrier frequencies. The prime purpose of the network was to provide data on satellite trajectories immediately following launch and during the first few passes around the Earth, in order to establish orbital parameters at the earliest possible time. The stations were tied to a data center at the Jet Propulsion Laboratory, by teletype, radio, and telephone. This network was located in such a manner that it covered an extensive area of the United States. The stations were located so that the base line distance between stations was comparable with the expected orbital altitude of the satellite.

### 2. Computational Technique

The basic computing scheme of the Spheredop network as performed at JPL was to make use of as much computing before the firing time as possible. A nominal orbit was specified before the firing and predictions were then calculated as to the exact frequency of the doppler shifted satellite tracking signal at the location of each Spheredop station. Other such calculations were run on orbits that represented small deviations from the so-called nominal orbit. For *Explorer I*, the IBM-704 computer group at ABMA calculated these theoretical doppler curves for the first pass of the satellite. Calculations were made for about 40 different sets of initial conditions near nominal. During the actual first pass of the satellite, data were transmitted in real time to the central data center and compared to each of the theoretical doppler curves. The orbital elements of the orbit best matching the observed data were then chosen to be the best approximation to the actual orbital elements. In this manner it was found that a fairly accurate idea of the orbital elements could be obtained within a few minutes after the first pass.

In addition to the above computing scheme, which was used only on the first pass, subsequent doppler data was used at JPL to refine the original orbit determination. Within the required accuracy, this could be done by using an analog interpreter consisting of a tabletop representation of the Earth, combined with simple hand computing methods. Reduced doppler data were also sent to ABMA, where a more sophisticated orbit computation was made by the IBM-704 computer group, using times of nearest approach and maximum slope of the doppler curve as program input. This technique was employed for *Explorers I* and *II*.

For the operation involving the launchings of *Explorers IV* and *V*, similar data reduction and analysis schemes were used. Data from the Spheredop network were transmitted to the JPL message center. At JPL the maximum slope and time of nearest approach was determined, and immediately transmitted to ABMA followed by transmission of the raw data. ABMA had primary responsibility for orbit determination. The ABMA computations were based on a program which had been prepared for the IBM-704 computer. Less extensive orbital computation was also made at JPL.

## C. System Operation

### 1. Doppler

The Microlock doppler system, being a one-way system, does not have the inherent accuracy of the two-way system commonly encountered at missile ranges. Neglecting the frequency drift of the transmitter, the limiting factor of the system accuracy is the stability of the reference oscillator used in the Microlock frequency counter which is within several parts in $10^7$. Since the counter counts the VCO frequency, it can introduce 20-to-30 cps error in the doppler shift data. The 455- and 5.455-mc reference oscillators in the Microlock receiver (Fig. 69) contribute approximately 1 and 5 cps error, respectively, during a pass. Therefore a total error of about 35 cps out

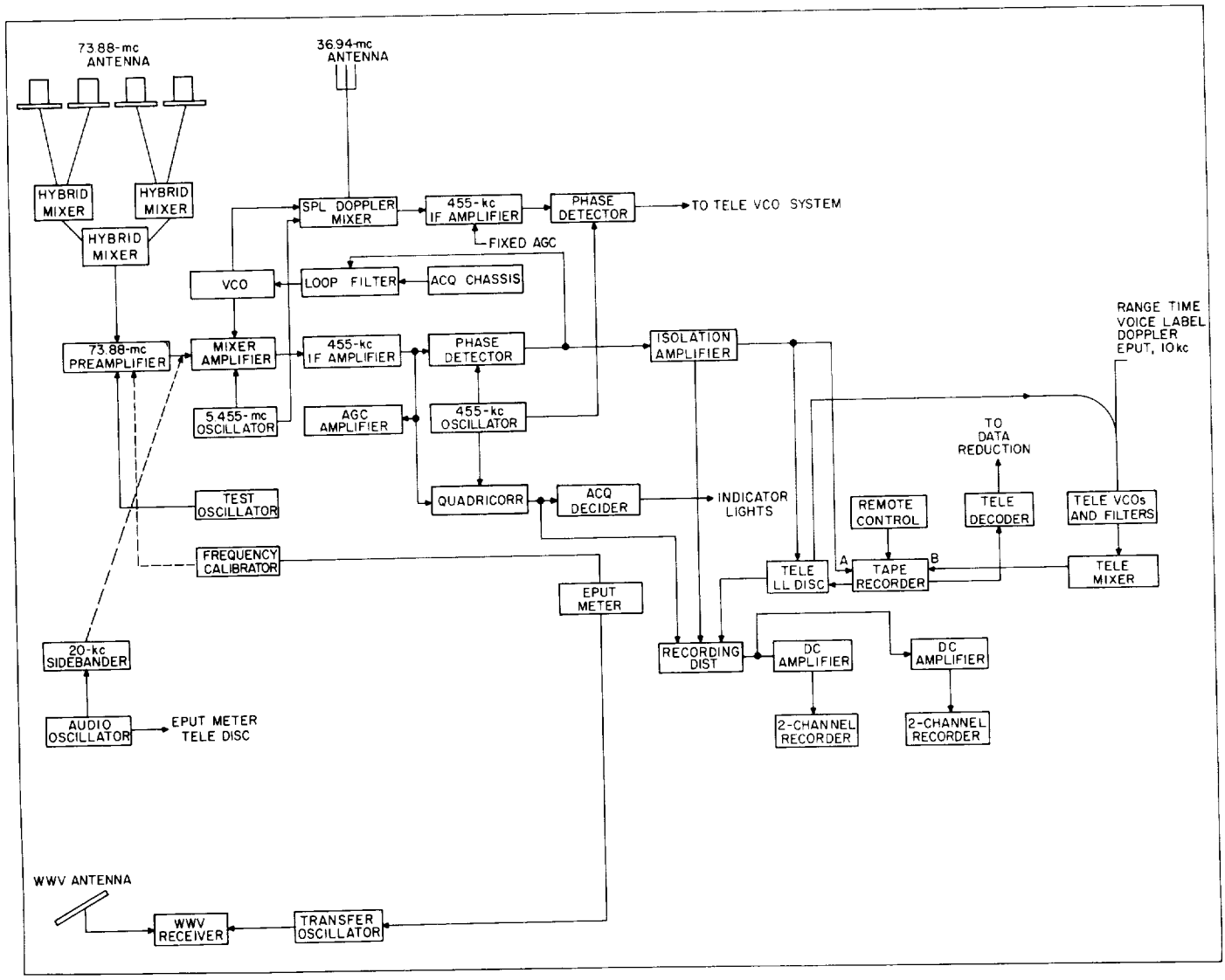


**Figure 69. Functional block diagram of Microlock ground station**

of about 5600 cps total frequency shift for *Explorer* orbits amounts to less than 1% error. Figures 70 and 71 show the data collected for *Explorers I, II,* and *III*. All curves are corrected to a nominal frequency of 108.00 mc, since the low-power transmitters of each payload had slightly different frequencies. Figure 71 also shows the burning periods of the high-speed stages; the horizontal sections between the steep portions are the coasting periods. Although analog data covering *Explorer* burning and coasting periods are far less accurate, they show the doppler signal as continuously functioning and verify the digital lengths of the coasting and burning periods. Digital information was averaged over 1-sec intervals (every other second) and this fact was taken into account when calculating the satellites' velocities.

### 2. Signal Strength

The AGC voltage of the Microlock receiver was recorded as a measure of receiver signal strength. Figures 72, 73, and 74 show the received signal strength for the three *Explorer* launchings. The low-power transmitters had a nominal output power of 10 mw, and all three were less than 1 db below this figure. The high-power beacon on *Explorer I* had a power output of 60 mw; the subsequent rounds used interrogated transmitters and were not tracked by Microlock, except to measure carrier frequency during preflight checkouts.

The motion of the payload after injection can be analyzed to some degree by examination of the variations in signal strength. The graphs shown are not plotted in

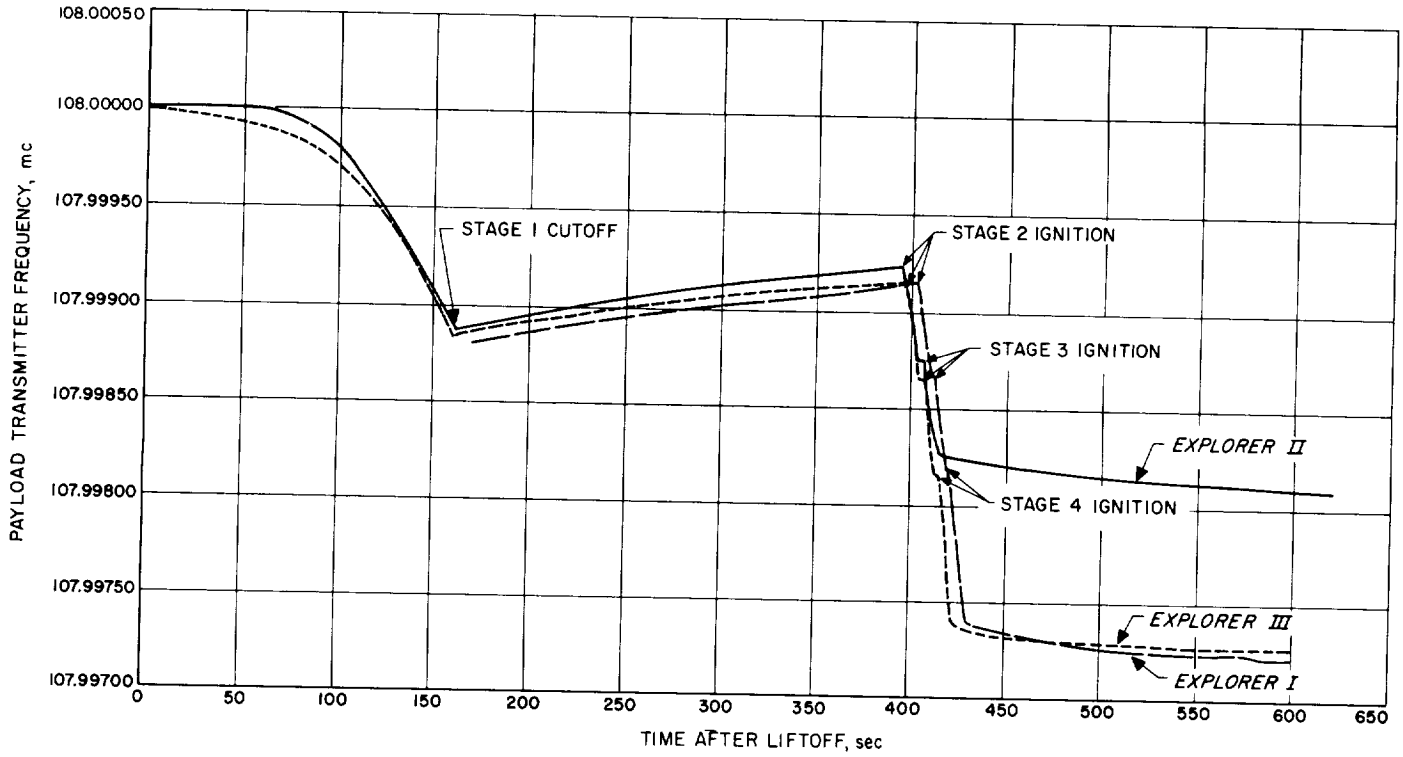


**Figure 70. *Explorer* doppler shift**

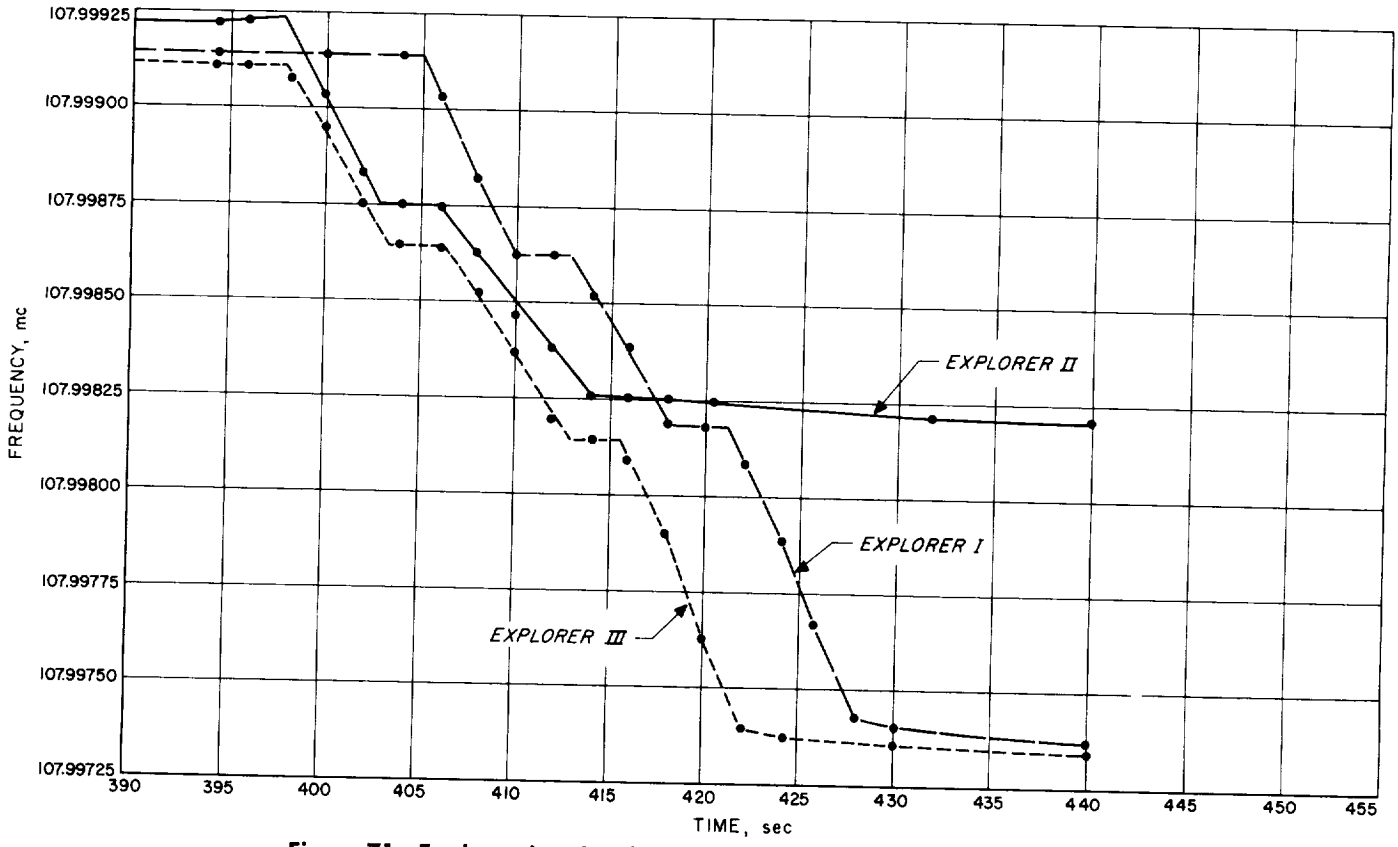


**Figure 71. *Explorer* doppler shift during burning of high speed stages**

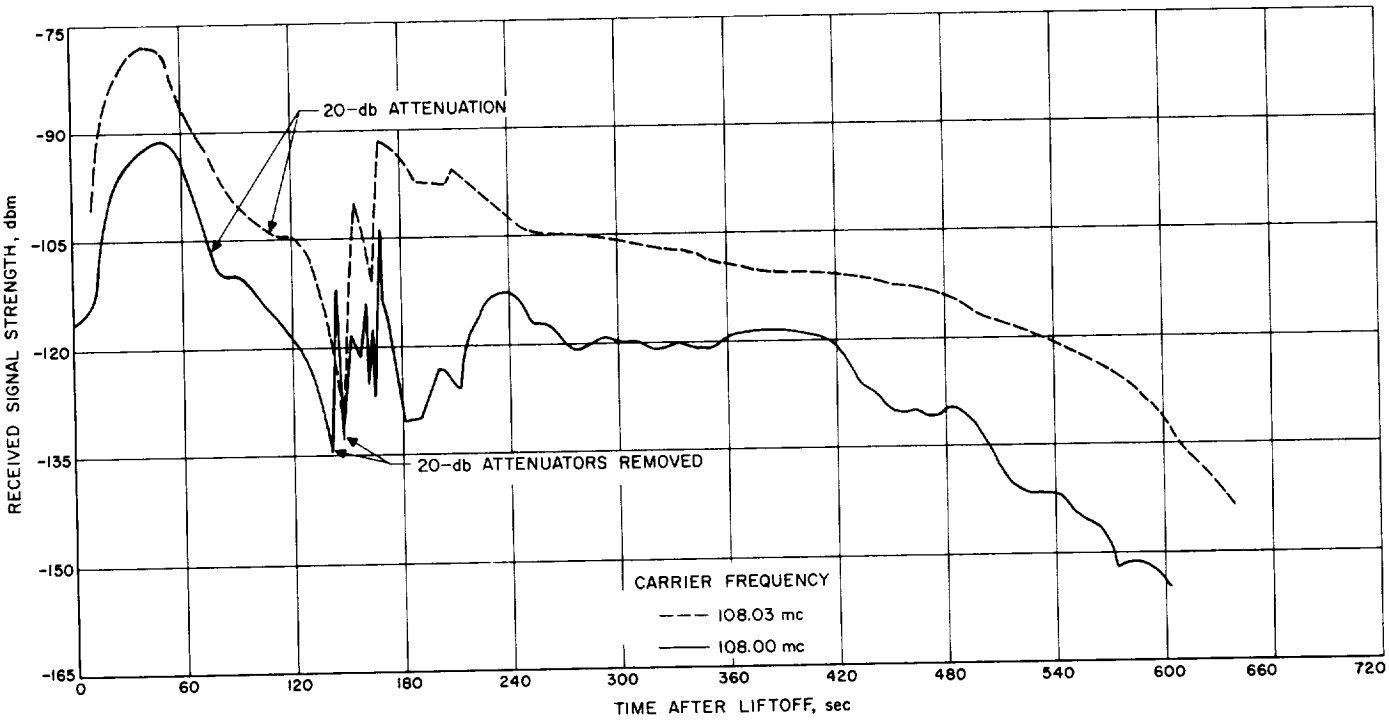


**Figure 72. *Explorer I* Microlock received signal strength vs time**

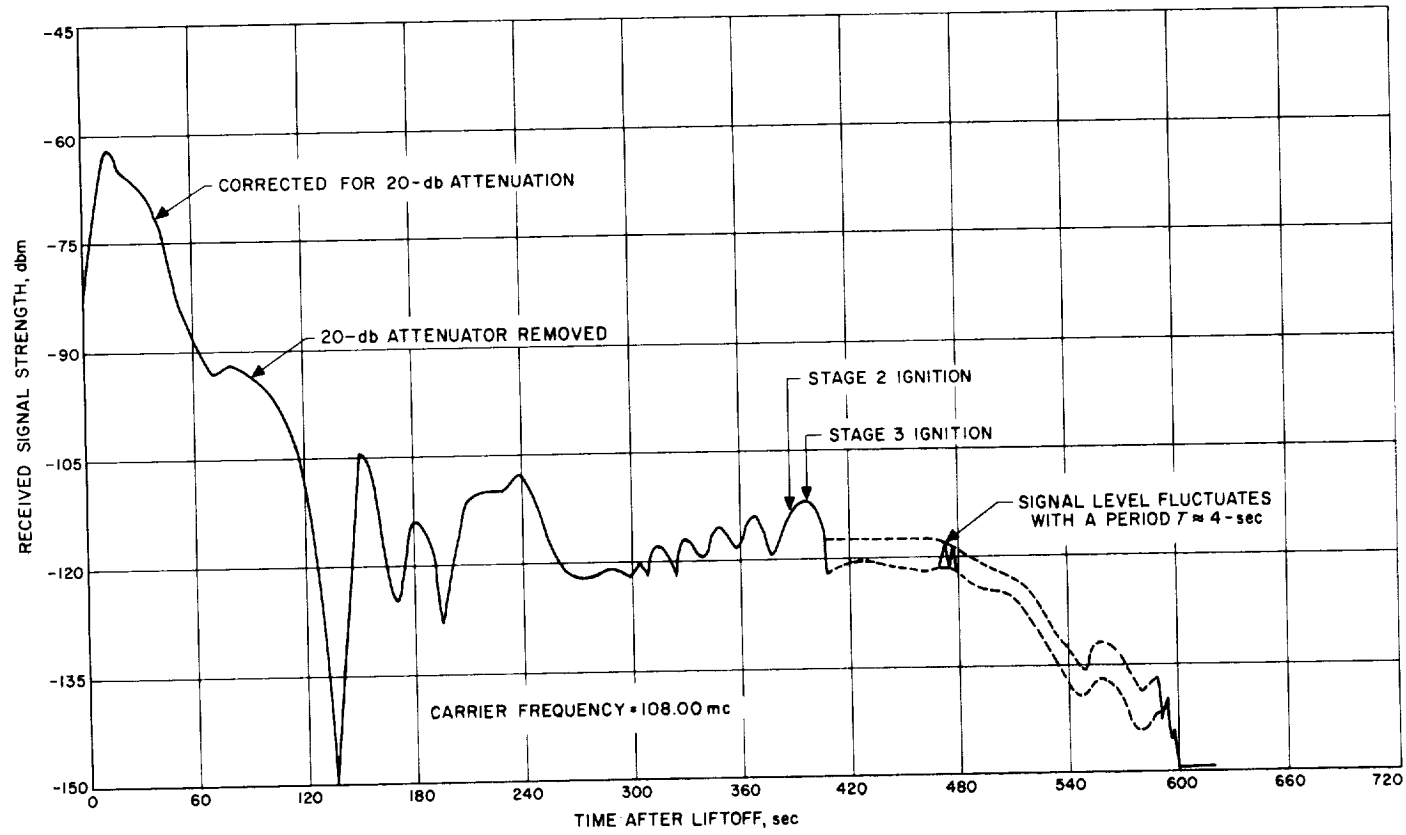


**Figure 73. *Explorer II* Microlock received signal strength vs time**

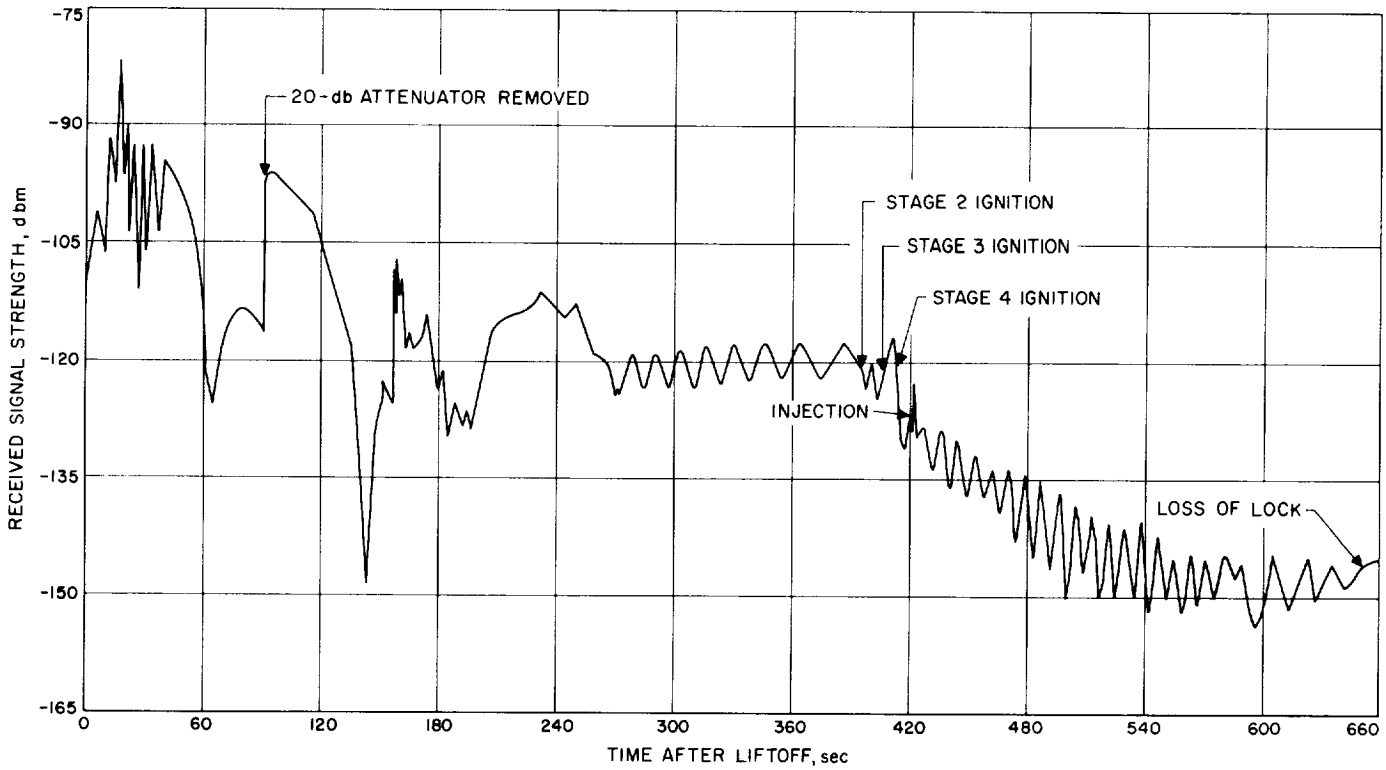


**Figure 74. *Explorer III* Microlock received signal strength vs time**

sufficient detail to indicate all the variations. The spin rate of the payload can be read from the fluctuations in the AGC voltage which are due to asymmetry of the antenna pattern. After fourth stage burning, the signal strength varied in a periodic manner. The period varied with time, and this effect has been correlated with precession of the payload.

The inherent sensitivity of the Microlock receiver and the fairly broad beam antenna employed allow the tracking of the *Explorers* essentially from horizon to horizon. When the perigee of the orbits was over a station tracking, periods were as short as 4 or 5 min with attendant high-signal strength ($-100$ dbm). When the orbit regressed to place the apogee over a station the observing times were as long as 30 min; 20-min passes were very common. In these cases signal strength was lower but adequate to extract telemetering data. During this time the satellite was at ranges of 2000 to 3000 miles from the receiver and traveled about 10,000 miles along its orbit.

### 3. Interferometer

The interferometer antenna system of Microlock was originally designed to provide the times of selected direction-cosines by means of the commonly used, crossed-axis system. These direction-cosines were determined by the nulls in the antenna patterns of the interferometer. The central null lay in a plane perpendicular to the axis of the antenna system. For the *Explorer* launchings, this null plane was oriented so that the firing azimuth lay in this plane (Fig. 75). With the null plane lying along the

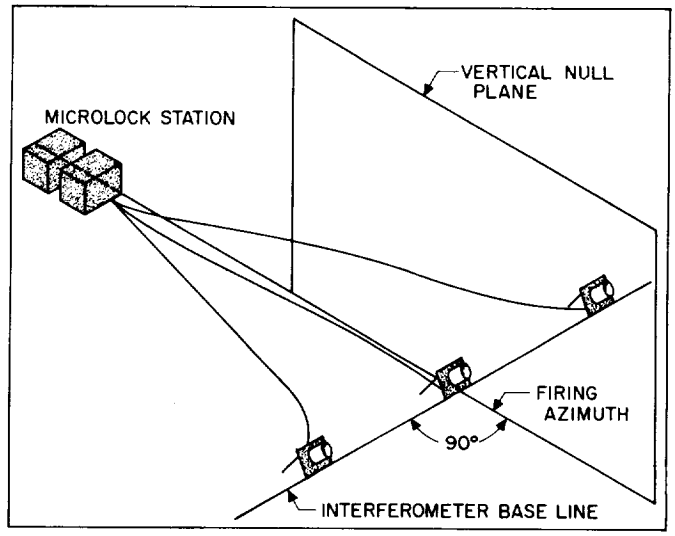


**Figure 75. Microlock interferometer antenna for *Explorer* launching**

nominal firing azimuth of 110 deg, deviations from the expected trajectory could be measured. The actual trajectory did not lie in this plane because of Coriolis acceleration, drift errors, and guidance corrections.

*Explorers I* and *II* were fired from ABMA Pad No. 26A at the AFMTC. The Microlock station was located so that the center null plane of the antenna passed almost directly through the pad. The mechanical axis of the antenna was accurately surveyed and the electrical axis was adjusted to coincide with it within ±0.1 deg by adjusting phase lengths in cables between the antennas and the differencing networks. After this adjustment the position of the null plane was measured by flying a transmitter in a helicopter, which was observed by a theodolite as it crossed the null plane. This boresighting technique supplied a number of check points as the helicopter flew up and down the 110-deg azimuth from the antenna on a slalom-type course. The position of the first side null was also checked.

In order to calculate the direction of the missile when not on a null of the antenna pattern, the output of the interferometer channel had to be calibrated as a function of angle. A switching scheme was used in which the interferometer was alternately switched from the difference terminal to the sum terminal of the hybrid network of the interferometer antenna. The antenna patterns at these two terminals are shown in Fig. 76. The solid line pattern is the difference pattern with the central null in the vertical plane and aligned with the firing azimuth. The dotted line is the sum pattern and has a maximum where the difference pattern has a minimum. At a switching point, the ratio of difference to sum signal is proportional to the angular displacement from a difference pattern null. Between the first two side nulls in the difference pattern, the ratio is ambiguous in magnitude, but the ambiguity may be resolved as shown in Fig. 77. The polarity of the signals depends on the relative phases of the two signals. In each of the quadrants I to IV, the combination of polarities of the two signals is unique, and the appropriate quadrant may be selected. This information and the magnitude of the ratio determine the angle. Outside the first two difference pattern nulls, the combination of polarities is repeated. This ambiguity must be resolved by prior information.

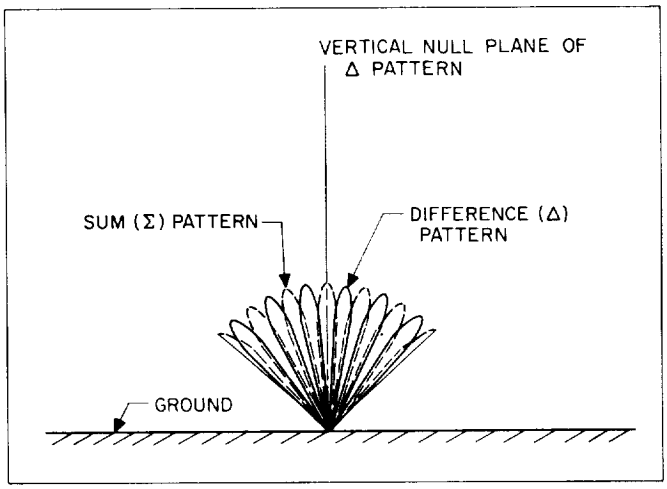


**Figure 76. Microlock interferometer antenna pattern**

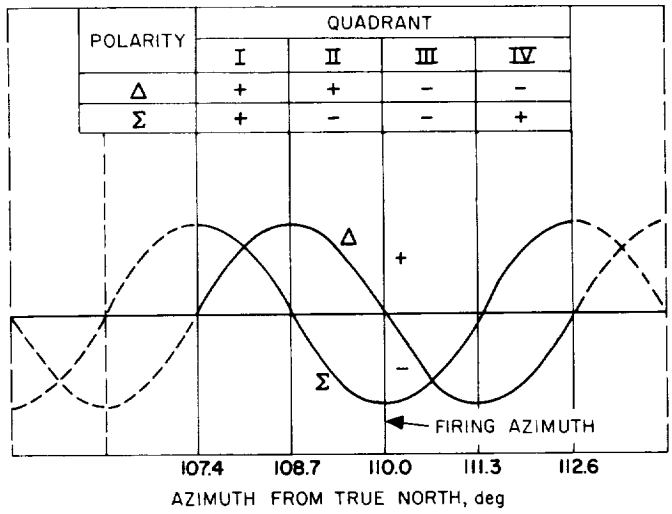


**Figure 77. Microlock channel output signal vs azimuth angle**

In the case of *Explorers I* and *II*, the angle always remained in the central four quadrants. *Explorer III* was fired from ABMA Pad No. 5. The Microlock station was not moved because of lack of time to properly set up the antennas. Therefore the missile was tracked with considerable parallax during the early portion of flight when the azimuth angle was initially far outside the central four quadrants. In order to resolve this ambiguity, the expected appearance of the output of the interferometer channel for both sum and difference patterns was precalculated as shown in Fig. 78. The flight data were examined to ascertain times of null crossings and positive and negative maxima. These were then plotted and a curve sketched through these points. These data converted to azimuth angle are shown in Fig. 79 and show how the parallax error decreased as the range increased. The curves clearly show how the missile was brought back to the firing azimuth after drifting slightly to the left. This method was successful in accounting for all the null crossings and resolving the ambiguities.

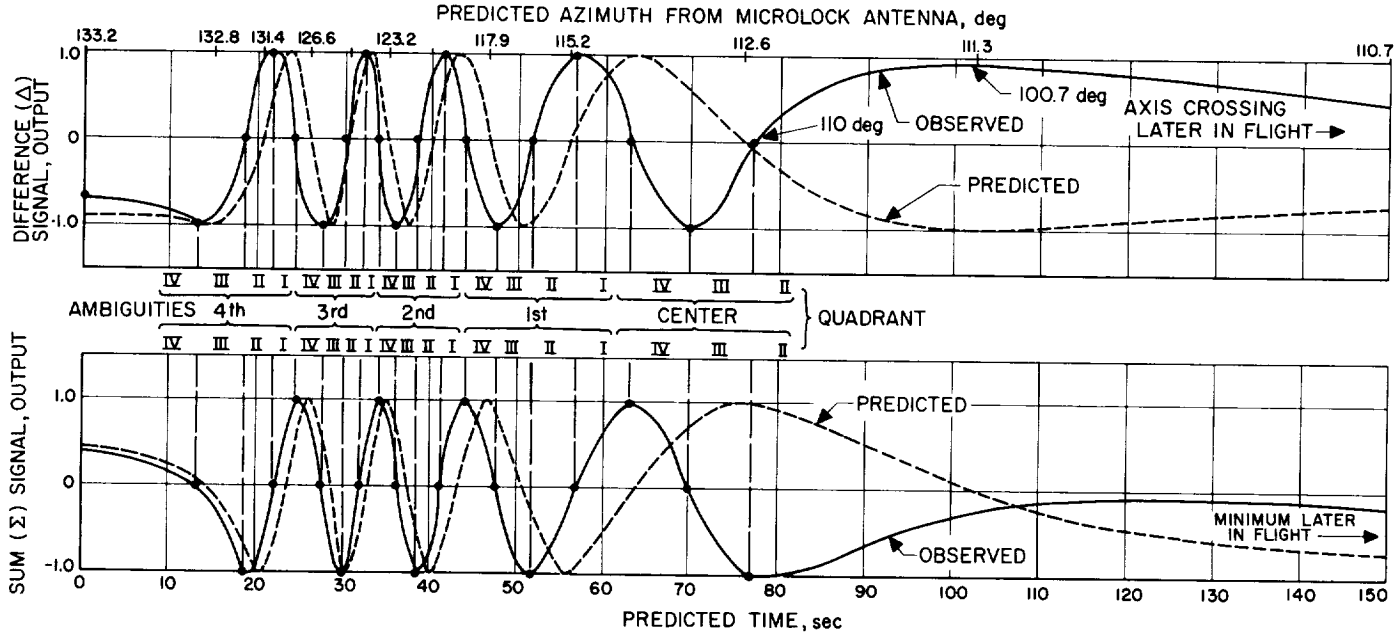


**Figure 78. *Explorer III* Microlock interferometer predicted and observed null crossings and maxima**

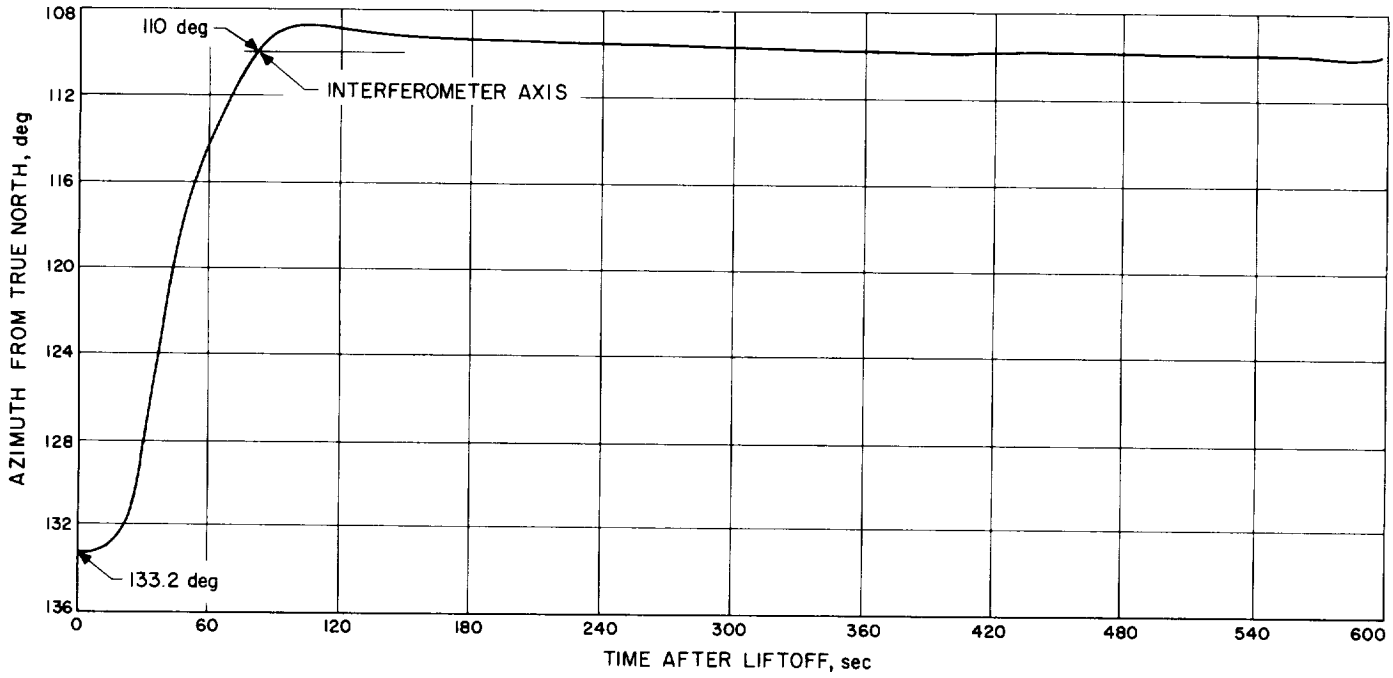


**Figure 79. *Explorer III* Microlock interferometer observed azimuth angle vs time**

## D. Summary

### 1. Apex position

Immediately after the launching of the high-speed stages, ABMA provided the JPL Message Center with slant range, altitude, and velocity of the *Redstone* nose at apex. In addition, time of launch of the high-speed stages was provided by a special apex computer. These data were required in order to make an early orbital determination.

**2. Interferometer**

The Microlock Gold Station obtained interferometric data during and immediately after the launching phase. These data, partially reduced, were forwarded to the JPL Message Center at AFMTC immediately after the signal was lost at the Gold Station receiver. The data were transmitted in the form of angle vs time.

**3. Doppler**

The Microlock Gold Station obtained doppler information from the payload during and after the launch sequence. These data were in the form of automatically printed frequencies counted over 1-sec intervals with 5-sec spacings between counts. Immediately after the signal was lost at the Gold Station, the data were transmitted to the JPL Message Center at AFMTC.

The doppler station at Antigua, B. W. I., received a doppler frequency tone from the Minitrack receiving station on that island. The JPL Station counted frequencies received from this signal in the same manner as that employed by the Microlock Gold Station. Data were transmitted to the JPL Message Center at AFMTC via the Minitrack Communication Network. These two doppler signals, one from AFMTC and the other from Antigua, were used in the early determination of the orbit.

**4. Event times**

Indications of the ignition times of the high-speed stages were obtained by the Microlock Gold Station. These times, together with the time at which the signal was lost by this station, were transmitted to the JPL Message Center at AFMTC, as were the times at which the signal was received and lost by the Antigua Station. This timing information also assisted in the early determination of the orbit.

# XVIII. INITIAL SCIENTIFIC MEASUREMENTS OF *EXPLORERS*

## A. Temperature Measurements

Exterior shell and internal temperatures were instrumented to provide data on primary environment and effectiveness of heat-isolation techniques. Data have been compared with precalculated shell temperatures and estimated internal temperatures to improve satellite design techniques. The temperature of the nose cone as a function of aerodynamic heating in the launch phase was difficult to determine analytically. This quantity has also been measured and telemetered to provide design information for future space vehicles.

## B. Micrometeorite Impact and Erosion Data

The distributions of space density and relative momentum of micrometeorites are of great importance. This experiment utilized two types of micrometeorite detectors:

1. Twelve wire-grid erosion detectors in parallel.

2. One impact microphone with amplifier and scaler.

The wire-grid detectors operated the channel 4 subcarrier of the low-power transmitter. As each wire grid was severed, the subcarrier experienced a small step-increase in frequency, indicating a high-velocity impact with a micrometeorite of 5 microns or larger.

The microphone was placed in spring contact with the outer shell of the satellite. When a particle of sufficient size and momentum hit the shell, the amplified pulse actuated the scaler. The output of the scaler controlled channel 4 of the high-power transmitter. Each time the frequency changed from low to high, or from high to low, the satellite had encountered a particle with a momentum of 1.6 x 10.2 gm-cm/sec or greater. Analysis of relative times in the high and low states has given an indication of the space density of the micrometeorites. An estimate of the absolute size and momentum of the particles was made by calibrations prior to flight. This experiment was performed in cooperation with the Air Force Cambridge Research Center (AFCRC). Results of this portion of the IGY satellite experiment were released by the AFCRC.

## C. Cosmic-Ray Count

Continuous cosmic-ray count was simultaneously measured and telemetered by both transmitters. The total count was scaled down by 32, and the channel 5 subcarriers experienced a step-change in frequency (either up or down) for each 16 cosmic-ray particles of sufficient intensity to trigger the Geiger-Mueller tube. The maximum square-wave response of channel 5 is 20 cps; therefore, the telemetering system is easily capable of transmitting information many times the normal rate, when such activity occurs during intense solar or magnetic storms. The results of the cosmic-ray experiment were prepared and released by Professor James Van Allen of the State University of Iowa.

## D. Geomagnetic Field Intensity

Damping of the spin rate has aided in indicating the magnitude of the geomagnetic field intensity and its effects upon the satellite. The spin rate was determined from amplitude modulation produced by one antenna which does not rotate about its symmetry axis. The low-power transmitter utilizes a dipole-like radiator, symmetrical about the spin axis. The satellite does not spin about its axis of symmetry; hence amplitude modulation of the received signal results. The displacement of spin axis from the symmetry axis was approximately ¼ deg; the energy in the spin-rate information-carrying sideband was approximately 50 db down from the carrier. Utilizing the sensitive Microlock receiving equipment and very narrow band phase-lock loop discriminators, data have been obtained under favorable conditions.

The high-power transmitter, which used a turnstile antenna, also provided information. The voltage ellipticity of the turnstile is approximately 1.1 along the symmetry axis, and, in the equatorial plane, had an amplitude modulation of approximately 5%. The linearly polarized ground antennas indicated the amplitude-modulated sidebands were in the order of 30 db down from the carrier.

## E. Ionospheric Measurements

At 108 mc, the ionosphere is believed to produce polarization rotation of a linear wave—the Faraday effect. Measurements of the relative intensity of two perpendicular and linear components at a ground station have provided data on the rate change with propagation angle of the ionosphere electron density. These data have been obtained from the linearly polarized Microlock dipole antenna.

Ray bending, due to index of refraction variations in the ionosphere, is 1 milliradian at 108 mc for propaga-

tion in a direction of 30 deg from the zenith (bending decreases as the zenith is approached). Measurements with the Minitrack interferometer, as compared with optical or post-calculated position data, have yielded ray-bending data, or, indirectly, integrated electron density.

### F. Atmospheric Density

From the evaluation of orbital decay, high-altitude atmospheric density data have been obtained. Estimates of payload attitude at perigee have aided in increasing the accuracy of these data.

# XIX. *EXPLORER I*

## A. General

On 31 January 1958 at 5 sec past 10:55 p.m., Eastern Standard Time, *Explorer I* was injected into orbit by *Jupiter-C* missile 29 (Fig. 80). The launching was a joint JPL-ABMA undertaking which took place at the Air Force Missile Test Center, Cape Canaveral, Florida. The orbital entry conditions were achieved by the combination of the *Redstone* booster to lift the missile to the desired altitude and the JPL high-speed stages to supply the additional velocity increment to place the payload in orbit. The Army Ballistic Missile Agency had the responsibility for the preparation and launching of the first or booster stage. The Jet Propulsion Laboratory prepared the high-speed stages of the launching vehicle, the satellite, and the satellite instrumentation.

*Explorer I* was identical to the satellite described previously in Sec. XIV.

The high-power transmitter radiated approximately 60 mw into a "turnstile" antenna. The information was amplitude-modulated for reception by the Minitrack stations and consisted of two temperatures, micrometeorite impact data, and cosmic-ray counts.

The low-power radiated 10 mw into a dipole antenna formed by electrically splitting the two halves of the payload. The stainless steel cylinder carrying the instrumentation was attached to the final stage rocket motor case by a cylinder of glass fiber which insulated the instrument cylinder from the motor case both electrically and thermally. Information was transmitted by four telemeter channels in the form of phase modulation, which was received by the Microlock stations. The two transmitters were completely independent of each other. Electronic tracking and telemetry records indicated that all systems functioned properly and that the missile closely followed the predicted trajectory. The high-power transmitter apparently exhausted its power supply 12 days after injection into orbit. It had been expected to last 14 to 21 days.

The missile was well controlled throughout the powered flight and coasting period, although the telemetered control frequencies differed from those predicted.

Cluster rotation occurred in three steps as scheduled, beginning with a speed of 560 rpm prior to liftoff, and reaching 751 rpm at 115 sec. Speed regulation of the cluster was maintained as desired.

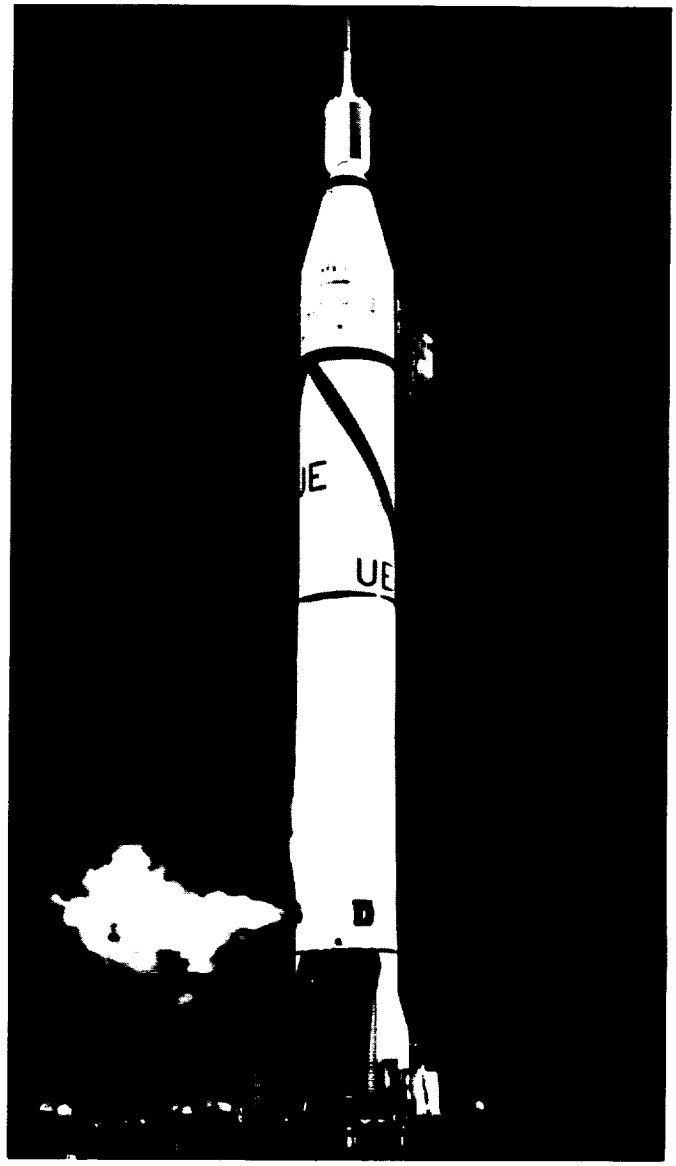

**Figure 80. The *Jupiter-C Explorer I***

Because the velocity at booster cutoff was about 250 mph higher than predicted, apex time was 10 sec later than predicted, and ignition of the second stage occurred 8 sec too early, only 0.7 sec before the timer setting. Table 9 shows conditions at second stage ignition.

Cluster stages performance was obtained by subtracting the data at second stage ignition from those at injection into orbit. The difference between predicted and actual performance was very small.

Table 10 gives a comparison of predicted conditions at the time of injection into orbit with actual conditions based on observations of the initial orbit. The values given correspond to the following initial orbital data:

| | |
|---|---|
| Perigee, miles | 223 |
| Apogee, miles | 1580 |
| Period, min | 113.2 |
| Estimated life, yr | 6 |

**Table 9. Conditions at second stage-ignition**

| Condition | Predicted | Actual |
|---|---|---|
| Time after liftoff, sec | 394.4 | 403.7 |
| Earth-fixed velocity, mph | 5230 | 5520 |
| Altitude, miles | 218 | 225 |
| Range, miles | 402 | 426 |
| Pitch angle, deg | 86.6 | 86.7 |
| Yaw angle, deg | 1.8 | 1.8 |

**Table 10. Conditions at injection into orbit**

| Condition | Predicted | Actual |
|---|---|---|
| Time after liftoff, sec | 419.3 | 428 6 |
| Earth-fixed velocity, mph | 17,180 | 17,680 |
| Altitude, miles | 218 | 228 |
| Range, miles | 474 | 501 |
| Pitch angle, deg | 89.9 | 89.1 |
| Yaw angle, deg | 1.1 | 0.1 |

## *B. Data Transmitted from* Explorer I

### 1. Fluctuations in Signal Strength

Long-period variations (1.5 min approximately) indicated that some Faraday effect was present. It is quite possible that these were due to the transmission of signals through the ionized layers of the upper atmosphere and the magnetic field of the earth. These variations were not due to tumbling of the satellite.

One very pronounced variation in signal strength had a fundamental period of about 7 sec. It is significant that the signals from the fixed linear antenna (but not the four flexible antennas) were of approximately the same strength when received by an east-west antenna as when received by a north-south antenna. Also, the 108.00-mc and the 108.03-mc signals were usually, but not always, out of phase. It was tentatively assumed that these fluctuations in signal strength were due to tumbling of the satellite.

### 2. Temperatures

There was continuous transmission of all telemetered data. Measurements of the stagnation point temperature and the nose-cone skin temperature were recorded at:

| Location | Latitude |
|---|---|
| Patrick Air Force Base | 28°N |
| Earthquake Valley | 33°N |
| San Gabriel | 34°N |
| Nigeria | 10°N |
| Singapore | 2°N |

Patrick Air Force Base, Earthquake Valley, and San Gabriel received data from approximately four passes a day; Nigeria and Singapore received data from about seven passes a day. Data from the low-powered transmitter were received at all stations, but information from the high-powered transmitter was received only at Patrick Air Force Base and San Gabriel.

The telemetered temperature data, including predicted internal temperatures for the nose cone and cylinder, were recorded for some 732 passes, covering the period from 1 February to 15 April 1958. Samples are given in Fig. 81 and 82.

Both the measured internal temperatures of the cylinder and the calculation of internal temperature in the nose cone showed a range of 35°C. This range was traversed semiperiodically, over an apparent period of approximately 2½ days. It is probable, however, that this temperature range was experienced during each orbit, since data were received during not more than 25% of any orbit. The records show an internal fluctuation of 0 to 35°C inside the cylinder and 5 to 40°C inside the nose cone. Shell temperature ranged from −25 to 75°C.

### 3. Cosmic Rays

As anticipated, the cosmic-ray count ran about 30 to 40 per sec at altitudes of 200 to 300 miles above southern California. However, at the satellite's highest altitude, above South America and adjoining waters, the count climbed to more than 35,000 per sec and completely saturated the instrumentation.

The radiation data were received only in the portions of the orbital band which were above ground stations. Since much of the surface of the Earth, particularly large bodies of water, over which *Explorer I* orbited had no receiving stations, the data were not representative of the total orbit.

### 4. Micrometeorites

The telemetered data indicated that one or two of the wire grids were fractured during the launching of the last

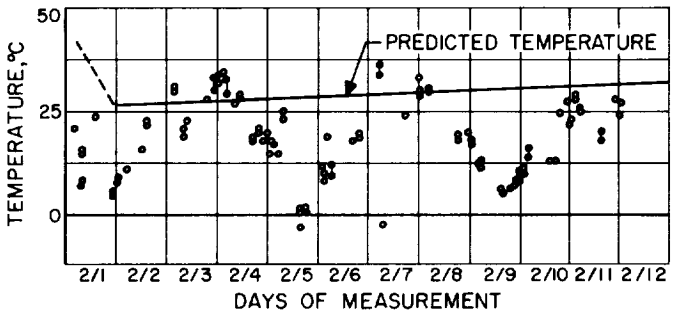


**Figure 81. Measured and predicted internal cylinder temperature vs time for 1958 Alpha, Feb. 1 through 12, 1958**

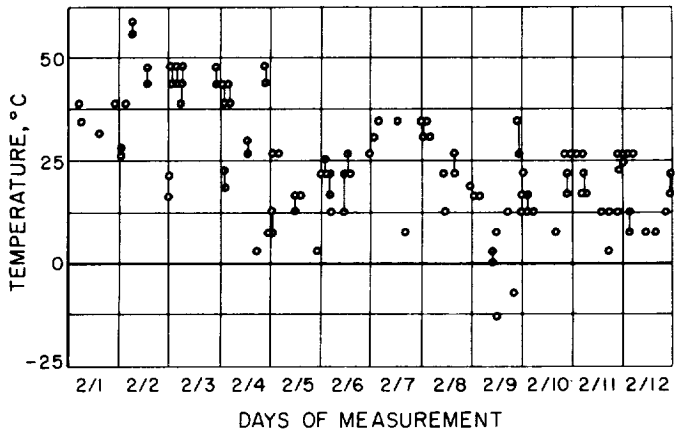


**Figure 82. Measured stagnation point temperature vs time for 1958 Alpha, Feb. 1 through 12, 1958**

stage. It was not possible to determine whether these breaks were due to micrometeorites. Indications were that *Explorer I* very frequently encountered micrometeorites of sufficient size to break the very fine wires.

Several impacts of small particles on the shell of the satellite were indicated by changes in the frequency of the telemetered signals from the impact microphone. In one record, two such events were observed during an interval of about two minutes.

# XX. *EXPLORER II*

Missile 26, carrying *Explorer II*, was fired on schedule at Cape Canaveral at 1327:59 hours EST on 5 March 1958 and was intended to place a second satellite in orbit. The flight was normal up to and including third-stage ignition. Failure of the fourth stage to fire prevented the attainment of orbital velocity.

Missile 26 was similar to missile 29 (*Explorer I*) and, in addition, carried a tape on which to store cosmic-ray information for broadcast through a Minitrack transmitter when interrogated by ground stations. A similar device was used in *Explorer III* and is described in Sec. XXI.

Table 11 shows the conditions at stage 2 ignition. Doppler frequency changes showed that both stages 2 and 3 produced a velocity increase of about 3000 mph, which added to the velocity produced by the booster totaled about 12,000 mph. Stages 3 and 4 impacted at a range of about 2000 miles.

**Table 11. Stage 2 ignition conditions**

| Condition | Predicted | Actual |
|---|---|---|
| Time after liftoff, sec | 394.4 | 390.4 |
| Earth-fixed velocity, mph | 5230 | 5290 |
| Altitude, miles | 218 | 234 |
| Range, miles | 402 | 396 |
| Pitch angle, deg | 86.6 | 84.3 |
| Yaw angle, deg | 1.8 | 1.2 |

# XXI. EXPLORER III

## A. General

On 26 March 1958, missile 24, carrying *Explorer III*, placed the second successful satellite of the *Explorer* series into orbit. *Explorer III* achieved orbital parameters of a 33.46-deg angle of inclination, a 1740-mile apogee, and a 115.65 min nodal period. Table 12 presents additional information on the flight.

The large deviation in local path resulted in high orbital eccentricity.

*Explorer III* weighed 18.53 lb and carried instrumentation for the following measurements:

1. Cosmic-ray count was recorded on a special miniature tape recorder developed by the University of Iowa. The stored information was transmitted by the high-power transmitter when interrogated by the Minitrack ground stations. This method enables conservation of battery power with prolonged life, since the high-power transmitter was required to operate only a short period each day.

2. Meteorite erosion, using wire gages similar to those used in *Explorer I*.

3. Temperature measurements were taken as in *Explorer I*. The data were telemetered in the same manner as for *Explorer I*. Tracking was done by Microlock and Minitrack stations (for signals from the transmitters on the satellite) and by radar.

## B. Data Transmitted from Explorer III

### 1. Communication

*Explorer III* carried two minimal-weight radio-frequency transmitters: the high-power transmitter having a power of 50 mw and a frequency of 108.03 mc, and the low-power transmitter having a power of 10 mw and a frequency of 108.00 mc.

The high-power transmitter used a dipole antenna in place of the turnstile antenna which had been employed in *Explorer I*. This was done by using the satellite itself as an antenna: a glass fiber ring in the midsection of *Explorer III* served as an insulator to divide the satellite in half, so that each half was one pole of the antenna. This system also served as the antenna for the radio receiver for the coded ground signal to activate the high-power transmitter. A similar dipole antenna in the forward half of the satellite provided the antenna for the low-power transmitter.

**Table 12. Flight data for *Explorer III***

| Condition | Predicted | Actual |
|---|---|---|
| Burnout of 1st stage, sec | 155.7 | 155.5 |
| Separation, sec | 157.7 | 160.9 |
| Stage 2 ignition, sec (timer) | 396.0 | 396.0 |
| Stage 4 ignition, sec | 412.0 | —— |
| Injection into orbit, sec | 420.0 | 424.0 |
| Altitude at injection, miles | 218 | 241 |
| Range at injection, miles | 480 | 500 |
| Earth-fixed velocity, mph | 17,260 | 17,400 |
| Local path angle at injection, deg | 90 | 84.5 |
| Perigee distance, miles | 218 | 117 |
| Apogee distance, miles | 1270 | 1740 |

### 2. Cosmic Rays

In an encapsulated package that also held the high-power transmitter, *Explorer III* contained a miniature tape recorder which "froze" on tape the data on cosmic radiation during the total orbit. While the satellite is making a full orbit around the Earth, the tape recorder makes a continuous record of the cosmic ray data. A tuning fork provides an internal time standard so that it is possible, when the tape is played back, to determine at what moment a given event occurred. The metal tape moves at a very slow rate of 0.005 in./sec. Less than 3 ft of tape is required for an entire trip around the Earth. When the satellite passes over or near one of the Minitrack stations along the 75th meridian, a coded command radio signal from the ground starts the tape over the playback head and simultaneously switches on the high-power transmitter. Thus, all the cosmic-ray information gathered during the entire orbit is sent to the ground station within 5 sec. The tape is then automatically erased and reset.

*Explorer III* thereby provided a comprehensive survey of the total cosmic-ray intensity at its orbital altitude above the Earth with respect to both time and position.

### 3. Temperature

In contrast to *Explorer I*, which had four temperature sensors, the number of temperature sensors in *Explorer III* was reduced to two, one for external and one for internal readings. The internal sensor was located in the cylindrical body of the satellite.

### 4. Micrometeorites

An impact microphone of the type carried in *Explorer I* was not used in *Explorer III*. However, the latter carried

an erosion gage, similar to that previously used, on the exterior of the instrument section. During the first week of May at approximately the time *Explorer III* was passing through an intense meteorite swarm called Eta Aquarids, two of the wire grids on the micrometeorite detector were broken.

Shortly afterwards, the cosmic-ray measuring device started to behave erratically and acted as if a wire had come loose. On May 10, the low-power beacon stopped sending signals, and on the same day the high-power transmitter, which had been growing weaker and more erratic, stopped sending signals in response to the interrogation command.

Because these systems had independent power supply units, the failure was presumed due to some occurrence common to both transmitters. From this evidence, it has been concluded that, between May 1 to May 7, when the Earth and *Explorer III* were in the meteorite belt, tiny meteor particles penetrated the instrumentation compartment.

On May 15, however, the low-power beacon returned to operation for a short period.

# XXII. *EXPLORER IV*

## A. General

On 26 July 1958, missile 44, carrying *Explorer IV*, placed the third satellite of the *Explorer* series into orbit. The orbit had a greater eccentricity and was at higher altitudes than previous *Explorer* satellites.

The carrier for *Explorer IV* differed from the previous *Explorer* carriers in that the third stage used JPL 136 solid propellant and the fourth stage used JPL 532A solid propellant, which improved overall performance.

*Explorer IV* was identical in size to *Explorers I* and *III* but was more than 7 lb heavier. It differed from previous *Explorers* principally in orbit, surface temperature control, and instrumentation.

## B. Injection into Orbit

The flight program for missile 44 (*Explorer IV*) differed greatly from that of the previous satellite launching vehicles, since it was intended to place the satellite in an orbit more eccentric and at a much higher altitude. Instead of 110 deg east of north, used in previous launchings, missile 44 was to be launched at 44 deg east of north. This was to result in an orbital inclination of about 50 deg to the equator. Table 13 compares predicted and actual flight results for *Explorer IV* at orbital injection.

**Table 13. Orbital data for *Explorer IV* at injection**

| Condition | Predicted | Actual |
|---|---|---|
| Earth-fixed velocity, mph | 18,000 | 17,750 |
| Altitude, miles | 179 | 161 |
| Pitch angle (local), deg | 90.0 | 89.6 |
| Yaw angle, deg | 0.8 | 0.8 |
| Perigee altitude, miles | 179 | 161 |
| Apogee altitude, miles | 1,755 | 1,388 |
| Inclination of orbit plane to equatorial plane, deg | 50.8 | 50.5 |

## C. Tracking

Initial tracking of missile 44 (*Explorer IV*) was done in the same manner as for previous satellite-carrying missiles, using the permanent camera, Microlock, and radar installations in conjunction with the radio beacons on the missile and payload.

Further orbital tracking was done by the Astrophysical Observatory of the Smithsonian Institution, and complete orbital information was available for each week, as soon as the necessary computations were completed.

## D. Orbit of Explorer IV

The orbit of *Explorer IV* was chosen to provide data from spaces not previously sampled. The orbital band covered most of the Earth's surface, with extremities at 51 deg north and south latitudes, compared to the 35 deg of *Explorers I* and *III*. The first pass of *Explorer IV* covered the East coast of the United States, Newfoundland, England, central Europe, southern Russia, India, and Australia. Subsequent passes covered the entire U.S., southern Canada, all of Australia, Africa, and South America, and the southern halves of Europe and Asia.

In addition to covering a large area, the orbit of *Explorer IV* was purposely chosen to have a high eccentricity, so that radiation could be recorded from farther out in space.

## E. Surface Temperature Control

The aluminum oxide strips, used on the previous *Explorers* to control temperatures, were not added, as higher temperatures were considered desirable for *Explorer IV*. The entire surface was sand-blasted stainless steel. Internal temperatures were expected to range from 0 to 65°C.

## F. Instrumentation of Explorer IV

The general arrangement of the instrumentation, including antennas and transmitters, of *Explorer IV* is shown in Fig. 83. The whip antenna was no longer used; the antennas were formed by cutting completely around the metallic cylindrical body in two places, and insulating the sections so formed from each other by structural phenolic plastic, similar to *Explorer III*. The front and rear antennas were used for the low- and high-power beacons, respectively. Radiation patterns of these antennas were such that the attitude of the satellite could be determined by studying the signal strength variations, which were periodic and corresponded to the tumbling periods of the satellite, as shown in Fig. 84. The radiation pattern for the forward antenna is illustrated in Fig. 85. The pattern for the rear antenna was similar but had only two lobes.

*Explorer IV* contained four separate radiation counters, instead of the single Geiger-Mueller counters carried by

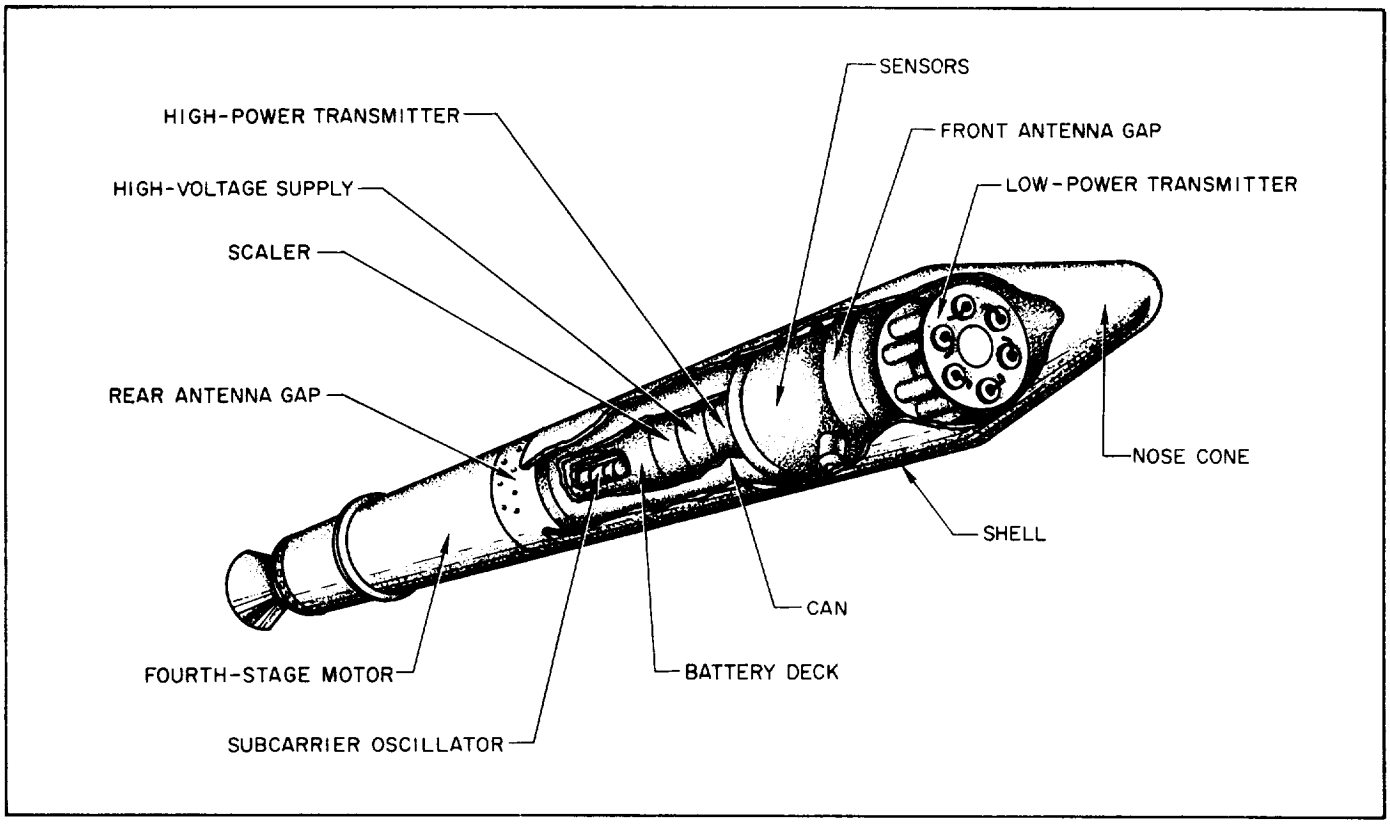


**Figure 83. *Explorer IV* instrumentation**

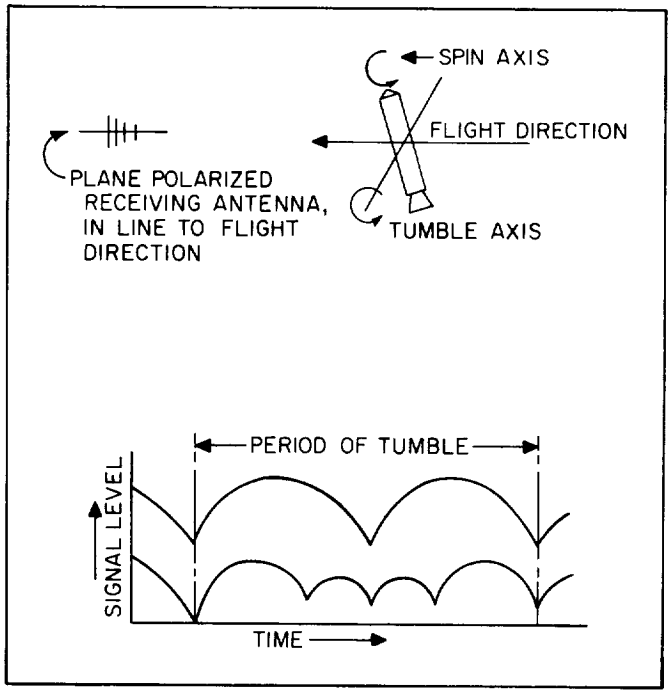


**Figure 84. *Explorer IV*, variation of signal level with tumble angle**

*Explorers I* and *III*. (The weight of the instrumentation in *Explorer IV* was almost twice that of the previous *Explorers*.) There were two Geiger-Mueller counters and two scintillation counters to measure radiation intensities. One of each of the Geiger-Mueller and scintillation counters was shielded with lead to exclude radiation below certain energy levels. In addition, the unshielded counters had special pickups to respond to various energy levels. Thus the new satellite differentiated various energy levels of radiation and indicated the relative quantities within these levels.

### G. *Data Transmitted from* Explorer IV

Unlike the two previous satellites placed in orbit by the Army, *Explorer IV* was devoted entirely to radiation studies. The decision to concentrate on such studies resulted from the extremely high cosmic-ray counts transmitted by the earlier *Explorers*. Information from the apogees of their orbits indicated pulse rates hundreds of times as high as expected, with counts higher than 35,000 per sec at the highest altitudes over South America. The unexpectedly high values exceeded the capacity of the

equipment used, so new types of equipment were developed for *Explorer IV* by the State University of Iowa Physics Department under Dr. James A. Van Allen. The new instruments could record up to 60,000 particles/sq cm/sec, several thousand times as many as previously measured.

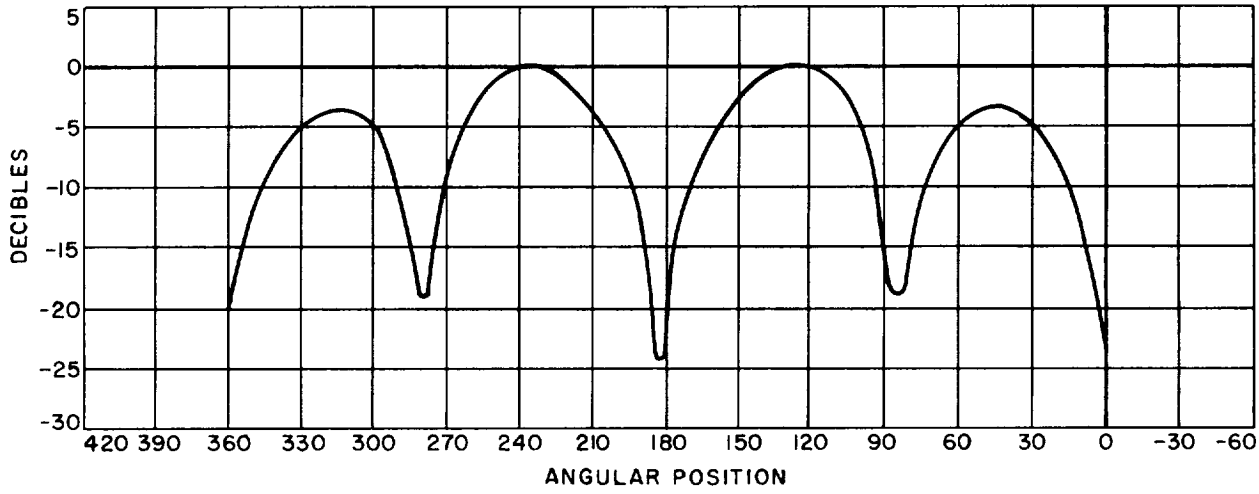


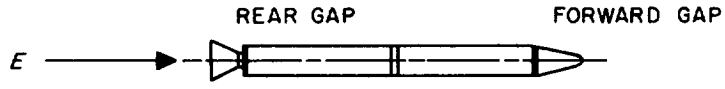


*EXPLORER IV* ANTENNA PATTERN, db

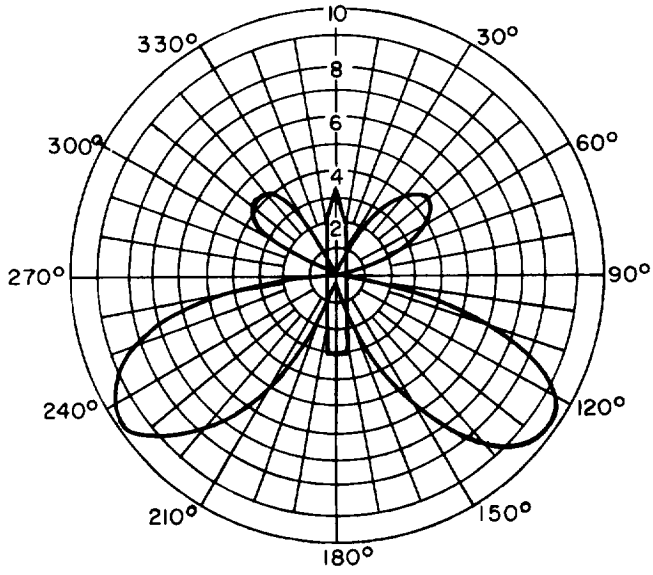


*EXPLORER IV* ANTENNA POWER PATTERN

**Figure 85. *Explorer IV* antenna pattern**

# XXIII. *EXPLORER V*

*Explorer V*, originally scheduled for August 9, 1958, was rescheduled for August 21 and was actually fired on August 24. The initial reschedule was to allow time for payload modifications dictated by the *Explorer IV* instrumentation results and to try to extend the payload lifetime. The last rescheduling was due to a leak in the fuel valve in the booster. *Explorer V* was unsuccessful in placing a payload into orbit.

The payload was similar to that of *Explorer IV* and the stage 4 propulsion unit was also similar. A polyurethane (Table 14) propellant-loaded stage 4 motor offers about 8% increase in the velocity increment over a motor loaded with JPL 136.

**Table 14. Composition of JPL 532A**

| Constituent | Amount, wt % |
|---|---|
| Ammonium perchlorate | 78.550 |
| Zirconium oxide, TAM Div. National Lead Co., Treopax grade | 2.000 |
| Polypropylene glycol, Carbide & Carbon Chemical Co., Niax 2025 | 16.354 |
| Trimethylol propane, Celanese Corp., Commercial grade | 0.268 |
| Alrosperse 11P, Geigy Chemical Corp. | 0.485 |
| Toluene diisocyanate, DuPont Hylene T | 2.060 |
| Phenyl B-naphtylamine, Eastman Organic Chemical Co. | 0.243 |
| Ferric acetylacetonate | 0.040 |

# XXIV. ROUND 49

## A. General

Round 49 carried as its main payload an inflatable plastic sphere covered with aluminum foil, a payload developed at Langley Research Center, Virginia. After inflation this sphere would have a diameter of 12 ft (Fig. 86 and 87).

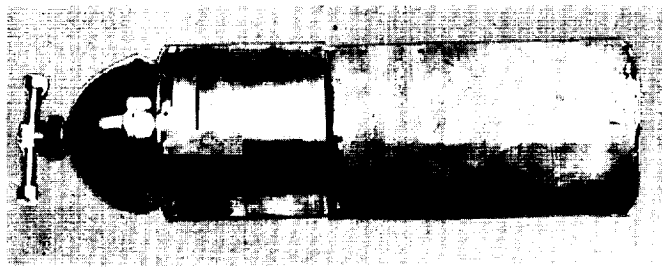

**Figure 86. Balloon assembly**

**Figure 87. NACA balloon**

The orbit intended for this sphere was approximately circular at an altitude of about 750 km. This comparatively high perigee would be achieved by the use of a "kick motor," or fifth stage, to be fired half way around the Earth (at the apogee) from the launching point. The principal effect of the kick motor was the increase in altitude at perigee from 120 to nearly 800 km. It was the purpose of the experiment to enable accurate measurements to be made of atmosphere density at high altitudes. The measurements were to be based on close observation of the satellite's orbit.

## B. Payload Design

### 1. Payload Components

The principal payload components (Fig. 88) included a 2-lb kick motor (Fig. 89), a Microlock beacon (Fig. 90), and NACA balloon package. To accommodate the larger volumetric requirements, the diameter of the payload cylindrical shell was increased from 6 to 7 in., still keeping the payload critical speed at reasonable value.

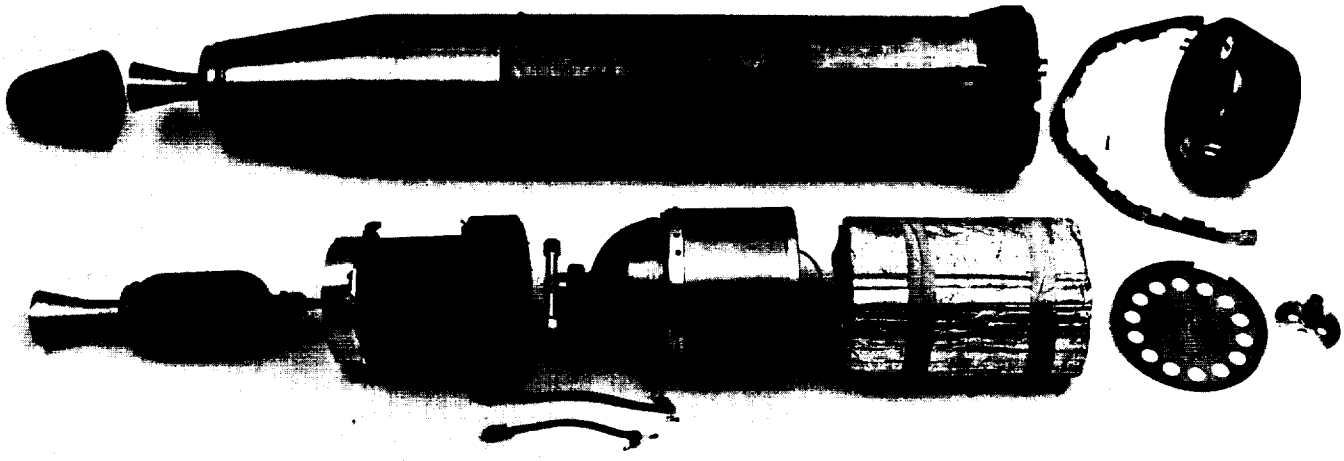

**Figure 88. Payload assembly**

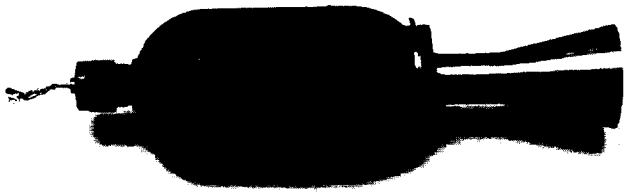

Figure 89. Two-pound solid-propellant motor

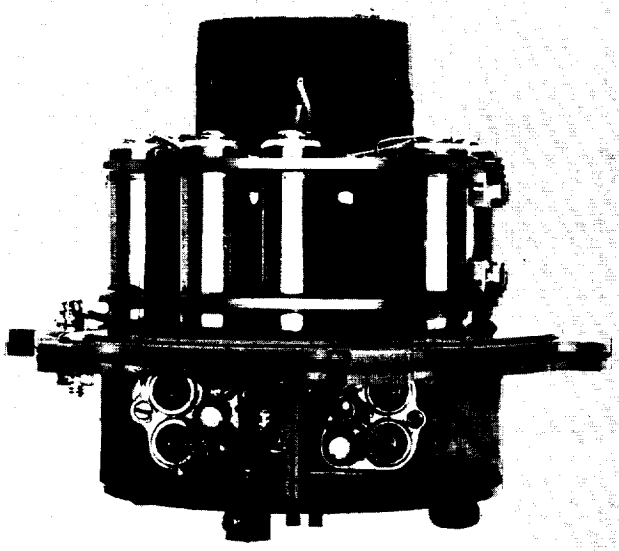

Figure 90. Low-power beacon

### 2. Balloon Ejection

To permit the balloon package ejection from the payload package, separation of the fourth stage motor was required, since the kick motor is located in the forward end of the payload. A timer simultaneously ignited the kick motor and a time delay mechanism which separated the payload from the stage 4 motor.

### 3. Transmitter

The transmitter beacon (Fig. 90) consisted of a redesigned 25-mw phase-modulated Microlock transmitter, two channels of telemetering (channels 3 and 4), and mercury batteries for a beacon life of at least one week.

### 4. Failure to Orbit

Round 49 (Fig. 91) was fired on 22 October as scheduled; however, at approximately 111.5 sec after liftoff, the payload, still attached to the fourth stage, broke off

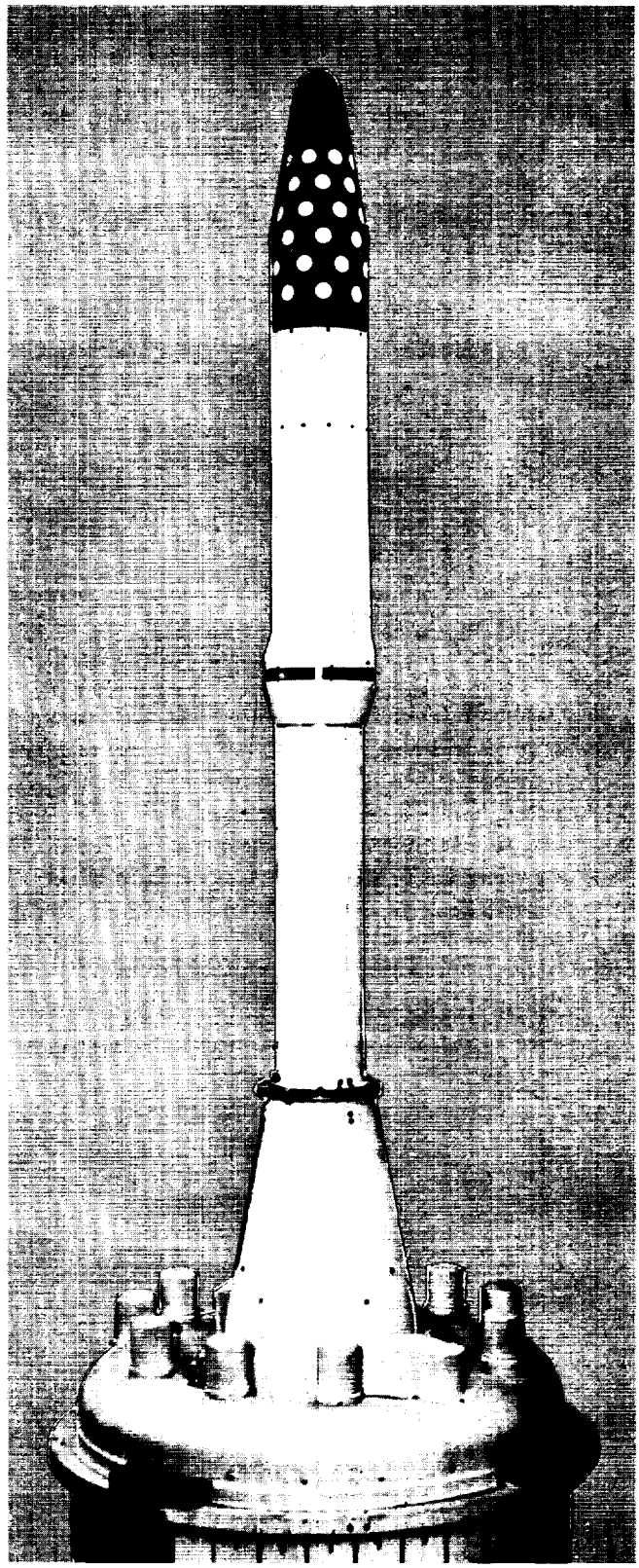

Figure 91. Round 49

from the cluster. This was deduced from interpretation of booster telemetering records and payload transmitter signal records. Cause of the failure may be due to resonance of the cluster, thermo buckling and differential expansion effects due to aerodynamic heating, and/or unbalance in the cluster due to failure of a payload component.

# BIBLIOGRAPHY

## General Documents


1. Hibbs, A. R., *Scientific Results from the* Explorer *Satellites,* External Publication No. 514, Jet Propulsion Laboratory, Pasadena, June 2, 1958.
2. Froehlich, J. E., *Contributions of the* Explorer *to Space Technology,* External Publication No. 526, Jet Propulsion Laboratory, Pasadena, July 7, 1958.
3. Pickering, W. H., *Results of the IGY Satellite Program,* External Publication No. 574, Jet Propulsion Laboratory, Pasadena, July 20, 1959.
4. Hibbs, A. R., *Scientific Results From the* Explorer *Satellites and the* Pioneer *Space Probes,* External Publication No. 649, Jet Propulsion Laboratory, Pasadena, May 15, 1959.
5. Stewart, H. J., Small, J. G., Robillard, F., *The* Explorer *Rocket System,* Publication No. 129, Jet Propulsion Laboratory, Pasadena, May 8, 1958 (CONFIDENTIAL).
6. Robillard, G., *The* Explorer *Rocket Research Program,* Publication No. 145, Jet Propulsion Laboratory, Pasadena, October 31, 1958.
7. Froehlich, J. E., and Hibbs, A. R., *Contributions of the* Explorer *to Space Technology,* Progress Report No. 20-359, Jet Propulsion Laboratory, Pasadena, September 3, 1958.
8. Shipley, W. S., *Absorptances to Solar and Terrestrial Radiation of Surface Considered for Use on the* Explorer *Satellite,* Section Report No. 12-161, Jet Propulsion Laboratory, Pasadena, September 15, 1958.
9. Froehlich, J. E., and Hibbs, A. R., *Ballistics of the* Explorer, Report 20-118, Jet Propulsion Laboratory, Pasadena, August 13, 1958.
10. Victor, Walter K., Richter, Henry L., and Eyraud, J. P., Explorer *Satellite Electronics,* Technical Release No. 34-12, Jet Propulsion Laboratory, Pasadena, January 29, 1960.
11. Merrick, William D., Valencia, Chris, Frazer, Robert E. and Stoller, Floyd W., *The Techniques, Equipment, Equations and Data-Reduction Procedures Used in the Alignment, Checkout and Evaluation of the 85-ft. Dish Radio Telescope Antenna at the JPL Goldstone Tracking Site,* Publication No. 30-9, Jet Propulsion Laboratory, Pasadena, September 7, 1959.
12. *Space Programs Summary No. 6 (for the period September 15 to November 15, 1959),* Jet Propulsion Laboratory, Pasadena, December 1, 1959 (SECRET).
13. Juno I *and* II *Stage 2 Rocket Motor,* Publication No. 169, Jet Propulsion Laboratory, Pasadena, October 15, 1959.
14. *Jupiter Bimonthly Summary No. 7 (for the period 15 May to 15 July 1957),* Jet Propulsion Laboratory, Pasadena, August 1, 1957 (SECRET).
15. *Jupiter Bimonthly Summary No. 8 (for the period 15 July to 15 September 1957),* Jet Propulsion Laboratory, Pasadena, October 1, 1957 (SECRET).
16. *Jupiter Bimonthly Summary No. 9 (for the period 15 September to 15 November 1957),* Jet Propulsion Laboratory, Pasadena, December 1, 1957 (SECRET).
17. *Jupiter Bimonthly Summary No. 10 (for the period 15 November 1957 to 15 January 1958),* Jet Propulsion Laboratory, Pasadena, February 1, 1958 (SECRET).
18. *Proposal for Modification of the State University of Iowa Cosmic Ray Experiment for the* Jupiter C *Vehicle,* Publication No. 115, Jet Propulsion Laboratory, Pasadena, December 2, 1957.
19. *Space Research Summary No. 1 (for the period 15 May to 15 July 1958),* Jet Propulsion Laboratory, Pasadena, August 1, 1958 (SECRET).
20. *Space Research Summary No. 2 (for the period 15 July to 15 September 1958),* Jet Propulsion Laboratory, October 1, 1958 (SECRET).
21. *Space Research Summary No. 3 (for the period 15 September to 15 November 1958),* Jet Propulsion Laboratory, Pasadena, December 1, 1958 (SECRET).
22. Dowler, W. L., Juno II *Fourth-Stage Motor (Titanium Case),* Publication No. 156, Jet Propulsion Laboratory, Pasadena, February 18, 1959 (CONFIDENTIAL).

23. Juno I *and* II *Stage 2 Rocket Motor,* Publication No. 169, Jet Propulsion Laboratory, Pasadena, October 15, 1959 (CONFIDENTIAL).

24. Mathison, Richard P., *Equations for the Radio System of the* Juno II *Downrange Tracking Station,* Section Report No. 16-61, Jet Propulsion Laboratory, Pasadena, July 8, 1958.

25. *Aeroballistics Evaluation of Jupiter C Test Flight C-26,* RTV 53710-13, ABMA, Huntsville, Ala., April 19, 1950 (SECRET).

26. Explorers *in Orbit,* No. 58472-91 and 58519, ABMA, Huntsville, Ala., November 10, 1958 (SECRET).

27. *Bound Volume of Papers Presented at the American Rocket Society 13th Annual Meeting,* No. 59314 and 59394, American Rocket Society, January 14, 1959.

28. Koelle, Heinz H., and Pauli, Fritz, *Secret Title on Performance and Design Considerations for the Jupiter-C Missile for Various Flight Missions,* No. 60447, ABMA, Huntsville, Ala., July 5, 1956 (SECRET).

29. Felix, A. Richard, *Static Stability and Drag Investigation of Jupiter C Boosted NASA Manned Space Capsule,* No. 62456 and 62547, ABMA, Huntsville, Ala., December 5, 1958 (CONFIDENTIAL).

30. *Proposal for an Advanced Reconnaissance System,* No. 62960, ABMA, Huntsville, Ala., April 1957 (SECRET).

31. Geissler, E. D., *ABMA Space Vehicles,* No. 70686, ABMA, Huntsville, Ala., November 24, 1959 (CONFIDENTIAL).

32. Potts, C. M., *Microlock Diary—Cape Canaveral,* Section Report No. 8-561, Jet Propulsion Laboratory, Pasadena, 1956 (CONFIDENTIAL).

33. Sola, Louis, *Two-Pound Motor Development (Kick Motor),* Section Report No. 4-4, Jet Propulsion Laboratory, Pasadena, March 5, 1958 (CONFIDENTIAL).

## Feasibility and Telemetering Studies

34. *Guided Missile Summary No. 45* (for the period November 1, 1954 to January 1, 1955), Jet Propulsion Laboratory, Pasadena, February 1, 1955 (SECRET).

35. *Guided Missile Summary No. 54* (for the period May 1, to July 1, 1956), Jet Propulsion Laboratory, Pasadena, July 15, 1956 (SECRET).

36. *Corporal Bimonthly Summary No. 33A* (for the period November 1, 1952, to January 1, 1953), Jet Propulsion Laboratory, February 1, 1953 (SECRET).

37. *Corporal Bimonthly Summary No. 34A* (for the period January 1 to March 1, 1953), Jet Propulsion Laboratory, Pasadena, April 1, 1953 (SECRET).

38. *Corporal Bimonthly Summary No. 35A* (for the period March 1 to May 1, 1953), Jet Propulsion Laboratory, Pasadena, June 1, 1953 (SECRET).

39. *Corporal Bimonthly Summary No. 36A* (for the period May 1 to July 1, 1953) Jet Propulsion Laboratory, Pasadena, August 1, 1953 (SECRET).

40. *Corporal Bimonthly Summary No. 37A* (for the period July 1 to September, 1953), Jet Propulsion Laboratory, Pasadena, October 1, 1953 (SECRET).

41. *Corporal Bimonthly Summary No. 38A* (for the period September 1 to November 1, 1953), Jet Propulsion Laboratory, Pasadena, December 1, 1953 (SECRET).

42. *Corporal Bimonthly Summary No. 39A* (for the period November 1, 1953, to January 1, 1954), Jet Propulsion Laboratory, Pasadena, February 1, 1954 (SECRET).

43. *Corporal Bimonthly Summary No. 40A* (for the period January 1 to March 1, 1954), Jet Propulsion Laboratory, Pasadena, April 1, 1954 (SECRET).

44. *Corporal Bimonthly Summary No. 41A* (for the period March 1 to May 1, 1954), Jet Propulsion Laboratory, Pasadena, June 1, 1954 (SECRET).

45. *Corporal Bimonthly Summary No. 42A* (for the period May 1 to July 1, 1954), Jet Propulsion Laboratory, Pasadena, August 1, 1954 (SECRET).

46. *Corporal Bimonthly Summary No. 43A* (for the period July 1 to September 1, 1954), Jet Propulsion Laboratory, Pasadena, October 1, 1954 (SECRET).

47. *The* Sergeant, *Report No. 20-76,* Jet Propulsion Laboratory, Pasadena, April 15, 1954 (SECRET).

48. *A Proposed Radio-Inertial Guidance System for a 1500-Mile Ballistic Missile,* Jet Propulsion Laboratory Publication No. 61, January 11, 1956 (SECRET).

49. *A Proposed Program for Joint Army-Navy Development of Radio-Inertial Guidance System for IRBM*—No. 2, Naval Research Laboratory and Jet Propulsion Laboratory Enclosure 3, March 13, 1956 (SECRET).

50. *Errors at Impact as Functions of Dispersion at Cutoff for Ballistic Rockets,* R. A. E. Technical Note G. W. 383, Farnborough, Hants, Great Britain, October, 1955 (SECRET).

## BIBLIOGRAPHY (Cont'd)


51. Cuccia, C. L., *Harmonics, Sidebands, and Transients in Communications Engineering*, p. 308, McGraw-Hill, New York, 1952.

52. Valley, G. E., Jr., and Wallman, H., *Vacuum Tube Amplifiers*, Radiation Laboratory Series, Vol. 18, McGraw-Hill, New York, 1958.

53. Hessel, J., Goubau, G., and Battersby, L. R., *Microwave Filter Theory and Design*, Proceedings of the IRE; Vol. 37, 990-1002, September, 1949.

54. *A Feasibility Study of the High-Velocity of a Minimum Orbiting Missile*, Publication No. 47, Jet Propulsion Laboratory, Pasadena, 15 July 1955 (SECRET).

55. Sampson, W. F., *A Feasibility Study for Minimum-Weight Radio Instrumentation of a Satellite*, Publication No. 48, Jet Propulsion Laboratory, Pasadena, 21 September 1955 (SECRET).

56. Sampson, W. F., *MICROLOCK: A Minimum-Weight Radio Instrumentation System for a Satellite*, Publication No. 63, Jet Propulsion Laboratory, Pasadena, 13 April 1956 (SECRET).

57. Jaffee, R. M., and Rechtin, E., *Design and Performance of Phase-Lock Circuits Capable of Near-Optimum Performance Over a Wide Range of Input Signals and Noise Levels, Transactions and Information Theory*, IRE, IT-1, No. 1, March 1955.

58. *Jupiter Bimonthly Summary No. 2*, Jet Propulsion Laboratory, Pasadena, California, 1 October 1956 (SECRET).

59. *Jupiter Bimonthly Summary No. 1*, Jet Propulsion Laboratory, Pasadena, California, 1 August 1956 (SECRET).

60. *Jupiter Bimonthly Summary No. 6*, Jet Propulsion Laboratory, Pasadena, California, 1 June 1957 (SECRET).

61. *Explorers in Orbit*, Army Ballistic Missile Agency, Redstone Arsenal, Alabama, 10 November 1958 (SECRET).


### RTV Rounds 27, 34, and 40


62. Benesch, S., *Estimated Dispersion for the High-Speed Stages of the RTV Round 34*, Section Report No. 1-28, Jet Propulsion Laboratory, Pasadena, April 12, 1957 (CONFIDENTIAL).

63. Eimer, M., *Preliminary Data Analysis of Redstone RTV Round 34*, Section Report No. 1-30, Jet Propulsion Laboratory, Pasadena, July 15, 1957 (CONFIDENTIAL).

64. Owens, J. D. and Clarke, W. G., *Jupiter C-RS 27 Flight Evaluation: Propulsion and Associated Systems*, RTV 51290, ABMA, Huntsville, Ala., September 20, 1956 (CONFIDENTIAL).

65. Saucier, Sidney P., Jupiter C-*RS 34 Flight Evaluation Propulsion and Associated Systems Launching No. 25 on May 15, 1957*, RTV 51291, ABMA, Huntsville, Ala., August 29, 1957 (CONFIDENTIAL).

66. Donehoo, Larry K., and Bacchus, David L., *Control Factors for First Stage of Propelled Flight for* Jupiter C *Missile RS 34, No. 60449, ABMA*, Huntsville, Ala., April 9, 1957 (SECRET).

67. *Dovap Flight Data:* Jupiter C *No. 40*, No. 60454, ABMA, Huntsville, Ala., September 20, 1957 (SECRET).

68. Miner, W. E., and Neighbors, Alice, *Trajectory Data for Firing of* Jupiter C *Missile No. 27*, No. 60455, ABMA, Huntsville, Ala., August 30, 1956.

69. McNair, Lewis L., *Trajectory Data for Firing of* Jupiter C *Missile No. 40, No. 60467, ABMA*, Huntsville, Ala., July 1, 1957 (SECRET).

70. *Observation of* Jupiter C *Re-Entry-Recovery Configuration (Missile No. 40) From Aboard Destroyer Escort USS H. D. Crow*, No. 60474, ABMA, Huntsville, Ala., August 22, 1957 (SECRET).

71. Schwaneger, Arthur J., Jr., and Miner, William E., *Trajectory Data for Firing of* Jupiter C *Missile RS-34 Azimuth of 105 Degrees*, No. 61497, ABMA, Huntsville, Ala., March 21, 1957 (SECRET).

72. *Remarks on Optical Tracking of Missile No. 27*, No. 63525, ABMA, Huntsville, Ala., September 11, 1956 (SECRET).

73. Emanuel, Garvin R., *Performance Evaluation Unit Systems Report of Propulsion and Associated Systems of* Jupiter C *Missile CC-40, Launching No. 29 on August 8, 1957*, No. 64849, ABMA, Huntsville, Ala., June 30, 1959 (SECRET).


### *Explorer I*, Round 29 (*Juno I, Jupiter C*)


74. Eyraud, John P., Shipley, William S., Randolph, Lee W., Richter, Henry L., and Pilkington, William, *Instrumenting the* Explorer I *Satellite*, No. 66551-52, Jet Propulsion Laboratory, Pasadena, 1959.

75. Potter, P. D., Davis, E. F., and Schuster, D., *Coaxial Turnstile Antenna Feed System*, Invention Report No. 20-94, Jet Propulsion Laboratory, Pasadena, September 3, 1958.

76. Randolph, L. W., Choate, R. L., *Calibration Record for the IGY Earth Satellite 1958 Alpha,* Publication No. 130, Jet Propulsion Laboratory, Pasadena, February 5, 1958.

77. *Preliminary Mass Characteristic Values for* Jupiter-C *Missile RS 29,* RTV 50653, ABMA, Huntsville, Ala., January 8, 1958 (SECRET).

78. Donehoo, Larry K., *Control Factors for First Stage of Propelled Flight for* Jupiter-C *Missile RS-29,* RTV 50997-98, ABMA, Huntsville, Ala., January 23, 1958 (SECRET).

79. Jupiter C *No. 29 Safety Analysis Data Azimuth 110 Degree RTV 51360,* ABMA, Huntsville, Ala., January 6, 1958 (SECRET).

80. Crenshaw, Joseph N., *Expected Normal Modes and Bending Frequencies of* Jupiter C *Missile No. 29 After Separation of Booster Section,* RTV 50999 and RTV 51000, ABMA, Huntsville, Ala., January 21, 1958 (SECRET).

81. Jean, O. C., and Sullivan, Elbert L., Jupiter C *No. 29 Error Analysis,* RTV 51289, ABMA, Huntsville, Ala., January 8, 1958 (SECRET).

82. Owens, J. D., *Preliminary Flight Evaluation of Propulsion and Associated Systems* — Jupiter C, RS-29, RTV 51292, ABMA, Huntsville, Ala., February 10, 1958 (CONFIDENTIAL).

83. Jupiter C *No. 29 Safety Analysis Data Azimuth 110°* RTV 51360, ABMA, Huntsville, Ala., January 6, 1958 (SECRET).

84. Speer, Fridtjof, *Aeroballistics Evaluation of Test Flight* Jupiter C-29, RTV 52686-9, ABMA, Huntsville, Ala., March 1, 1958 (SECRET).

85. Crenshaw, Joseph N., *Expected Normal Modes and Bending Frequencies of* Jupiter C *Missile No. 29 After Separation of Booster Section,* No. 60453, ABMA, Huntsville, Ala., January 21, 1958 (SECRET).

86. Miner, William E., and Jean, O. C., Jupiter C *No. 29 Preliminary Trajectory Data,* No. 60494, ABMA, Huntsville, Ala., November 19, 1957 (SECRET).

87. *Preliminary Mass Characteristic Values for* Jupiter C *Missile RS 29,* No. 60866, ABMA, Huntsville, Ala., January 8, 1958 (SECRET).

### *Explorer II,* Round 26 (*Juno I, Jupiter C*)

88. Jupiter *Missile, Serial RSUV Master Operational Schedule,* No. 838, Jet Propulsion Laboratory (PAFB Office), February 18, 1958 (CONFIDENTIAL) (Modified Handling Authorized).

89. Choate, Robert L., *Calibration Records for the IGY Earth Satellite 1958 Gamma,* Publication No. 126, Jet Propulsion Laboratory, Pasadena, June 27, 1958.

90. Trostle, H. G., and Scott, M. P., *Doppler Data on Cluster No. 26 (RS 24),* Section Report No. 1-41, Jet Propulsion Laboratory, Pasadena, August 4, 1958 (CONFIDENTIAL).

91. Emanuel, Garvin, R., Jupiter C *Missile RS-26 Thermal Environment Analysis Systems Report. Temperature and Pressure Control Systems, Special Measurements and Skin Temperature Data Launching No. 38 on March 5, 1958.* RTV 54891-93, ABMA, Huntsville, Ala., May 23, 1958 (CONFIDENTIAL).

92. Emanuel, Garvin E., and Vaughan, Otha, H. Jr., *Performance Evaluation Unit Systems Report of Propulsion Unit and Associated Systems of* Jupiter C *Missile RS-26 Launching No. 38 on 5 March 1958,* No. 70847, ABMA, Huntsville, Ala., January 21, 1960 (SECRET).

### *Explorer III,* Round 24 (*Juno I, Jupiter C*)

93. Minor, Wm. E., and Jean, O. C., Jupiter C *No 24 Final Trajectory Data,* RTV 52078-9, ABMA, Huntsville, Ala., March 13, 1958 (SECRET).

94. *Flight Test Data*—Jupiter C *No 24 Launched March 26, 1958,* RTV 53452-53, AFMTC (PAFB), Florida, April 2, 1958 (SECRET).

95. Fulmer, C. R., *Trajectory for* Jupiter *Flight Test C-24,* RTV 54303-6, ABMA, Huntsville, Ala., May 23, 1958 (SECRET).

96. Vaughan, Jr., Otha, H., Jupiter C *Missile RS-24 Thermal Environment Analysis Systems Report Temperature and Pressure Control System, Special Measurements, and Skin Temperature Data Launching No. 39 on March 26, 1958,* RTV 54894-96, ABMA, Huntsville, Ala., May 19, 1958 (CONFIDENTIAL).

97. *Aeroballistics Evaluation of Test Flight* Jupiter C-24, RTV 55250, ABMA, Huntsville, Ala., June 14, 1958 (SECRET).

98. Trostle, H. G., and Scott, M. P., *Doppler Data on Cluster No. 26 (RS-24),* Section Report No. 1-41, Jet Propulsion Laboratory, Pasadena, August 13, 1958 (CONFIDENTIAL).

### *Explorer IV,* Round 44 (*Juno I, Jupiter C*)

99. Jean, O. C., and Schrader, Martin J., *Missile No. 44 and 47 Preliminary Trajectory Data,* RTV 54307-10, ABMA, Huntsville, Ala., June 2, 1958 (SECRET).

## BIBLIOGRAPHY (Cont'd)


100. *Missile No. 44, Final Trajectory Data,* RTV 55161, ABMA, Huntsville, Ala., July 3, 1958 (SECRET).

101. Jupiter C No. *44, Safety Analysis Data Azimuth 44°,* RTV 55248, ABMA, Huntsville, Ala., July 2, 1958 (CONFIDENTIAL).

102. Speer, Fridtjof, *Aeroballistics Evaluation of Test Flight* Jupiter C *44 and 47,* RTV 58022-23, ABMA, Huntsville, Ala., September 26, 1958 (SECRET).

103. Speer, Fridtjof, *Aeroballistics Evaluation of Test Flight* Jupiter C *44 and* C *47,* RTV 69949, ABMA, Huntsville, Ala., September 26, 1958 (SECRET).

104. *Missiles No. 44 and 47 Preliminary Data,* No. RTV 54308, ABMA, Huntsville, Ala., June 2, 1958 (SECRET).


### *Explorer V,* Round 47 (*Juno I, Jupiter C*)


105. Dowler, W. L., Explorer IV *4th Stage Motor (410 Stainless Steel Case),* Publication 30-1, Jet Propulsion Laboratory, Pasadena, April 3, 1959 (CONFIDENTIAL).

106. Jean, O. C., and Schrader, Martin J., *Missile No. 44 and 47 Preliminary Trajectory Data,* RTV 54307-10, ABMA, Huntsville, Ala., June 2, 1958 (SECRET).

107. Speer, Fridtjof, *First Result Test Flight* Jupiter C *47* Explorer V, No. 56220-22, ABMA, Huntsville, Ala., August 29, 1958 (SECRET).

108. *Missile No. 47, Final Trajectory Data,* RTV 57656-8, ABMA, Huntsville, Ala., August 8, 1958 (SECRET).

109. Speer, Fridtjof, *Aeroballistics Evaluation of Test Flight* Jupiter C *44 and 47,* RTV-58022-23, ABMA, Huntsville, Ala., September 26, 1958 (SECRET).

110. Speer, Fridtjof, *Aeroballistics Evaluation of Test Flight* Jupiter C *44 and 47,* No. 69949, ABMA, Huntsville, Ala., September 26, 1958 (SECRET).

111. *Missiles No. 44 and 47 Preliminary Data,* RTV 54308, ABMA, Huntsville, Ala., June 2, 1958 (SECRET).


### Round 49, *Deal III, Beacon* (*Juno I, Jupiter C*)


112. Teague, E. Rober, and Jean, O. C., Jupiter C *Missile No. 49: Error Analysis,* RTV 57106-7, ABMA, Huntsville, Ala., September 23, 1958 (SECRET).

113. Hoelker, R. F., and Jean O. C., Jupiter C No. *49: Preliminary Trajectory,* RTV 57282, ABMA, Huntsville, Ala., September 12, 1958 (SECRET).

114. Schrader, M. J., and Jean, O. C., Jupiter C *Missile No. 49 Trajectory Outlay Considerations,* RTV 57471 and 57515, ABMA, Huntsville, Ala., October 7, 1958 (SECRET).

115. Flight Test Data, Jupiter C *No. 49 Launched October 22, 1958,* RTV 58048, AFMTC, October 31, 1958 (SECRET).

116. Lindberg, J. P., Fulmer, C. R., et al, *Aeroballistics Evaluation of Test Flight Jupiter C 49,* No. 60708-11, ABMA, Huntsville, Ala., February 14, 1958 (SECRET).

117. Hopkins, Chester L., and Vaughan, Otha H., Jr., *Performance Evaluation Unit Systems Report on Propulsion and Associated Systems of* Jupiter C *Missile C-49 Launching No. 47 on 22 October 1958,* No. 65764, ABMA, Huntsville, Ala., July 31, 1959 (SECRET).

118. Schrader, Martin J., and Jean, Otha C., Jupiter C *Missile No. 49 Final Trajectory,* No. 69939, ABMA, Huntsville, Ala., October 13, 1958.

119. *Actual Trajectory for* Jupiter *Flight Test C-49,* No. 15265, ABMA, Redstone Arsenal, January 22, 1959 (SECRET).